Accurate Node Localisation in Ad Hoc Networks Using Directional Pulsed Infrared Light Communications

A thesis submitted for the degree of

Master of Engineering Science (Research)

by

Joseph Violi

Department of Electrical and Computer Systems Engineering
Monash University
Australia

January 2009

Summary

This thesis presents a localisation scheme for ad hoc networks which use pulsed infrared light as the communication medium. Data transmission with infrared light has shown great potential for various applications such as ambient intelligence or indoor broadband communication systems. Infrared light has very attractive properties for indoor applications as it is inherently secure due to the fact that infrared signals do not penetrate walls. This property also reduces the interference and increases available bandwidth to individual devices. Infrared systems can be built with low-cost components, and are thus suitable for inexpensive consumer applications.

Localisation in wireless ad hoc networks is important since it allows the nodes to learn their precise location, and use this information for higher layer mechanisms. These include topology configuration, fault tolerance, routing, mapping of measured data to physical locations, or support for mobile devices. The dissemination of accurate localisation information allows nodes to interact more intelligently with their environment and other nodes in the network.

Typically, in wireless ad hoc networks, nodes estimate their position relative to their neighbours by processing the location information, and certain physical properties of the signal they receive, such as signal strength, bit error rate, or time difference of arrival. Unfortunately, widely used low-cost infrared transmitters and receivers for indoor applications do not allow measurement of these properties easily. To overcome this, we have developed a system which only relies on the reception of a data frame and is capable of estimating the angular direction of the infrared signal source within an error margin of ± 5 degrees. Then, through the application of triangulation, a node estimates its relative position with respect to its neighbours.

One effective method of translating a relative location to an absolute one is to use anchor nodes. These nodes know their exact location and broadcast this information to their neighbours. Each node then progressively fixes its position and broadcasts the position updates, leading to the entire network localising itself. A major drawback of this approach arises in large networks, where the average

hop distance between the anchor and ordinary nodes is large, and position estimation errors inevitably start to accumulate. In order to alleviate this problem, we have developed the Anchor Hop Distance Weighted Localisation (AHDWL) algorithm to selectively weigh position estimates at each hop. We have found that the AHDWL algorithm is very effective in reducing propagation of positioning errors.

A small size test network using directional pulsed infrared light was created to evaluate the performance of the localisation system. Also, a simulator based on the experimentally obtained channel characteristics was developed for rapid evaluation of the localisation algorithm on large networks. Results show that using our approach, an infrared network built with low-cost consumer grade components which lack explicit signal strength or bit error rate measurement capabilities, can accurately estimate the position of its member nodes.

Declaration

I declare that, to the best of my knowledge, the research described herein is original except where the work of others is indicated and acknowledged, and that the thesis has not, in whole or in part, been submitted for any other degree at this or any other university.

Joseph Violi
Melbourne
January 2009

Acknowledgments

This work would not have been possible without the support and guidance of my supervisors, Dr. Ahmet Şekercioğlu and Dr. Andrew Price. Their enthusiasm and knowledge in the area made for an interesting and challenging project. A special thanks goes to Dr. Ahmet Şekercioğlu for his continued patience during the write up stage, the seemingly endless corrections which he meticulously made in his patented handwriting style greatly improved my technical writing skills.

I also would like to thank all of the ECSE staff, in particular the workshop staff, for their support and insightful advice on various design techniques. My sincere appreciation goes to the office and administration staff for ensuring the countless forms and paperwork were correctly completed and filed.

I wish to thank all of my fellow students, in particular Sophia Kaplantzis, Iris Yan, Summer Li, Sorrell Grogan and Dinesh Segaran, mainly for providing distractions from my work, but also for their help with mathematical concepts, software packages such as Matlab and LaTeX, and for generally acting as sounding boards for my ideas.

Lastly, and most importantly, I wish to thank my parents and brothers for their continued love and support. Without their support and encouragement, this thesis would not have been possible.

Contents

List of Figures

List of Tables

List of Acronyms

ADC	Analog to Digital Converter
AHDWL	Anchor Hop Distance Weighted Localisation
AoA	Angle Of Arrival
APIT	A Point In a Triangle
BER	Bit Error Rate
BPF	Band Pass Filter
CTS	Clear To Send
DMAC	Directional Media Access Control
DV	Distance Vector
EWMA	Exponentially Weighted Moving Average
GCC	GNU C Compiler
GNAT	Georgia Tech Network of Autonomous Tasks
GPS	Global Positioning System
IC	Integrated Circuit
ID	Identification
IR	Infrared
JTAG	Joint Test Action Group (IEEE 1149.1)
LED	Light Emitting Diode
LoS	Line of Sight
LPR	Local Positioning RADAR
MAC	Media Access Control
ML	Maximum Likelihood
MMSE	Minimum Mean Square Estimation
PD	Photo Diode
PCB	Printed Circuit Board
PWM	Pulse Width Modulation
RADAR	Radio Detection and Ranging
RF	Radio Frequency
RLS	Recursive Least Squares
ROCRSSI	Ring Overlapping based on Comparison of RSSI
RSS	Received Signal Strength
RSSI	Received Signal Strength Indicator
RToF	Round Time of Flight

RTOS	Real Time Operating System
RTS	Request To Send
RTT	Round Trip Time
TDOA	Time Difference Of Arrival
TDOF	Time Difference Of Flight
TOA	Time Of Arrival
WSN	Wireless Sensor Network

List of Symbols

$(\hat{x}_i, \hat{y}_i)$	Current position estimate of node i
$\|i - j\|$	Euclidean distance between nodes i and j
ϕ_{ij}	Relative bearing to node j from node i
Δ_{ijk}	Clockwise angle formed between nodes i and k at node j
d_i	Anchor hop distance of node i
w_i	Weighting applied to sample i
φ_i	Angle of IR receiver module i relative to the node's local $0°$ bearing

Chapter 1

Introduction

1.1 Background and Motivation

Infrared and visible light communication systems are being developed to provide high speed data connectivity for indoor wireless communication applications, such as high speed internet to portable devices (Figure 1.1). The line of sight requirement of optical communication systems increase overall network capacity while also reducing the risks of eavesdropping and interference from outside sources.

Optical communication systems also have an exciting potential to be used in aquatic environments due to the fact clean water provides reasonably low attenuation of visible and near-visible light. Festo [Fes] have created the "Aquajelly", an underwater device capable of swimming like a jellyfish. The Aquajellies are able to communicate with each other underwater using infrared channels to share information.

In such networks, localisation allows nodes to discover their relative position, and in many cases their position within the world. Position information is vital for many applications such as monitoring and tracking[ZG04], geographical
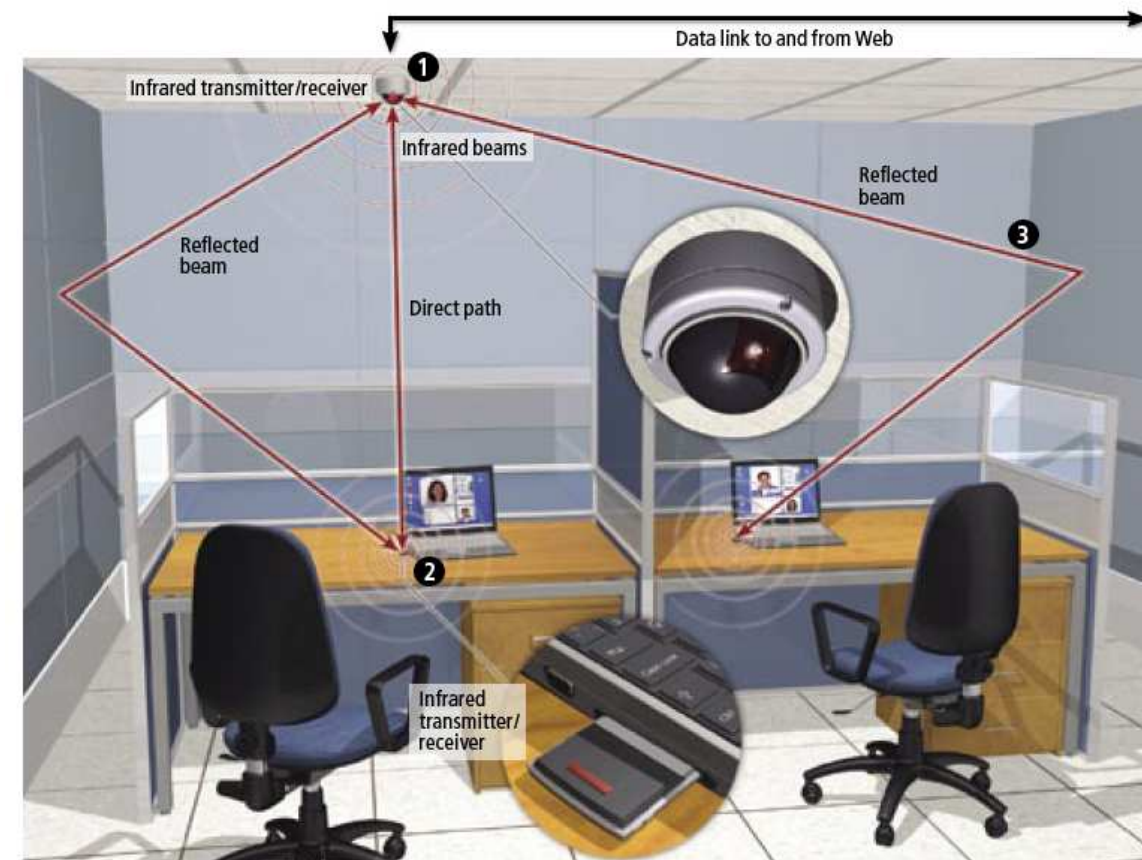
Figure 1.1: An indoor optical wireless network application example for providing broadband communication capability to individual devices [Kav07].

addressing and routing [Sto02] and topology control [GZT+05]. Position information becomes even more critical in mobile networks, where nodes must be able to determine their location and the location of neighbours in order to intelligently interact with one another.

1.2 Basic Concepts

Optical components are typically available in narrow beam-width configurations, allowing easy and cost effective directional communication links to be developed

using only off-the-shelf, consumer grade, components. Directional communication links provide higher network capacity as a greater number of data packets can be transmitted simultaneously without interfering with one another. Also, as most of the transmission power is directed towards the intended recipient, it reduces the energy consumption, thus increasing the life span of battery operated devices.

Directional optical transmissions allow nodes to estimate the relative angular position of the neighbouring nodes. This information, along with the application of basic geometric principles, can be used to calculate position estimates leading to localisation of the entire network.

Localisation in networks of devices can be broken into two broad categories: range-based, and range-free. Range-based systems rely on nodes measuring distances or angle to neighbouring nodes in order to calculate a position estimate. Whereas range-free techniques do not require the nodes to measure any distances or angles. Both categories are discussed in detail in Chapter 2. This project exploits the advantages offered by the physical properties of the pulsed infrared light transmission to create a range-based localisation system based on estimation of the relative angular location of the transmission sources.

Range-based localisation systems can usually be broken into three distinct stages:

1. Angle/distance estimation (Figure 1.2),

2. position calculation, and

3. localisation algorithm.

Figure 1.2 shows the interaction between each stage. Initially nodes measure the distance or angle to neighbouring nodes. These measurements are then combined with the application of basic geometric principles to develop a position
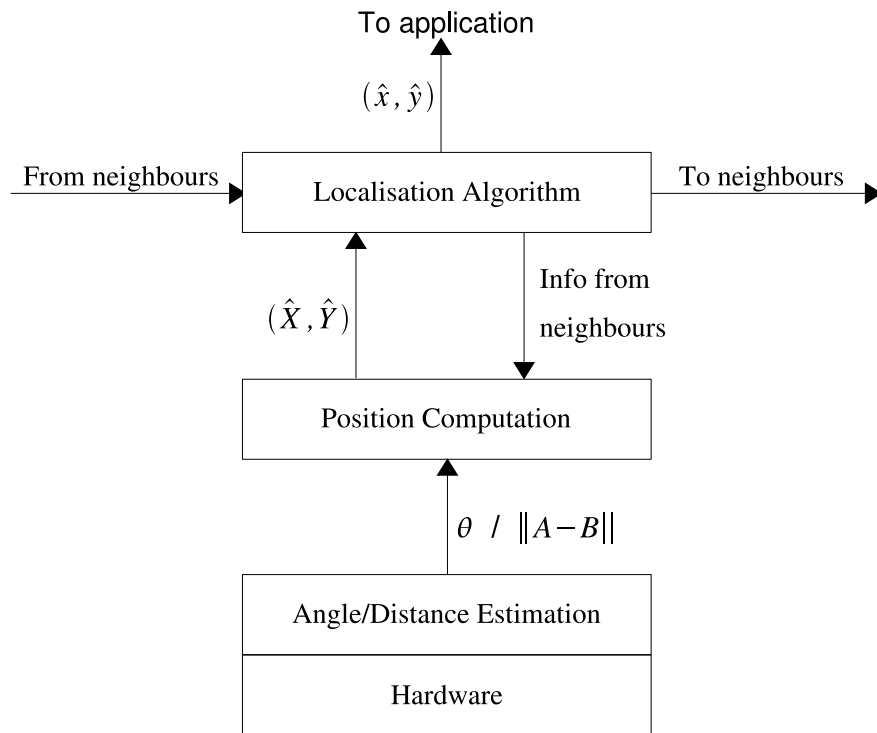
Figure 1.2: Components of a typical localisation system. A node calculates an instantaneous estimate of its position $(\hat{X}, \hat{Y})$ and the localisation algorithm improves the accuracy of this position estimate over time using various methods to give $(\hat{x}, \hat{y})$.
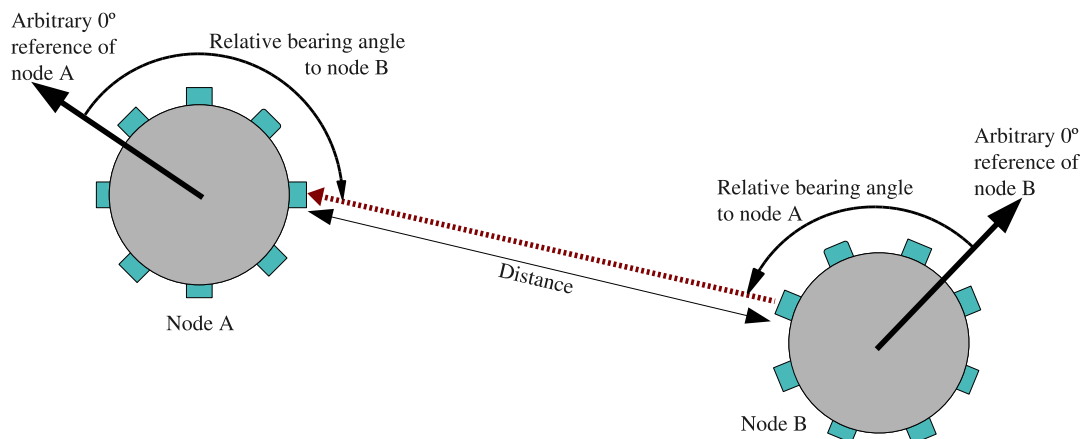
Figure 1.3: Range-based localisation systems rely on distance or angle estimation to compute a position estimate.

estimate. Once a position estimate is calculated, it is passed to the localisation algorithm. The localisation algorithm is responsible for sharing position estimates with neighbouring nodes and combining the measured data with the information obtained from the neighbouring nodes, in order to develop a more accurate position estimate. The localisation algorithm is also designed to ensure that as many nodes as possible are able to localise themselves accurately.

1.3 Critical Issues and Research Aims

This project aims to develop a testbed and localisation system for networks with directional infrared communication links without explicit received signal strength indicators. The localisation system will consist of angle estimation using the directional infrared communication channels, standard geometric principles for the position estimation and a novel localisation algorithm based on an exponentially weighted moving average (EWMA) filter with weighting coefficients based on anchor hop distance to mitigate the propagation of position errors.

In many networks there are a limited number of anchor nodes which independently know their position, either having it preprogrammed or from an external localisation system such as the Global Positioning System (GPS) [Dal93]. Ideally all nodes in the network should have this property. However, preprogramming position information becomes prohibitively complex for large networks and the use of external localisation systems becomes expensive and requires more complex hardware and larger batteries, which is typically undesirable in large networks consisting of a large number of nodes.

In localisation systems where only a small number of nodes are anchor nodes and the rest must rely on their immediate neighbours for localisation information, there is a very real possibility of an accumulation of position errors. Obviously in

5

all localisation systems the accuracy of the position estimates is important, but in iterative localisation systems where nodes rely on neighbours, it is more critical as any errors will be propagated across the network and affect the accuracy of the position estimates of all nodes. Therefore the suppression of position errors at each hop is critical to ensure the accurate localisation of all nodes in the network.

To determine the suitability of directional infrared channels without explicit received signal strength measurements, detailed channel characteristics will be measured for a number of components to determine the expected channel quality and variability across a sample of components. This will be used for the angle estimation, which will form the bases of the position estimation and localisation algorithms.

1.4 Thesis Overview and Contributions

This thesis first presents a review of existing localisation techniques for ad hoc networks, along with a summary and comparison of existing testbeds in Chapter 2. The custom designed testbed with directional infrared channels is described in Chapter 3, along with the results of the angle estimation method. The proposed anchor hop distance weighting localisation (AHDWL) algorithm for mitigating the effect of error propagation in multihop localisation schemes is described in Chapter 4, and comparative results of its performance over a variety of wireless sensor network topologies presented in Chapter 4. Finally, concluding remarks and future research directions are discussed in Chapter 5.

Chapter 2

Localisation Techniques For Wireless Ad Hoc Networks

2.1 Introduction

Localisation techniques for wireless ad hoc networks can be split into two families:

- **Range-based** techniques rely on nodes measuring distances or angles to reference nodes.

- **Range-free** techniques do not require nodes to measure distances or angles to reference nodes.

The families of localisation algorithms are shown in Figure 2.1 [EH07]. Range-based techniques rely directly on measured distances, and do not have specific topology requirements beyond basic geometric constraints (eg, nodes must not be colinear (i.e., the angles between each of the nodes must be greater than $0°$)). Conversely, range-free techniques do not require the nodes to measure distances or angles to neighbours, and instead rely only on connectivity as the basis for

Localisation

Range Based   Range Free

Distance   Angle   Area   Hop Count
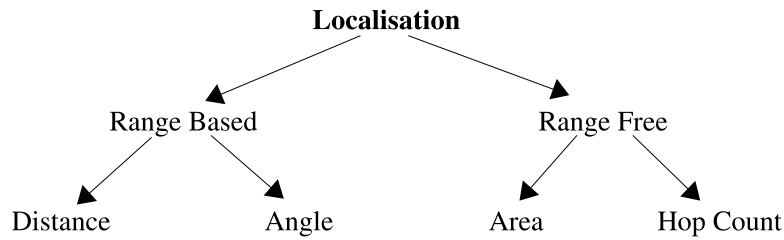
Figure 2.1: Categories of localisation algorithms.

determining their position within the network. This reduces the hardware requirements of the nodes, and eliminates the possibility of measurement errors as no direct measurements are taken by the nodes. However, many of the range-free algorithms have certain topological requirements [EH07] for the network which must be fulfilled to ensure accurate localisation estimates. Range-free techniques can be further broken down into two groups. Area based localisation [WX07] which works with areas to determine the most likely area a node is located in. Whereas hop count based approaches count the number of hops to anchor nodes, which is then used to estimate distances to each of the anchor nodes, from which a position estimate can be calculated [HHB+05].

This chapter reviews the range and angle measurement techniques, and position estimation methods based on trilateration and triangulation, followed by an extensive comparative review of both range-based and range-free localisation algorithms. A comparison of existing wireless testbeds with localisation capabilities is also presented.

2.2 Challenges of Distributed Localisation in Wireless Ad Hoc Networks

Localisation in wireless ad hoc networks suffers from many challenges which are not encountered in traditional localisation techniques. A major limitation of

wireless ad hoc networks is the limited transmission range of the nodes due to the low energy and long lifespan requirements of the nodes [ASSC02]. It is therefore not typically possible to receive position information directly from the anchor nodes (i.e., nodes with a priori position information). Instead, the localisation information (usually in the form of position information) will traverse a multi-hop path where each hop along the path will typically introduce small position errors caused by measurement errors when calculating its own position estimate. In multi-hop localisation, errors begin to accumulate and propagate throughout the network as nodes rely on nodes with inaccurate position estimates to calculate their own estimates, and this eventually renders the position estimates unreliable as they are overshadowed by errors and uncertainty.

Ubiquitous localisation systems such as GPS [Dal93] exist which can provide position information anywhere on the planet. However, GPS style systems are not suitable for a majority of wireless ad hoc network applications due to the power requirements, cost and/or form factor of the receiver circuitry and/or antenna [BHE00, CHH01]. GPS type systems are referred to as 1-hop localisation systems as the receiving node is within the direct transmission range of the landmark (i.e., the GPS satellites). Large scale networks with many simplistic nodes give rise to the multi-hop class of localisation algorithms [Nic04], where nodes are no longer in direct contact with anchor nodes, and must instead rely on intermediate nodes to propagate localisation information across the network.

WSN type networks usually consist of a large number of nodes which may be prone to failures, with relatively low speed and short range communication links that cover a wide geographical area [VCdSdM03, CCL03]. In WSN type networks it is preferred that all algorithms are decentralised and distributed to help distribute the load evenly across the network to reduce the required communications between nodes, reduce potential performance bottlenecks and eliminate

single points of failures. Localisation algorithms for such networks should also be distributed [LR03], and therefore no global map of the network can be made. Due to memory limitations, each node can only retain information about a limited number of nodes, typically no more than its immediate neighbours.

2.3 Measurement Techniques for Range-Based Localisation

Range-based localisation schemes begin by estimating either the distance or relative bearing to neighbours, which are then used, along with geometric position estimation algorithms, to estimate a node's position. Position estimates can either be represented in an arbitrary coordinate system such that each node has its own unique coordinate system, or in an absolute coordinate system where all nodes share the same coordinate system, similar to the information obtained from a GPS receiver.

The underlying geometric principles used in range-based systems such as triangulation and trilateration are relatively simple and intuitive [ECC03, TR05]. The majority of research efforts have been concentrated on improving the accuracy of measurement techniques or noise mitigation to estimate a node's position in the presence of errors in range and angle measurements.

In this section, reference nodes are defined as remote nodes which know their position, either from being initialised at a known location (i.e., anchor nodes) or from previously estimating their position. These nodes can be thought of as landmarks which other nodes within the network use to calculate their own position estimates.

2.3.1 Range Estimation

Range estimation techniques involve finding the distance to reference nodes to determine a node's current position relative to the reference nodes. There are a number of range estimation methods. They all have the same underlying requirement of being able to determine distances to at least three reference nodes in order to unambiguously determine their position in two dimensions. If the distance to only one reference point is available the location can be resolved to any point on a circle, if the distance to two reference points is known the two circles will typically intersect at two points (possible locations), a third distance measurement is required to determine the position uniquely in two dimensions. The situation can be described as an intersection of three circles with known radii where the node with an unknown position (x_A, y_A) can be determined by solving the following system of quadratic equations [TR05] (referred to as trilateration, Figure 2.3.1)

$$
\begin{aligned}
R_1^2 &= (x_A - x_1)^2 + (y_A - y_1)^2, \\
R_2^2 &= (x_A - x_2)^2 + (y_A - y_2)^2, \\
R_3^2 &= (x_A - x_3)^2 + (y_A - y_3)^2.
\end{aligned}
\qquad (2.3.1)
$$

A commonly used range estimation method is based on the measurement of the received signal strength (RSS) of the incoming signals to estimate the distance the signal travelled through the models of signal propagation, and the expected attenuation. Signal propagation and attenuation models may be determined analytically or via experimentation. RSS measurements are available on many RF devices [SKOM06, FKZL03] therefore there is typically minimal additional hardware requirements to implement RSS based range estimation. The distance estimation quality in RSS systems is heavily dependant on the model used, which should take into account multipath fading and shadowing [Feh95] that dominate
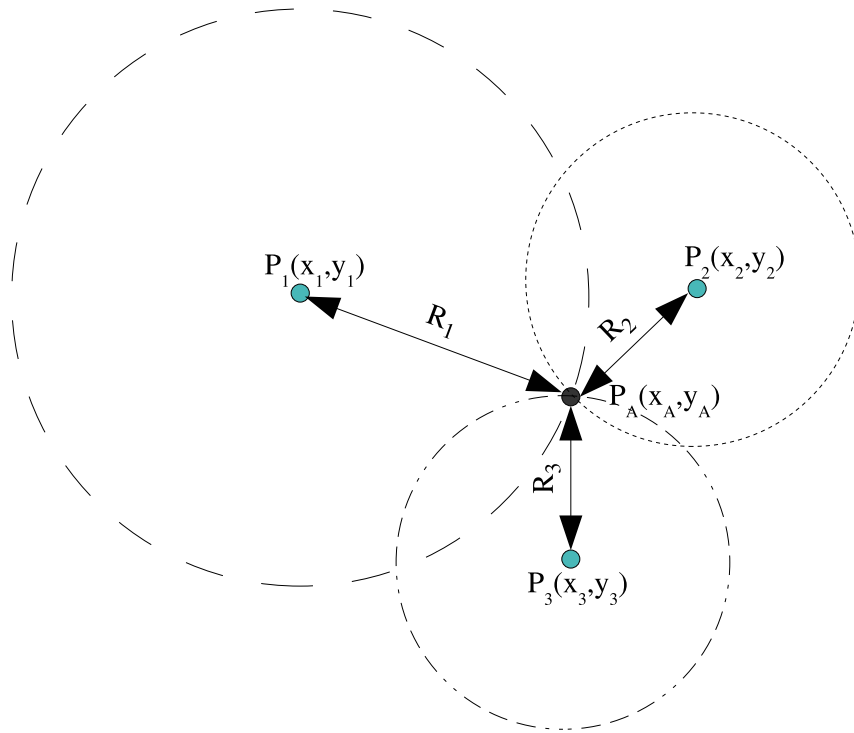
Figure 2.2: Position calculation using trilateration.

at short distances [BHE00], and makes it unreliable for short range distance estimation. Differences in signal attenuation in different media, or due to environmental effects (such as precipitation) and differences in components [ZHKS04] also affect the ability to accurately determine distance from RSS alone. These properties are typically different for each location and time varying. This greatly affects the ability to use RSS to accurately measure distances without good radio propagation models based on the antenna systems being used, such as the work presented in [SWH06] related to the antennas on the Crossbow MICA Mote [Cro] modules.

Algorithms such as [KKK07] aim to overcome these problems, by allowing nodes to dynamically calibrate their RSS systems autonomously. If RSS is not directly available from the module, bit error rate(BER) can be used as an indicator of signal quality, and hence, can be used to estimate the attenuation of the signal resulting in a pseudo-RSSI measurement [VWG$^+$03, KH06b]. The lower the BER

Medium	Propagation Speed	1/Propagation Speed
Light/RF	300×10^6 m/s	3.33 ns/m
Sound	340 m/s	2.94 ms/m

Table 2.1: Approximate propagation speed of light vs sound

the better the channel characteristics, and the lower the signal attenuation for a given power level.

Another family of ranging techniques is based on the assumption that the communication channel usually has a known propagation velocity. This knowledge can be used to construct ranging systems in a number of different ways. If the nodes employ a communication system which operate at only one propagation velocity, methods such as Time Of Arrival (TOA), Time Difference Of Arrival (TDOA) or Round Trip Of Flight (RTOF) [PLY$^+$00] can be implemented.

If the system uses at least two different media with known propagation speeds (such as light and sound), other methods such as Time Difference Of Flight (TDOF) can be used, which exploits the difference in the propagation speeds of the communication media, to estimate the distance between the transmitter and receiver, based on the time difference of arrival of two or more messages sent using the separate media.

TOA and TDOA can be used to estimate distance based on the one way flight of the signal. TOA relies on the propagation time of the signal to a node with a known position, if TOA distance estimates to three or more unique reference nodes are available, then classical trilateration techniques can be used to calculate a position estimate. The TOA method requires tight time synchronisation between all of the nodes, as the precise time that the message was sent must be known, in order to determine the time of flight. The tight time synchronisation requirement of TOA can be eliminated by using RTOF which works like RADAR. In
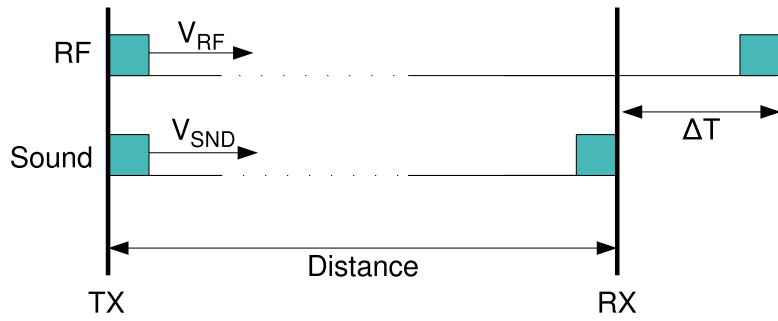
Figure 2.3: Time difference of flight method.

RTOF, a node sends a message which is echoed by the remote node, the message therefore encounters a total round trip distance of twice the distance between the two nodes. However, RTOF requires the processing delay in the remote node to be known, as this has to be subtracted from the RTT observed. Systems such as Local-Positioning Radar (LPR) [VWG⁺03] overcome this by using a modulated reflector on the remote nodes, such that no processing needs to be done on remote nodes, which in turn eliminates processing delays in the remote node.

Systems consisting of two or more communication media with different propagation speeds, such as RF and ultrasound, allow methods such as TDOF (Figure 2.3.1) to be used. TDOF measures the time difference between the arrival of two different mediums to determine the distance travelled. Table 2.1 lists the approximate propagation speed of light vs sound. As light travels almost 1,000,000 times faster than sound, it allows for the time difference of arrival between light and sound to be easily measured using relatively simple hardware with limited timing resolution. The propagation delay for each medium is given by,

$$T_{\text{RF}} = \frac{d}{V_{\text{RF}}}, \tag{2.3.2}$$

$$T_{\text{SND}} = \frac{d}{V_{\text{SND}}}. \tag{2.3.3}$$

Where d is the distance between the transmitter and receiver. Therefore the time

difference between the arrival of each of the signals is,

$$\Delta_T = T_{\text{SND}} - T_{\text{RF}}, \tag{2.3.4}$$

$$\Delta_T = d\left(\frac{1}{V_{\text{SND}}} - \frac{1}{V_{\text{RF}}}\right). \tag{2.3.5}$$

Rearranging Equation (2.3.5) gives distance in terms of time difference of arrival as,

$$d = \frac{\Delta_T}{\left(\frac{1}{V_{\text{SND}}} - \frac{1}{V_{\text{RF}}}\right)}. \tag{2.3.6}$$

2.3.2 Angle Estimation

Angle estimation, such as the angle of arrival (AoA) technique [RS06] (Figure 2.4a), can be achieved through the use of directional antennas, where the transmission and/or reception elements are designed to operate in a relative narrow beam, or have characteristics which allow directional transmission, or angle of arrival to be determined. In RF systems, directional antennas can be implemented in a number of ways, such as switched beam antennas or, the more advanced, adaptive antenna arrays [JCLR99, Pat00]. In optical communication links, such as infrared, directional communication systems are realisable due to the availability of narrow beam width optoelectronic devices, such as narrow beam LEDs and lasers, or by placing a lens to focus the beam. By placing a number of components in different directions it is possible to create a directional optical network which allows full $360°$ coverage. Therefore it is possible to use angle estimation techniques where only the transmit or receive antennas are directional.

The angle of arrival (AoA) scenario, presented in Figure 2.4(a), shows that to localise a point (X) correctly there must be a minimum of two remote nodes (A and B), any further nodes (C) should result in the same point. However, due to

(a) Angle of arrival   (b) Angle of transmission
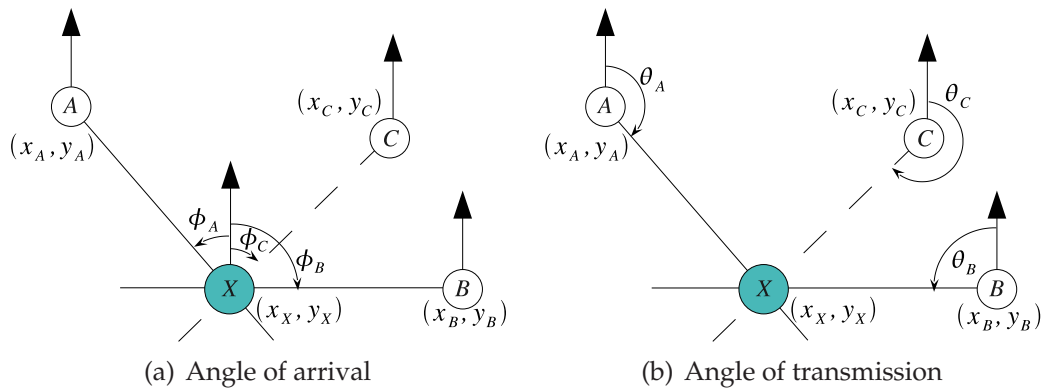
Figure 2.4: Angle-based localisation.
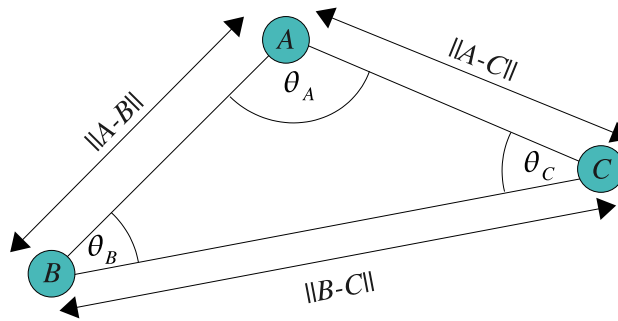
Figure 2.5: Triangulation systems can be reduced to trilateration problems if sufficient information is available.

errors in angle measurement, there will be uncertainty in the point. The accuracy of AoA in static networks can be increased by using filtering or averaging across many individual samples [RS03]. The methods presented in Figure 2.4 require all nodes to have a common bearing. Nodes can unify their bearings by utilising a bearing propagation algorithm, such as the one presented in [CHH01]. Another option is to require nodes to form triangles, such as shown in Figure 2.5, which eliminate the unified bearing requirement of the nodes.

Angle based systems can be reduced to trilateration systems [TR05] (if sufficient information is known) by calculating the distances to neighbours based on the measured angles and some distance information. For example, consider a triangle (Figure 2.5) with 2 vertices representing nodes with a known position (nodes B and C) and the remaining vertex being the unknown location node (node A).

The length of the edge joining the two nodes whose locations are known can be calculated as the Euclidean distance between the nodes. By combining this with the measured angular information, the Sine Rule

$$\frac{\|A - B\|}{\sin(\theta_C)} = \frac{\|A - C\|}{\sin(\theta_B)} = \frac{\|B - C\|}{\sin(\theta_A)} \tag{2.3.7}$$

can be used to calculate the lengths of the remaining edges of the triangle (assuming all the angles are known). However, this requires all nodes to be within transmission range of each other.

Directional communication links can be used to determine the discrimination angles between nodes relatively easily in ad hoc networks. While directional communication systems can increase the total capacity of the network [Pat00, RRS+05], they present media access control (MAC) issues [CV04, ZWCF06] which are not encountered in traditional omnidirectional systems such as 802.11 [Gas02]. It has been shown that 802.11 RTS/CTS MAC is not effective in ad hoc networks [XGB02], and does not offer effective MAC in directional networks. Schemes such as DMAC [RRS+05] provide MAC schemes designed specifically for directional communication systems.

2.4 Localisation Algorithms for Ad Hoc Networks

Localisation algorithms allow nodes to estimate their position based on information which it learns from its surroundings. Range-free based algorithms do not require any explicit ranging (or angle) information from the node to estimate its position, thus reducing the need for specialised hardware/channel models on each node. Whereas range-based algorithms require nodes to undertake range and/or angle estimation using methods as described in Section 2.3 and form the

basis of many position estimation algorithms.

2.4.1 Range-Free Localisation Algorithms

Range-free algorithms do not rely on explicit ranging or angle information. Instead, they rely on using information about neighbours to infer their positions [HHB+03]. Range-free techniques have the advantage that they do not require additional hardware which are required for obtaining ranging/angle information. However, to compensate for the limited environmental information, there usually are assumptions/restrictions placed on the topology of the network, such as the arrangement of nodes and minimum density requirements of the network to improve the accuracy of position estimations.

It could be argued that the cost saved by designing simpler nodes would allow for a higher density of nodes to be deployed, in which case there is no reason not to deploy a higher density network which could also lead to higher redundancy, or higher sensing resolution in WSN type applications.

One of the most intuitive range-free methods is centroid localisation [BHE00] which relies on the connectivity between nodes to determine proximity to reference nodes. The metric used to determine connectivity between nodes is based on the ratio of sent and received messages. Ideally, the nodes that are connected will receive all sent messages and have a connectivity metric of 100%, although, to account for packet losses a lower threshold is typically set. Nodes which maintain a connectivity metric greater than a defined threshold are deemed to be within range and therefore are used for determining a position estimation. The position estimation is based on the average of the advertised positions of all neighbours which have a connectivity metric greater than the threshold. The node calculates

(a) One triangle   (b) Two triangles   (c) Three triangles
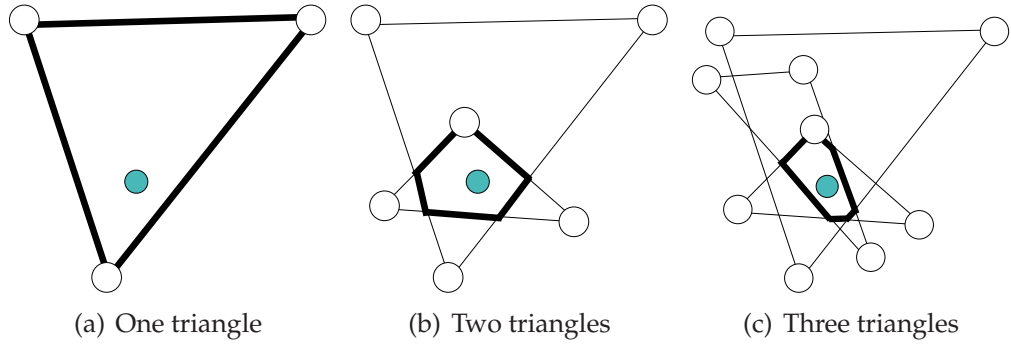
Figure 2.6: APIT localisation refinement.

its position estimation as the average position of all connected neighbours as follows,

$$(X_{\text{est}}, Y_{\text{est}}) = \left(\frac{X_1 + \cdots + X_k}{k}, \frac{Y_1 + \cdots + Y_k}{k} \right), \qquad (2.4.1)$$

where the node has k neighbours, and (X_1, Y_1), (X_2, Y_2) ... (X_k, Y_k) are their advertised positions.

A method similar to centroid localisation, from a conceptual point of view, is the 'A point in a triangle' (APIT) [HHB+05] approach. Instead of taking the average position of neighbouring nodes, triangles which bound the node are formed (Figure 2.6). It is known that (in an error free world at least) that the point will lie at a point which all triangles enclose. A node using the APIT algorithm begins by finding sets of three remote nodes, and determines which sets create a triangle which encloses itself. As shown in Figure 2.6 as the number of triangles increases, the position estimation certainty increases. Obviously, in order to have a large number of enclosing triangles, and hence a higher position accuracy, a relatively high network density is required. This in turn necessitates more nodes to be deployed in a given area. However, the simple hardware requirements of nodes makes the APIT method an attractive localisation option for WSN type networks where node density is typically high.
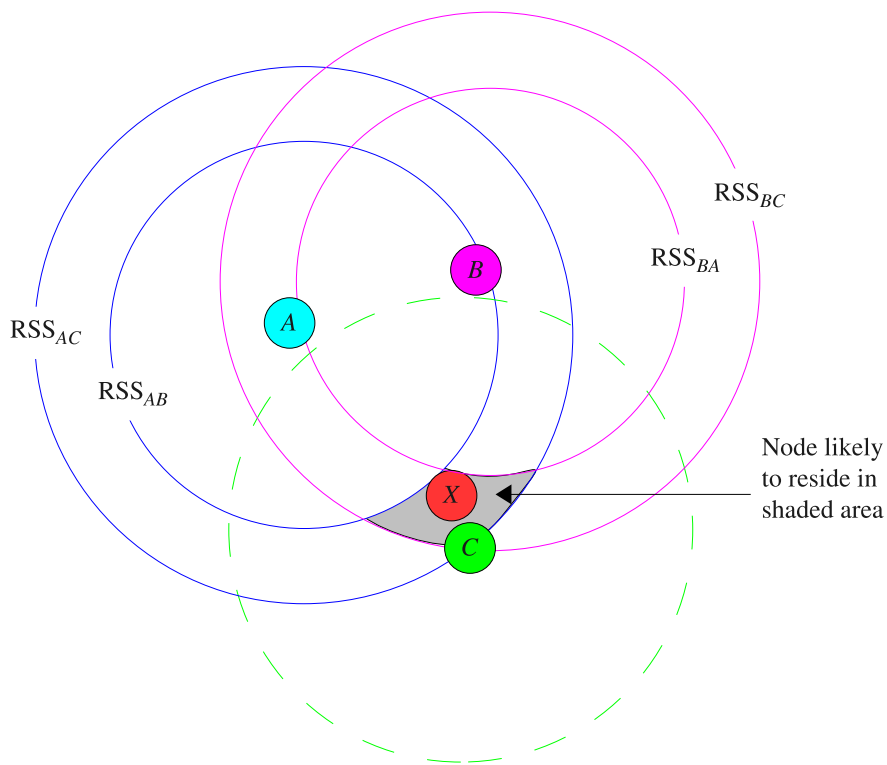
Figure 2.7: Ring overlap based on comparison of RSSI.

Ring overlap based on comparison of received signal strength indicator (RO-CRSSI) method [LWH04] uses differences in RSSI to determine the location of the node. ROCRSSI uses RSSI to find the relative distance between nodes by comparing different signal strengths to determine an area where these signal strengths overlap, the area of overlap indicates the area which the node must be located in. Figure 2.7 shows the basic operation of ROCRSSI where A, B and C are reference nodes. If node X can determine that it is located between RSS_{AB} and RSS_{AC} the likely area where X is located is reduced to a ring around node A. If node X is also known to exist within a similar ring around node B the intersections of these rings narrow the likely location to two smaller areas. If another reference node (Node C) is available this area can be reduced to a single area (shaded area in Figure 2.7)

The APIT, ROCRSSI and centroid approaches are called area based localisation

schemes, as they work with areas to determine the likely position of the nodes. Not all range-free are area based, the DV-Hop family of localisation algorithms rely on hop count between anchor nodes to calculate node position estimations.

DV-Hop localisation [NN03] works by determining the average hop count between anchor pairs, by counting the number of hops between anchor nodes. From this, the average distance per hop can be calculated resulting in a range estimation to the anchor nodes. Once three (or more) range estimations are found, trilateration techniques can be used to estimate the position.

The DV-Distance [NN03] method consists of the same basic underlying technique as DV-Hop, but it uses ranging information to determine the distance between nodes. It then propagates the distance in metres instead of hop count. DV-Distance is less coarse than DV-Hop as it takes into account the variation in distances between nodes. However, as it relies on measured distances, it is sensitive to errors in range estimations.

2.4.2 Range-Based Localisation Algorithms

Range-Based techniques require nodes to directly measure distances and/or angles to reference nodes. Such methods typically require nodes to have additional hardware to measure angles or distances to neighbours, but allow the nodes to more directly estimate their position, without reliance on specific topology constraints, such as higher minimum network connectivity, and isotropic network configurations, as discussed in the previous section.

Range-based localisation can generally be regarded as a two stage process:

1. Measure distance or angles to remote reference nodes,

2. Calculate and update position based on the reported position of neighbours

<div style="text-align:center">(a) Local coordinate system   (b) Global coordinate system</div>
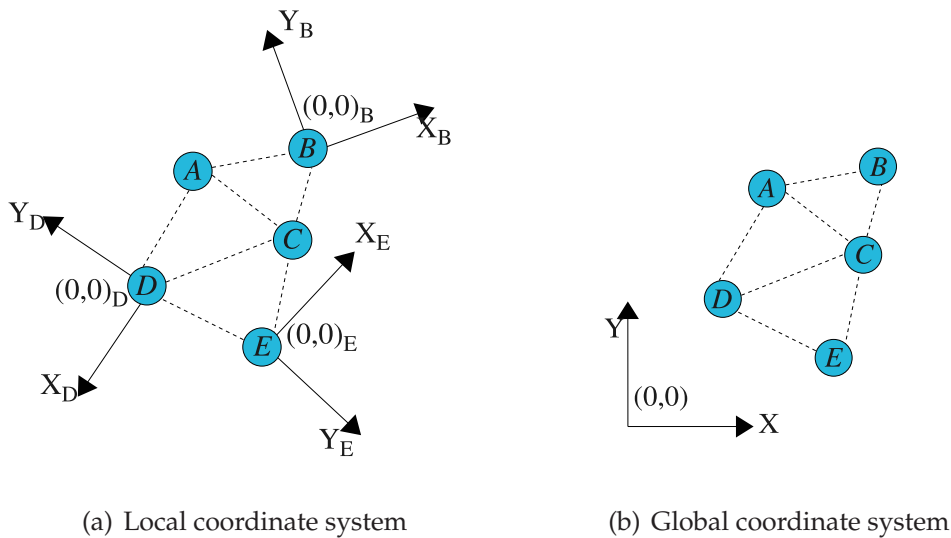
<div style="text-align:center">Figure 2.8: Local vs global coordinate systems.</div>

and distance/angle information.

Most range-based localisation schemes use the same underlying principles for determining position from range/angle measurements such as triangulation [KH06a] or trilateration [TR05]. The algorithms differ in the way in which they aggregate and filter different estimations, as well as how they develop coordinate systems and propagate information to neighbours.

The GPS-free positioning algorithm [CHH01] uses range estimations to neighbours and trigonometry to estimate positions relative to a local coordinate system (Figure 2.8(a)), where each node has its own coordinate system where the node is positioned at (0,0). Nodes have no sense of bearing, and hence, the individual coordinate systems do not necessarily have the same direction or orientation. An algorithm is also presented to allow all nodes in the network to align their local coordinate systems into a unified global coordinate system (Figure 2.8(b)), which allows all nodes to be represented in a single coordinate system with the same direction and orientation, providing a more functional position estimations for each node in the network.

Multilateration

Multilateration algorithms [SHS01] use the principles of trilateration while utilising the position estimates of multiple neighbours. There are many variations of the multilateration algorithm, but they all are based on the same underlying technique of atomic multilateration [SHS01].

Atomic multilateration allows nodes to estimate their position if they are within one hop distance from at least three reference nodes. If four or more reference nodes are within one hop transmission range, the propagation speed of the signal can also be determined. Figure 2.9(a) shows a typical multilateration situation. In this case, node A has four neighbours (B, C, D, E) each of which have a known position. If a time based ranging method is used, the distance R between node i and A can be given by

$$R_{i,A} = st_{iA}. \tag{2.4.2}$$

Where s is the estimated propagation speed of the range measuring medium being used, and t_{iA} is the time it took for the signal to propagate from each neighbouring node i to node A. Therefore, the error $e_i(x_A, y_A, s)$ between the measured and estimated position of node i can be expressed as the difference between the estimated and measured distances as,

$$e_i(x_A, y_A, s) = st_{iA} - \sqrt{(x_i - x_A)^2 + (y_i - y_A)^2}. \tag{2.4.3}$$

If a sufficient number of reference nodes are available, a maximum likelihood (ML) estimate of the position of node A can be obtained by minimising the error terms using a method such as minimum mean square estimation (MMSE) by

23

(a) Atomic multilateration   (b) Two hop multilateration
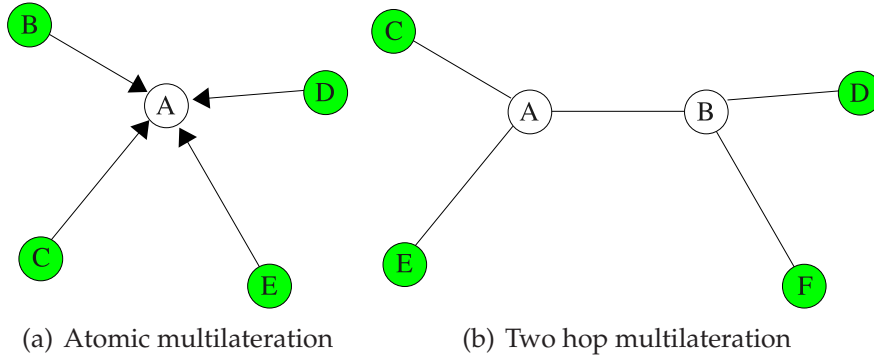
Figure 2.9: Multilateration scenarios.

minimising

$$E\left(x_A, y_A, s\right) = \sum_{i=1}^{N} \alpha^2 f_i \left(x_A, y_A, s\right)^2. \tag{2.4.4}$$

Where α represents a weighting coefficient which is typically set to 1.0 in the case of multilateration [SHS01].

Multilateration techniques can be extended such that the nodes no longer need to be within one-hop of a reference node. Due to geometric constraints, nodes must be within one-hop of at least three other reference nodes to receive an unambiguous position estimate. However, n-hop multilateration [SPS03] allows nodes to use non-reference nodes to assist in localisation. Consider the example illustrated in Figure 2.9(b), two nodes A and B each have three one-hop neighbours. However, each only have two reference nodes within one-hop distance, but they both have four neighbours within two-hop distance, this allows n-hop multilateration to be used. The n-hop multilateration method uses the same principles as atomic multilateration. The difference between the calculated and measured distances can be found, and the residuals minimised, through the use of a least squares method [ABKR07] or a Kalman filter [WB].

In ad hoc networks, iterative multilateration [SHS01] can be used to obtain position estimates of each node within the network, even if there are only a limited

number of anchor nodes. Iterative multilateration can be implemented in a number of ways in ad hoc networks. The first is to simply use atomic multilateration at each node in the network. As time passes, a larger number of nodes can estimate position based on neighbours, who have calculated their own estimates, and then become a reference nodes for other nodes. Iterative multilateration can also be implemented as a centralised algorithm or in clusters, depending on the structure and requirements of the network.

Iterative multilateration relies on ordinary nodes becoming reference nodes after estimating their own position, the estimate at each hop may introduce errors, giving rise to the possibility for errors to propagate and accumulate across the network [SHS01].

2.5 A Comparative Evaluation of Localisation Techniques

Localisation techniques are largely dependant on the capabilities of the nodes, desired accuracy and control over the topology of the network. If nodes are capable of range or angle estimation, one of the range-based algorithms can be used. These algorithms are not highly dependant on network topology, however, such methods are affected by measurement errors at each hop. On the other hand, if nodes are simplistic in design without explicit range or angle estimation capabilities, range-free algorithms still allow nodes to determine their position.

The operating environment and maximum distance between nodes will influence which communication and localisation medium to use. For instance, infrared and ultrasonic transmissions are obscured by walls, making them unusable where

nodes do not have direct line of sight to one another. For TDOF implementations the range and operating environment must be within the working values of both medium otherwise one medium will not be received, and hence, no time difference can be calculated.

Systems such as TOA and TDOA rely on tight time synchronisation between nodes [VWG$^+$03]. On the other hand TDOF, RTOF and AoA do not require any time synchronisation between nodes, thus saving the complexity of time synchronisation and time keeping of nodes. However, if nodes within a network are synchronised sufficiently, TOA and TDOA provide localisation information based on only one communication medium.

Range estimates based on RSS methods typically rely on idealistic propagation models for estimating distance from RSSI information, however, in real life, affects of multipath and shadowing [Feh95] will greatly affect the ability to estimate distance from RSS alone. As BER is usually related to RSS [VWG$^+$03], it may face the same problem as range estimation with RSSI, however with sufficiently complete realistic models, relatively accurate range estimations can be achieved. It has been found by Savvides et al. [SHS01], that using TDOF with RF and ultrasound was more reliable than RSSI, however TDOF requires extra timing abilities, whereas RSSI may be easier to directly obtain from demodulator circuitry, but typically requires at least an additional analog to digital converter.

If nodes are not capable of determining distance or angles to neighbours they must rely on range-free techniques for localisation. However, range-free techniques typically require either, higher node density, or specific network topology properties, which must be considered when choosing an appropriate localisation method to provide accurate position estimates.

Family	Advantages	Disadvantages	Methods
Range-based - Distance	Distance estimate can be formed from relatively cheap hardware	Accuracy dependant on method, models and environmental factors or tight time synchronisation	RSSI, TOA, TDOF, TDOA, RTOF
Range-based - Angle	Can be implemented using directional antennas, easy in optical domain.	Directional RF systems may be complicated	AoA
Range-free - Area	Requires no additional hardware	Requires relatively high node density	ROCRSSI, APIT
Range-free - Hop count	No additional hardware, lower node density than area based methods	Accuracy is usually dependant on network topologies	DV-HOP

Table 2.2: Comparison of families of localisation methods.

Choosing coordinate systems for position estimates must take into account the intended application of the localisation information. Local coordinate systems provide each node with a view of their neighbours, but do not fully describe a node's location within the context of the entire network. Global coordinate systems provide each node with a position estimate relative to a globally defined point within the network. Global coordinate systems require additional algorithms to ensure nodes have a unified, consistent and accurate view of the world.

2.6 Research Testbeds

Many researchers around the world have developed testbeds for localisation and team based algorithms. There is no universal standard testbed as each research group focuses on different techniques with different requirements. Amongst the testbeds, there are some common themes and groupings. One of the most basic grouping is mobile and static networks (i.e. do the nodes have the ability

to move or not). Another grouping that can be easily categorised, is that of the communications medium (e.g. radio/infrared/ultrasound). Both mobility and communication medium play an important role in determining the design of the localisation system. For the purposes of this work, we will only consider static networks, and therefore, will focus on the communication medium being used by the nodes.

2.6.1 Radio Based Testbeds

Radio frequency (RF) based implementations generally use unlicensed frequencies in the industrial, scientific and medical (ISM) band in order to take advantage of pre-built, readily available modules and to avoid spectrum licensing requirements. Due to the unlicensed nature, ISM band devices may be subject to interference by other ISM users. However, intelligent channel coding, along with error detection and correction, can help to reduce the effect of such problems.

The Milibot [NSGPK02] team consists of a heterogeneous network of small nodes which communicate using RF and is primarily used for mapping and exploring work. Localisation in the Milibot environment is achieved using TDOF with RF and ultrasound. RF based communications usually lends itself to inter-room communications as it will typically penetrate walls, however the secondary localisation medium, ultrasound in this case, will require nodes to be within line of sight (LoS) of one another in order for localisation to take place.

2.6.2 Optical and Infrared Based Testbeds

Optical and infrared based systems use light type communication systems which all have similar properties to visible light, in terms of absorption and reflection. As optical/IR channels will not easily pass through walls it reduces interference

from outside sources. However, the sun emits IR radiation, as do some fluorescent tubes, which may emit modulated IR radiation, which can be a major source of interference for indoors IR based networks. These sources of interference must be taken into account to ensure effective communication and localisation.

Many IR based testbeds for localisation have been designed and constructed by researchers around the world. The Pushpin [LBP05] network consists of small non-mobile nodes inserted into a foam type substrate, which provides power to the nodes. Pushpin nodes communicate with their neighbours using four IR transceivers placed $90°$ apart. Localisation in the Pushpin network has been demonstrated [BLP06] using TDOF with a flash bulb and ultrasonic transmitters to allow nodes to find their distance to the "pinger".

Localisation techniques which rely solely on IR tend to be primarily angle based, which is usually achieved by placing many IR receivers and transmitters around the node then determining the angle to neighbours based on which receiver/transmitter was involved, along with the components angular position on the board. Researchers at the University of Washington developed an infrared communication and localisation system [HMB05], which consists of 8 IR transmitters and 7 IR receivers, placed evenly around the perimeter of a circular PCB. The received bits are sampled, using an ADC, to determine the RSS. The angle of arrival is then determined using a centroid approach based on the measured RSS and the angular position of the receiver θ_i of the incoming signal as follows:

$$C_\theta = \frac{\sum_i \mathrm{RSSI}_i \times \theta_i}{\sum_i \mathrm{RSSI_i}}. \qquad (2.6.1)$$

The localisation system of the Moorebot [Mar04] also estimates the angle of arrival using a ring of IR components (12 IR LEDs and 4 receivers), along with the RSS information from the demodulator IC. The RSS is used to estimate distance

to neighbouring nodes and along with the $90°$ spacing of the receivers allows the angle of the signal, and hence angle to neighbours, to be calculated.

The GNATS [OWB04] network consists of static IR based nodes which run a distributed distance vector path planning algorithm to guide a mobile node to a location via the shortest path. The IR receiver modules used on the GNATs testbed do not have explicit RSSI information available. Therefore, the GNATs project investigated the possibility of using pulse width/loss measurements to estimate RSS as the basis of a trilateration localisation system. However, localisation does not appear to have been implemented in the actual network.

2.6.3 Summary of Existing Testbeds

Table 2.3 summarises the key functionalities and localisation systems used on each testbed. It can be seen that there has been much research effort spent on creating physical testbeds for wireless ad hoc networks. However, each testbed was designed for a particular purpose/environment, and there is no single testbed which is suited to all applications. While the testbeds reviewed are all well designed, none fully suit the requirements of this research. Hence, a custom testbed was developed, based largely on the findings and design of existing testbeds.

2.7 Conclusion

In this chapter, a review of existing localisation techniques for large scale ad hoc wireless networks has been presented. The localisation techniques were broken into two broad categories, range-free and range-based. A comparison of each technique was undertaken with an emphasis on improving position estimates in

Testbed	Primary Task	Comms.	Localisation	Other
Milibot [NSGPK02]	Distributed mapping and exploring	Radio	TDOF - Radio + Ultrasound	Heterogeneous mobile network
GNATS [OWB04]	Path planning - Distance vector	Infrared	Infrared angle/distance based possible	Localisation not fully implemented
Pushpin [LBP05]	Experimental testbed	Infrared	TDOF - Light (flash) + Ultrasound	Static network
Moorebot [Mar04]	General purpose	Infrared	AoA + RSSI - Infrared	Mobile testbed
Hoyt [HMB05] - University of Washington	General purpose	Infrared	AoA - Infrared	Add-on to K-Team Khepera II robots [HLM01]

Table 2.3: Summary of existing testbeds.

ad hoc networks for networks with a large number of nodes.

From the review of existing techniques it can be seen that, while there are a number of existing localisation techniques for ad hoc network, there has been little research into methods of mitigating the effect of error propagation in range-based localisation schemes. Methods such as multilateration allow weighting of individual samples which could be used to implement weighting of individual position estimates based on anchor-hop distance to reduce the number of hops which position errors can propagate.

Also, a review of existing wireless ad hoc testbeds with localisation capabilities has been presented. The review study has revealed that there was no universal testbed available for research into localisation in ad hoc networks, and it is common for researchers to design testbeds tailored to their specific requirements. Based on the work of GNATs [OWB04] and the other infrared based testbeds

mentioned, a custom testbed was developed with a view of providing angle esti-
mation using directional infrared channels without the explicit RSSI measured.

Chapter 3

Localisation with Pulsed Infrared Light

3.1 Introduction

In this chapter the findings of the experimental work focusing on quantifying the localisation potential of directional pulsed infrared light channels are presented, as well as the detailed evaluation of estimation of angular direction of received infrared signals.

The location estimations of the nodes are based on the calculation of the relative bearing of neighbours, which are estimated by aggregating the angular direction of the received signals. The results obtained were used to develop the anchor hop distance weighted localisation (AHDWL) algorithm presented in Chapter 4.

3.2 Ad Hoc Network Testbed and Experiments

A small scale experimental ad hoc network testbed was developed that uses pulse infrared light as its communication medium. The testbed was designed as a multi-purpose system, and has capacity to conduct follow-up research studies

<center>(a)   (b)</center>
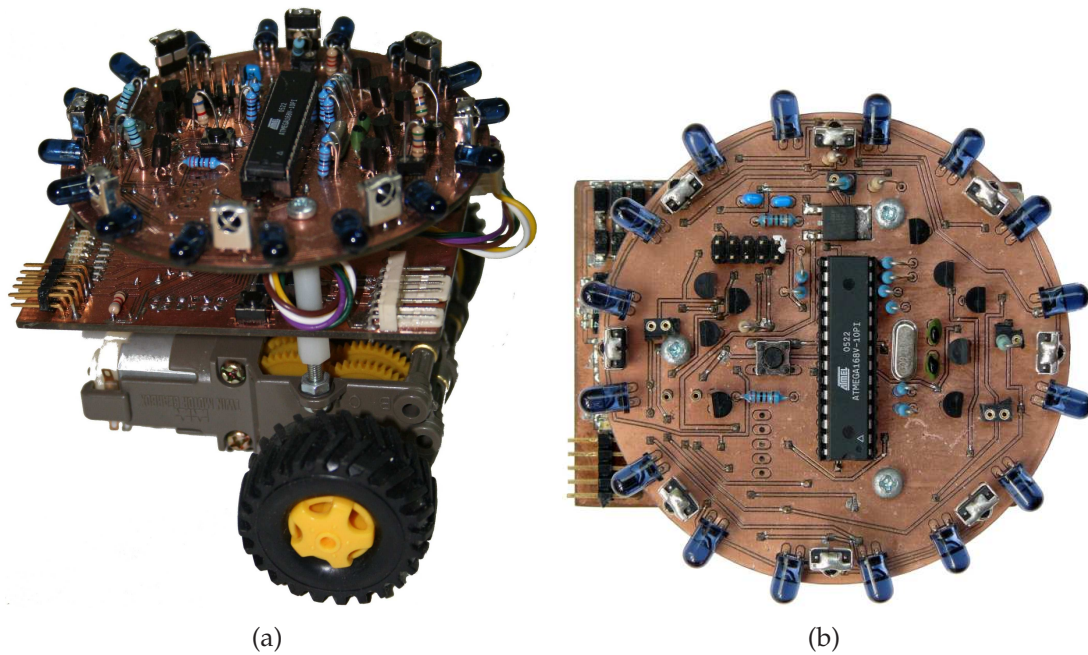
Figure 3.1: One of the wireless ad hoc testbed nodes, and close-up view of the circular communication board containing 16 infrared LED transmitters and 8 receivers.

on various applications which rely on directional antenna arrays, such as directional media access control (MAC) algorithms [RRS+05]. Additionally, mobility support was added so that the testbed could be used to do research on data harvesting [GBBE06], topology control [San05] and self-healing networks [SF04].

Figure 3.1 shows one of the nodes (the hardware overview and detailed circuit diagram can be found in Appendix A). Each node consists of two distinct subsystems: The main processing subsystem which is based on an Atmel ATmega128 microcontroller [Atma] running MicroC/OS-II [Lab02] real time operating system to provide multitasking and programming support such as intertask communication and resource sharing for high level algorithms and functionality. The communication subsystem consists of an Atmel ATmega168 microcontroller [Atmb] running custom designed software written in C to control the IR transmitter and receiver arrays.

<center>**34**</center>

RX ID	Angle	TX ID	Angle	TX ID	Angle
0	0°	a (0)	11.25°	i (8)	191.25°
1	45°	b (1)	33.75°	j (9)	213.75°
2	90°	c (2)	56.25°	k (10)	236.25°
3	135°	d (3)	78.75°	l (11)	258.75°
4	180°	e (4)	101.25°	m (12)	281.25°
5	225°	f (5)	123.75°	n (13)	303.75°
6	270°	g (6)	146.25°	o (14)	326.25°
7	315°	h (7)	168.75°	p (15)	348.75°

Table 3.1: Angular placement of the IR transmitters and receivers.

3.2.1 Overview of the Infrared Communication system

The infrared transmitters and receivers are placed evenly around a circular printed circuit board (Figure 3.1(b), the angular placement of each IR component is listed in Table 3.1).

The BRM-1030 [Bri] is a typical low-cost integrated IR receiver module, and is used for remote control applications requiring low data rates, such as TV remote controls. These types of modules, in general, consist of a five stage system: a photo diode, amplification circuits with automatic gain control, a band pass filter centred around a carrier frequency, an integrator circuit, and a comparator to provide a thresholding function to output a digital signal. Unfortunately, due to the tight integration of these stages within a small package, it is not possible to directly measure the physical properties of the received signal, especially the received signal strength (RSS), as the output of the BRM-1030 is the result of processing by this multi stage system, with unknown gains and nonlinearities.

3.2.2 Infrared Channel Experimental Setup

A series of experiments were conducted to determine how relative angular position of transmitters and receivers, distance between them, and transmission power, affect the quality of the IR channel. The following scheme was devised

to empirically obtain the channel characteristics: transmitter receiver distance, transmission power, and relative angular position of transmitter and receiver were changed systematically. For each configuration, 20 blocks of 30 pulses (600 total) were transmitted and the number of correctly received pulses was recorded (details of the experimental procedure can be found in Appendix B).

The primary aim of the experiments was to quantify how distance, transmit and receive angles, along with transmission power levels influence the communication channel quality without any access to direct measurements of the RSS at the receiver. Additionally, the secondary aim was to find out whether RSS can indirectly be estimated by counting the number of correctly detected pulses at the receiver and calculating the *pulse detection ratio* (the ratio of the number of correctly received and transmitted pulses).

The developers of the GNATs [OWB04] project had a similar approach and investigated the possibility of estimating the RSS via measuring the received pulse width and pulse detection ratio, where only a binary output is available from the receiver modules. However, they have not completed their studies and never reported the outcome of their work.

3.3 Pulse Detection Ratios

3.3.1 Pulse Detection vs Distance

It was found that there is a nonlinear relationship between pulse detection ratios and transmitter-receiver distances for a given power level as shown in Figure 3.2. Not surprisingly, the higher the transmission power, the further the receiver can be from the transmitter while still maintaining a high pulse detection ratio. The sharp fall off in the pulse detection ratio indicates that the channel very abruptly
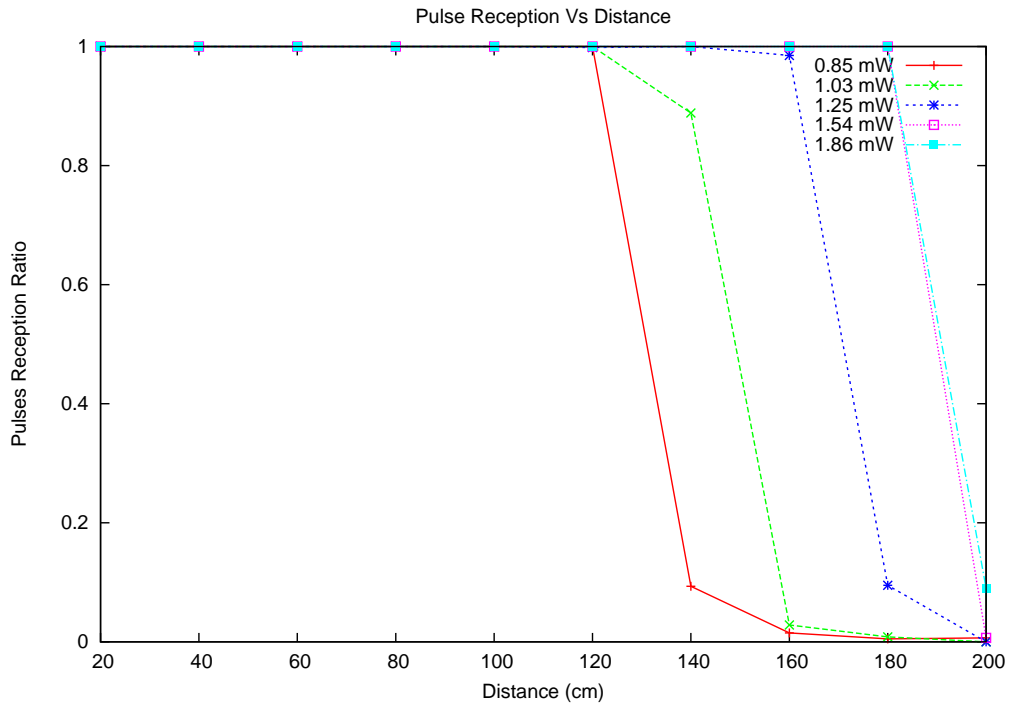
Figure 3.2: Pulse detection ratio vs distance for given transmission powers.

becomes unusable due to extremely high number of pulses becoming undetected (i.e., either all 600 pulses were correctly received, or very few, if any, were received).

The experiments also revealed that the IR modules were most sensitive in darkness, and when subjected to high intensity light (possibly containing IR spectrum components) the sensitivity was reduced, Figure 3.3 illustrates such a case. This was also observed in the GNATs [OWB04] project. Therefore, it was important to perform the experiments without changing the lighting conditions. The experiments showed that as long as there are only minor variations in lighting between measurement points, the IR modules may provide a consistent and usable base for distance based localisation.

However, as the channel quality also intrinsically depends on the angular orientation of the transmitter and receiver for a given distance (see Figures 3.4 and
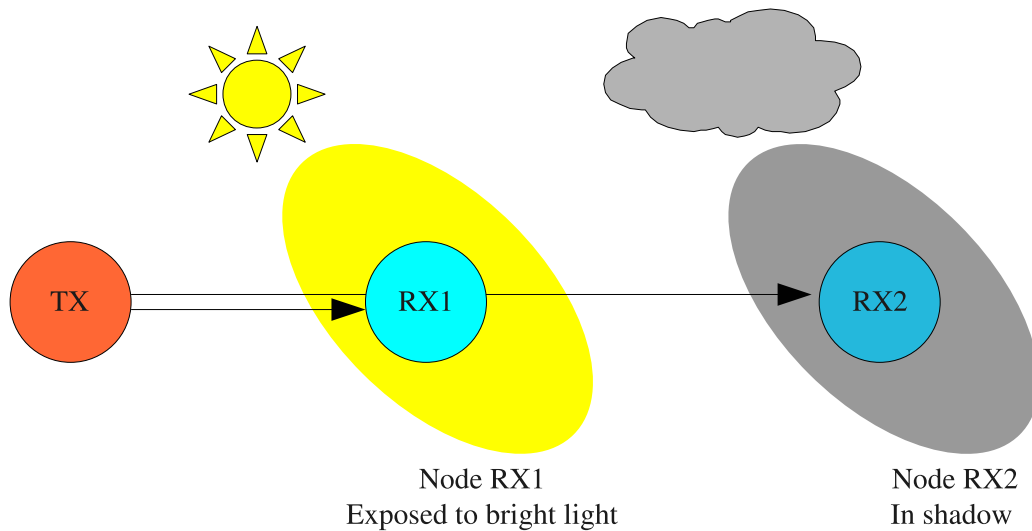
Figure 3.3: Illustration of the detrimental effects of ambient light. Node TX is transmitting a message at different power levels. Ideally RX1 will receive a message at a lower transmission power level than RX2. However, if RX1 is subjected to high intensity ambient light, which reduces its sensitivity. Conversely, RX2 is currently under a shadow (i.e., low external light) and may have improved sensitivity. This results in RX2 requiring less transmit power to communicate to than RX1.

3.5), the transmission and reception angles should be known before attempting to estimate distance based on the IR channel quality alone. This issue complicates the estimation since without first knowing the transmission and reception angles, it is not possible to determine the absolute distance between nodes based on received signal characteristics alone.

3.3.2 Pulse Detection vs Transmission and Reception Angles

Both transmission and reception angle experimental results, shown in Figures 3.5 and 3.4 respectively, appear to correlate well with the specifications provided by the manufacturers of the IR LEDs and receiver modules [Bri], specifically with regard to the transmission intensity and reception sensitivity of the components with respect to angle relative to the components optical axis. Figure 3.4 shows that the transmitter LED intensity falls off significantly between $10°$ and $15°$, with

(a) Distance = 0.20 m

(b) Distance = 0.60 m

(c) Distance = 1.00 m

(d) Distance = 1.40 m

(e) Distance = 1.80 m

(f) Distance = 2.00 m

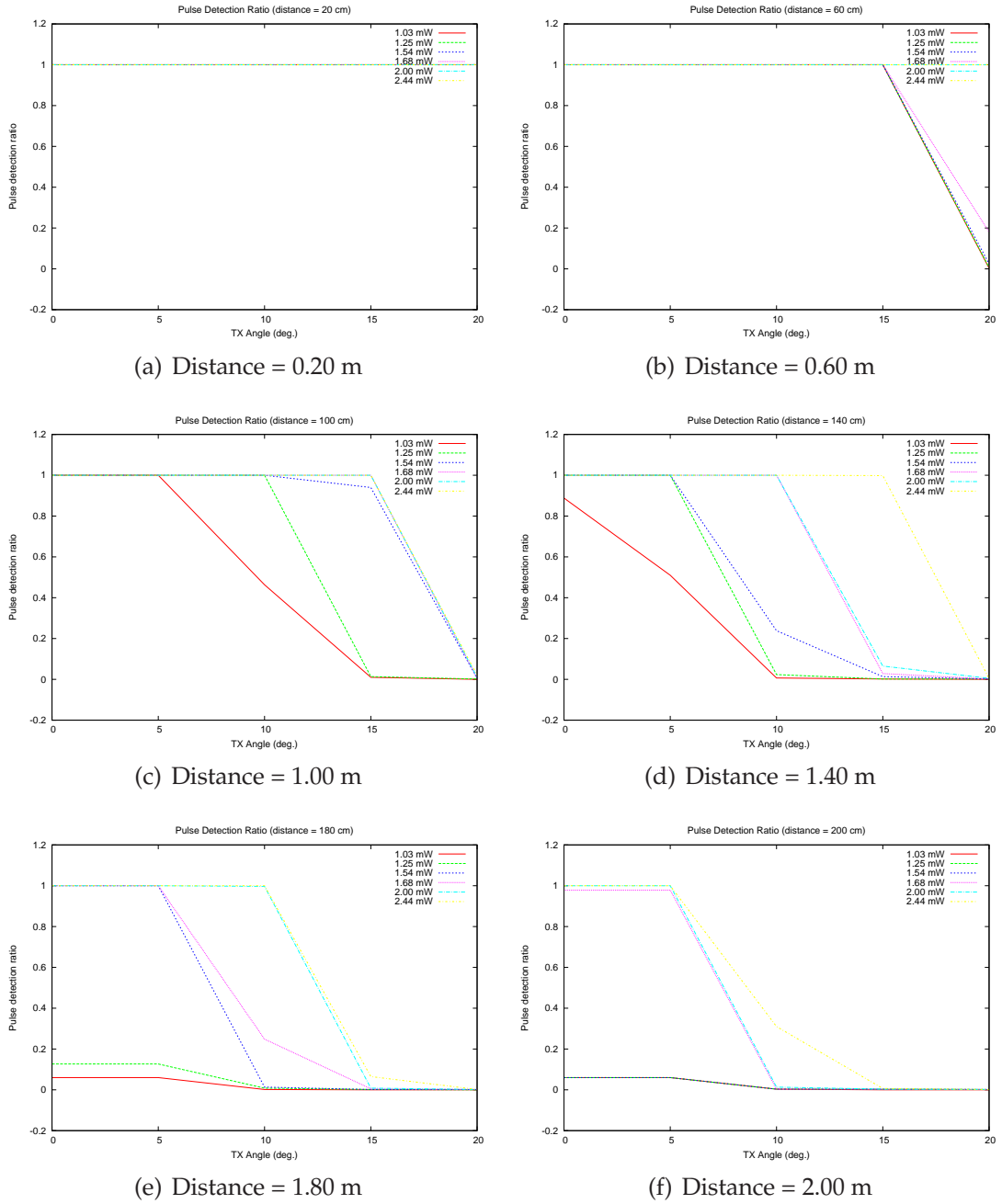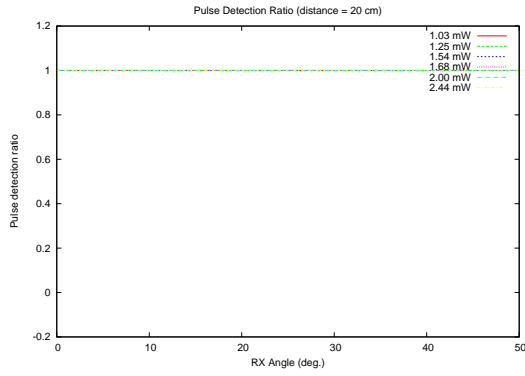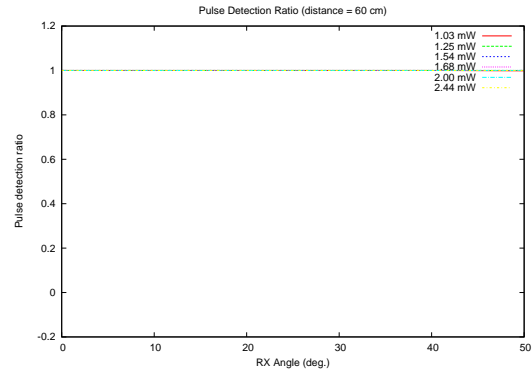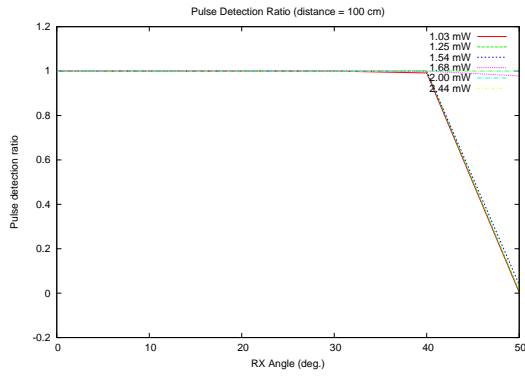Figure 3.4: Pulse detection ratio vs transmission angle for various distances.

(a) Distance = 0.20 m

(b) Distance = 0.60 m
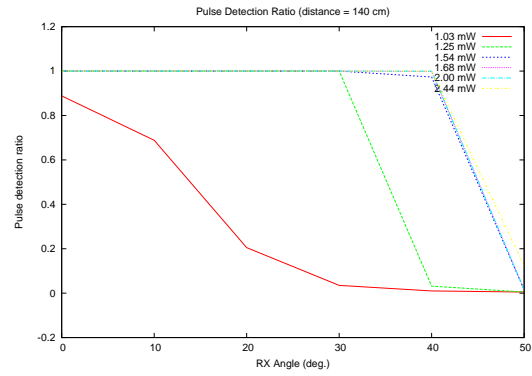
(c) Distance = 1.00 m
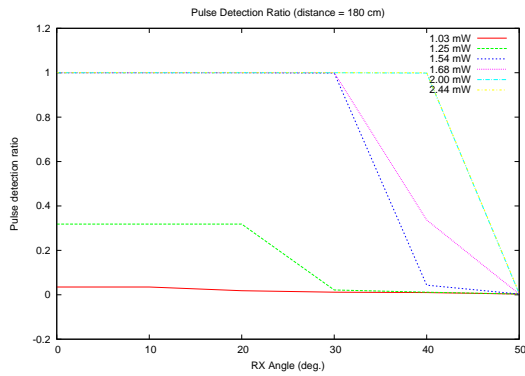
(d) Distance = 1.40 m

(e) Distance = 1.80 m
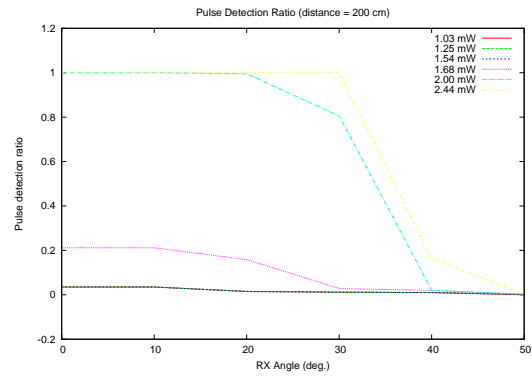
(f) Distance = 2.00 m

Figure 3.5: Pulse detection ratio vs reception angle for various distances.

a low probability of connection beyond $20°$ for any tested power level. Figure 3.5 shows that the reception sensitivity drops off significantly at approximately $40°$ for most power levels, but at sufficiently high transmission intensities the module is still able to detect most the transmitted pulses. For most power levels tested there is an upper limit of between $30°$ to $40°$. Again, the pulse detection rate of both the transmission and reception angle display sharp fall-off characteristics, indicating that the channel is typically either fully connected, or unconnected.

Furthermore, there is a monotonically decreasing relationship between channel connectivity and angle of transmission/reception, and a monotonically increasing relationship between transmission power and channel connectivity. This indicates, as expected, that the IR channel quality decreases as reception or transmission angle increases, and channel quality increases as the transmission power is increased.

3.4 Using Channel Connectivity for Indirect RSS Estimation

Experimental data on pulse detection ratios show that, due to internal characteristics of the BRM-1030 infrared receiver module, the receiver either detects almost all the transmitted pulses or detects none, i.e. there is a sharp and well defined boundary between these two cases. This is illustrated in the histogram in Figure 3.6, which accounts for all collected data points (1500 sets of 600 pulses, across five randomly selected transmitter-receiver pairs). They show that in 95% of the cases, either all 600 pulses were decoded correctly (i.e., pulse detection ratio is equal to one), or no pulses were detected. Only 5% of the tests resulted in partial
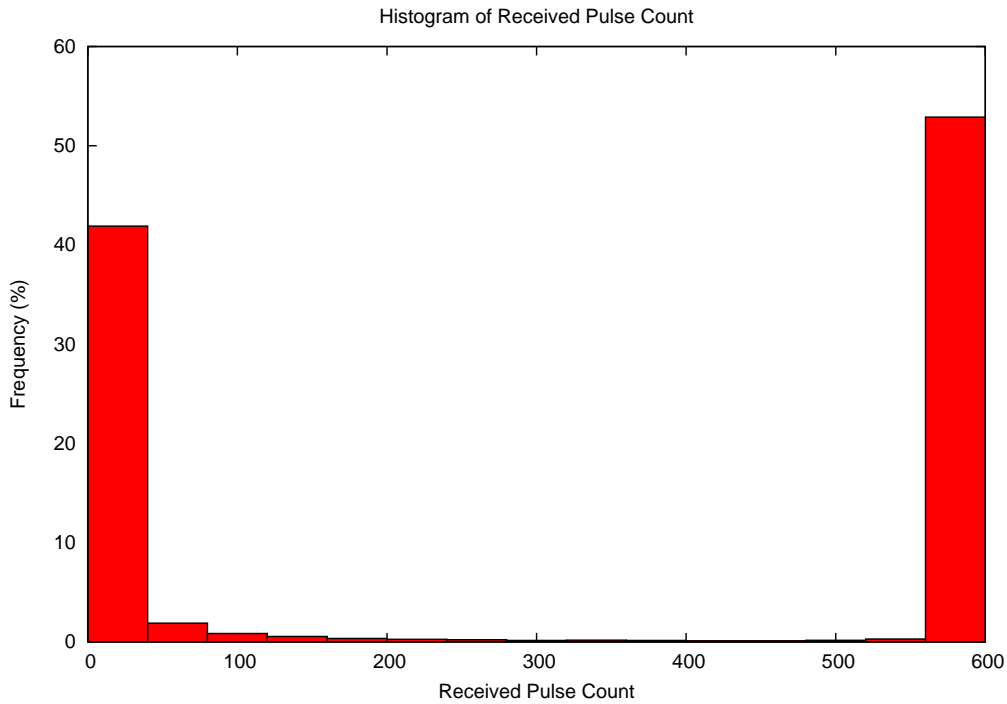
Figure 3.6: Infrared pulse detection histogram.

pulse losses. The histogram also shows that the majority of partial pulse detection cases typically result in an extremely high number of pulse losses, indicating that the communication channel is essentially unusable.

Based on these results, we define the concept of *channel connectivity*: If the pulse detection ratio is greater than 0.92 we define the channel as "connected", and use this as the basis of the created localisation algorithms. The next section provides more details.

Figure 3.7 shows the communication boundaries (in other words, the conditions in which a channel is connected). The shaded areas indicates where the pulse detection ratio is greater than 0.92 and the channel is connected. The graph shows a clear relationship between both transmission and reception angles, and transmission power, at a given distance, which indicates that channel connectivity can be used instead of direct RSS measurements.
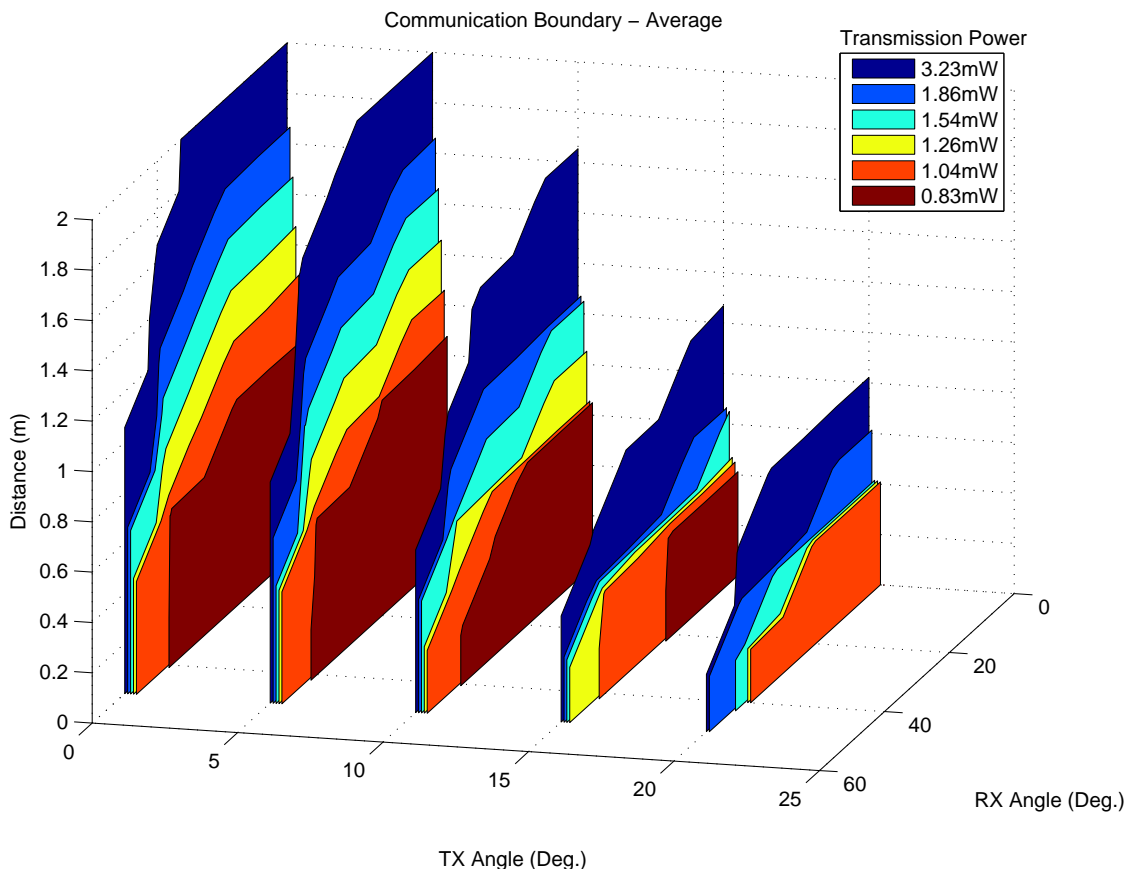
Figure 3.7: Average of the communication boundaries for the five pairs of infrared components tested. In the shaded areas a channel is connected and be used for communications. See Appendix B for individual results. The individual pairs exhibited some variations, although they all display clear connected/unconnected states. This variation is likely caused by difference in components which is unavoidable when using these low-cost components. All pairs indicate that channel quality reduces monotonically with distance, transmission and reception angles, and distance for a given power level.

Receiver	Transmitter	Minimum power level at which a valid Hello message was received
RX_{90}	$TX_{258.75}$	1.26 mW
RX_{135}	$TX_{258.75}$	0.83 mW
RX_{180}	$TX_{258.75}$	1.54 mW
RX_{90}	$TX_{281.25}$	1.04 mW
RX_{135}	$TX_{281.25}$	1.04 mW

Table 3.2: Active infrared transmitter-receiver pairs for nodes shown in Figure 3.8 with minimum transmission power for successful reception of Hello messages.
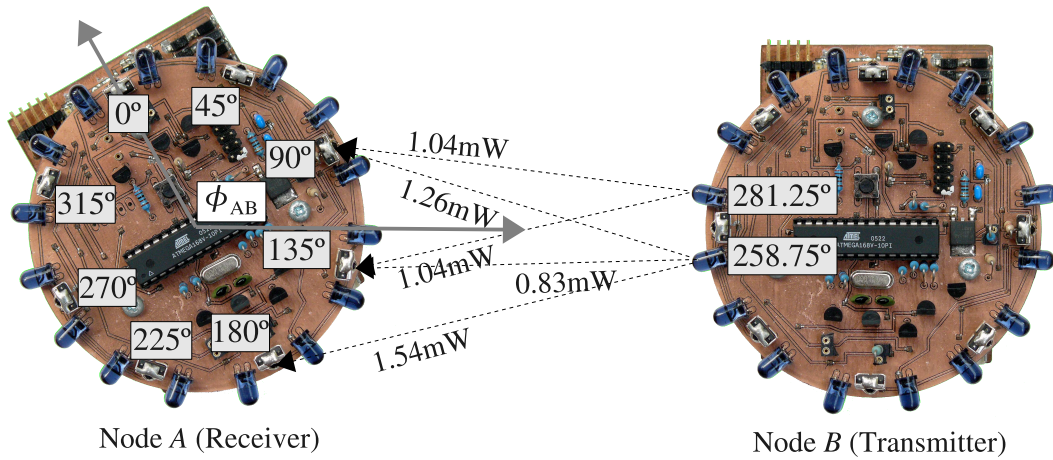
Figure 3.8: Example of relative bearing (ϕ_{AB}) estimation based on received Hello messages. See Table 3.2 for listing of connected IR components along with minimum power for reception of Hello messages.

3.5 Angle Estimation Using Directional Infrared Channels

Angle or relative bearing estimation was chosen as the basis of the localisation system described in this thesis. As discussed earlier distance based methods were not able to accurately determine distance from power intensity alone. Distance estimation requires both the relative angular position of the transmitter and receiver to be known, due to the fact that transmission intensity and reception sensitivity vary depending on the orientation of the transmitter-receiver pairs towards each other. The estimation is based on transmitting a series of packets,

called "Hello" packets, with increasing power levels to discover the communication boundary between a transmitter and a receiver. The method can be implemented in two ways: *Angle estimation at the transmitting node* can be used if the receiver sends back a response to a correctly received Hello packet, this information can be used to estimate the relative bearing. Since the nodes have twice the number of transmitters than receivers, the estimation accuracy will be higher than the second method explained next. But, this method has disadvantages, since the responses will typically be generated by multiple receivers, they will possibly collide and the protocol will require fairly sophisticated media access control [RRS$^+$05] algorithms. On the other hand, *angle estimation at the receiver node* does not require replies to be sent and eliminates the requirement of media access control. The receiver can passively determine the angle to the transmitting node simply by listening to the packets[1].

This method is similar to Hoyt's approach [HMB05]: the centroid of the received signals is calculated by taking into account the power levels of each received signal in order to estimate the relative bearing angle to a neighbour. Note that, Hoyt's approach uses RSS measurements to calculate an angle of arrival estimate. In Hoyt's method the transmission power is kept constant, and nodes receiving the transmission measure the RSS of the incoming signal. By measuring the RSS and receiver angle ($\hat{\varphi}$) an estimate is calculated as follows

$$\hat{\phi}_{ij} = \frac{\sum \text{RSS}_i \varphi_i}{\sum \text{RSS}_i} \tag{3.5.1}$$

where RSS_i is measured at the receiver which is placed at φ_i angle relative to the node's arbitrarily $0°$ bearing.

---

[1]While media access control is not strictly required for angle estimation based solely on received messages, it is highly recommended. Without media access control, Hello messages may be corrupted, due to nodes transmitting simultaneously. Lost Hello messages may result in lower quality angle estimates.

Our method does not rely on RSS measurements and performs the angle estimation as follows.

$$\hat{\phi}_{ij} = \frac{\sum_{n=1}^{N}(P_{\max} - P_n)\varphi_n}{\sum_{n=1}^{N}(P_{\max} - P_n)} \qquad (3.5.2)$$

where,

N = Total number of Hello messages node i received from node j with minimum transmission power.

$P_{\max}$ = Maximum possible transmission power level, in our hardware it is 3.25 mW.

φ_n = The receiver angle relative to local $0°$ which decoded Hello message n with minimum transmission level.

P_n = Power level advertised in the Hello message n.

Due to circular geometry of the receiver and transmitter arrays, the distance at which they are placed is not critical, as symmetric pairs effectively cancel out. But, it should be noted that, at large distances fewer pairs will be connected which may result in a lower quality angle estimate.

Example of Relative Bearing Estimation

An example of relative bearing estimation is illustrated in Figure 3.8. The centroid of the received messages at node A shown in Table 3.2 can be calculated to find the estimate of the angle to the node B, relative to node A's $0°$ bearing,

$$\hat{\phi}_{AB} = \frac{\sum_{n=1}^{N}(P_{\max} - P_n)\varphi_n}{\sum_{n=1}^{N}(P_{\max} - P_n)}. \qquad (3.5.3)$$

Using the data in Table 3.2 the following can be calculated:

$$\sum P_{\text{max}} - P_i \quad = \quad 10.54 \tag{3.5.4}$$

$$\sum \left(P_{\text{max}} - P_i \right) \varphi_n \quad = \quad 1310.85 \tag{3.5.5}$$

Therefore, the relative bearing angle, when using receiver ID, can be calculated as,

$$\hat{\phi}_{ij} = \frac{1310.85\,^{\circ}}{10.54} \tag{3.5.6}$$

Which gives an angle estimate of $124.37°$. Representing an angle estimation error of $5.63°$ from the actual angle of $130°$.

3.5.1 Simulation Results

A simulator was developed (see Appendix C for details) to allow rapid evaluation of angle based localisation in larger network topologies. The simulator included the physical infrared channel characteristics from the experimental data collected in section 3.2.2 to ensure a realistic and accurate simulation environment.

Different component configurations were tested using the simulator to understand how the number of IR components affect the accuracy of the angle estimates. The following configurations were tested using the simulator:

- 16 transmitters / 8 receivers (Sens-R configuration)

- 16 transmitters / 16 receivers

- 32 transmitters / 8 receivers

Each experiment was based on 10,000 simulation runs, using two nodes at a given distance, with random orientation and random experimental infrared data set for each pair. The experiments were repeated at different distances up to a maximum

of 2 metres, which was the limit set on the IR transmitters in this project.

The accuracy of the inter-node angle estimation using the Sens-R configuration, as described in Section 3.2, is presented in Figures 3.9(a), 3.9(b). It can be seen that the angle estimation error is centred around zero, and that the standard deviation of the estimates increases as distance increases. The poor performance at 2 metres is due to fewer infrared pairs being active (as they were limited to approximately 2-3 metres at ideal orientation). Angle estimation based on transmitter ID results in a more accurate angle estimation, due to the fact that there are more transmitters than receivers on the Sens-R platform.

Figures 3.9(c), 3.9(d) shows the second component layout tested, which was the Sens-R layout with twice as many receivers (i.e., 16 receivers). As expected, this improved the angle estimate, as there were more in range pairs available to calculate the estimate. Angle estimation based on transmitter ID was also improved.

Figures 3.9(e), 3.9(f) shows the third component layout tested, which was also based on the Sens-R layout, but with twice as many transmitters (i.e., 32 transmitters). This configuration resulted in slightly better angle estimation when using received messages, but the main improvement was to the transmitter LED ID based estimate, as there were more transmitters available, resulting in a higher angular resolution.

The accuracy of the transmitter ID based estimate is higher than the receiver ID based estimate due to the fact there is more transmitters than receivers, and also the transmitters have a much narrower beam. For practical purposes it is beneficial to increase the number of transmitters, as they are significantly less expensive than the receiver modules and result in more accurate angle estimations. However, there must be sufficient receiver modules to ensure complete $360°$ coverage.
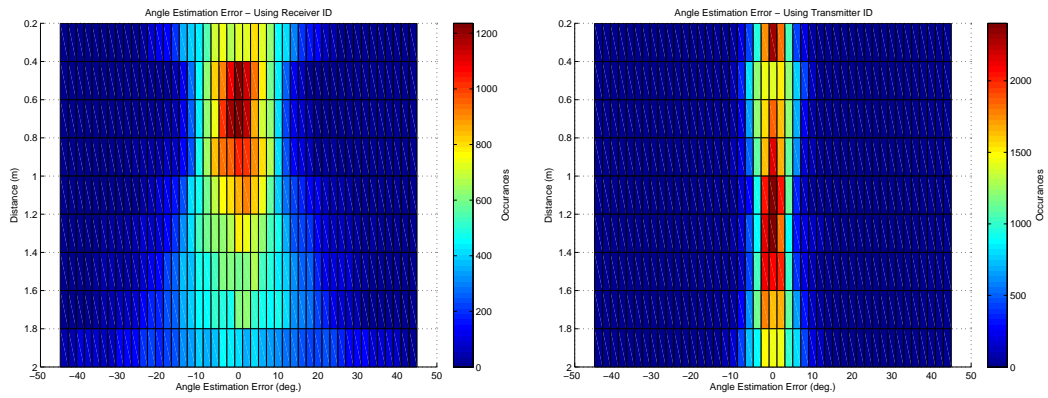
(a) 16 transmitters and 8 receivers: Receiver estimates the angular direction of the transmitter

(b) 16 transmitters and 8 receivers: Transmitter estimates the angular direction of the receiver
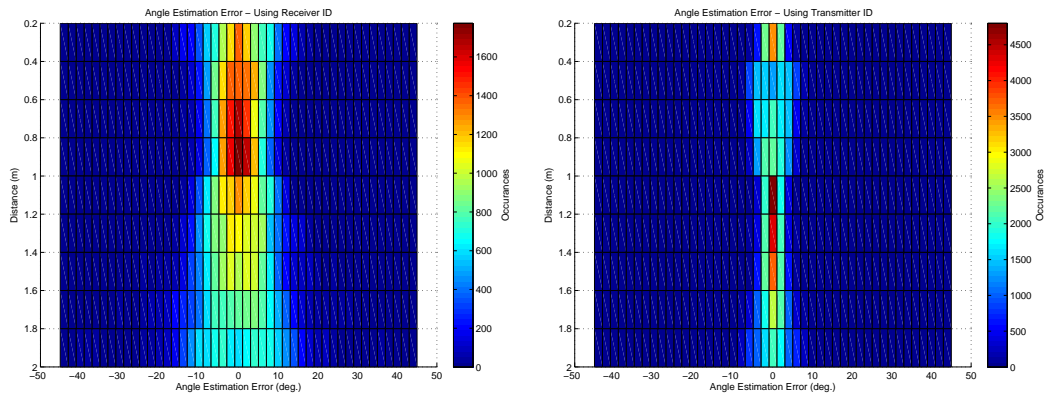
(c) 16 transmitters and 16 receivers: Receiver estimates the angular direction of the transmitter

(d) 16 transmitters and 16 receivers: Transmitter estimates the angular direction of the receiver
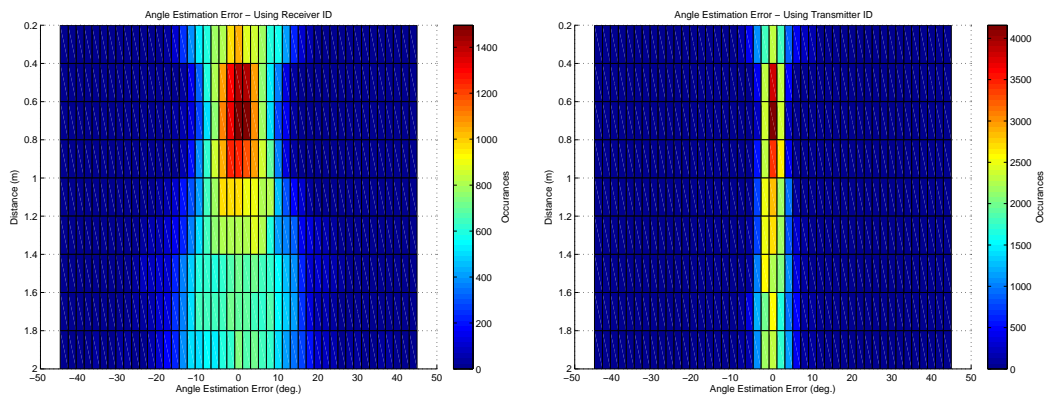
(e) 32 transmitters and 8 receivers: Receiver estimates the angular direction of the transmitter

(f) 32 transmitters and 8 receivers: Transmitter estimates the angular direction of the receiver

Figure 3.9: Angle estimation accuracy for various configurations. The decreased accuracy at short distances is due to many transmitter-receiver pairs being active, as the lowest power setting used on the Sens-R nodes does not allow accurate angle estimation to be achieved at extremely short distances.

For the Sens-R configuration (i.e., 16 transmitters/8 receivers), estimating angles at the transmitter node, resulted in an angle estimate with a standard deviation of approximately $2.5°$ centred around the actual angle. Angle estimation based on receiver ID on the Sens-R configuration provided an angle estimate centred around the true angle with a standard deviation of approximately $10°$. In a static network the angle estimates could be averaged, which may improve the angle estimate over time.

Angle estimation based on transmitter LED ID resulted in more accurate angle estimates between nodes using the Sens-R configuration. However, this requires neighbouring nodes to reply back to the transmitter. Replying back would require media access control, or else nodes would attempt to reply back at the same time, and potentially interfere with one another. Angle estimation utilising receiver ID information only does not require the receiving node to reply back, so the receiver node can be totally passive during the angle estimation phase.

3.6 Position Estimation using Directional Infrared Channels

Using a weighted centroid approach to determine the relative angle to neighbouring nodes using directional infrared channels (see section 3.5), a trilateration based localisation was developed, such that a node could estimate its position based on two neighbours acting as reference nodes, where each neighbour already has an estimate of their own position.

In traditional trilateration based localisation systems, a node requires three external reference points to unambiguously calculate its position in two dimensions. However, as the Sens-R nodes are able to determine the size of the angle between

the nodes, it is possible to calculate a position estimate with just two reference nodes. By knowing the (x,y) coordinate estimates of each of the neighbours, along with the angle between them, it is possible to eliminate the phantom position estimate relatively easily and accurately.
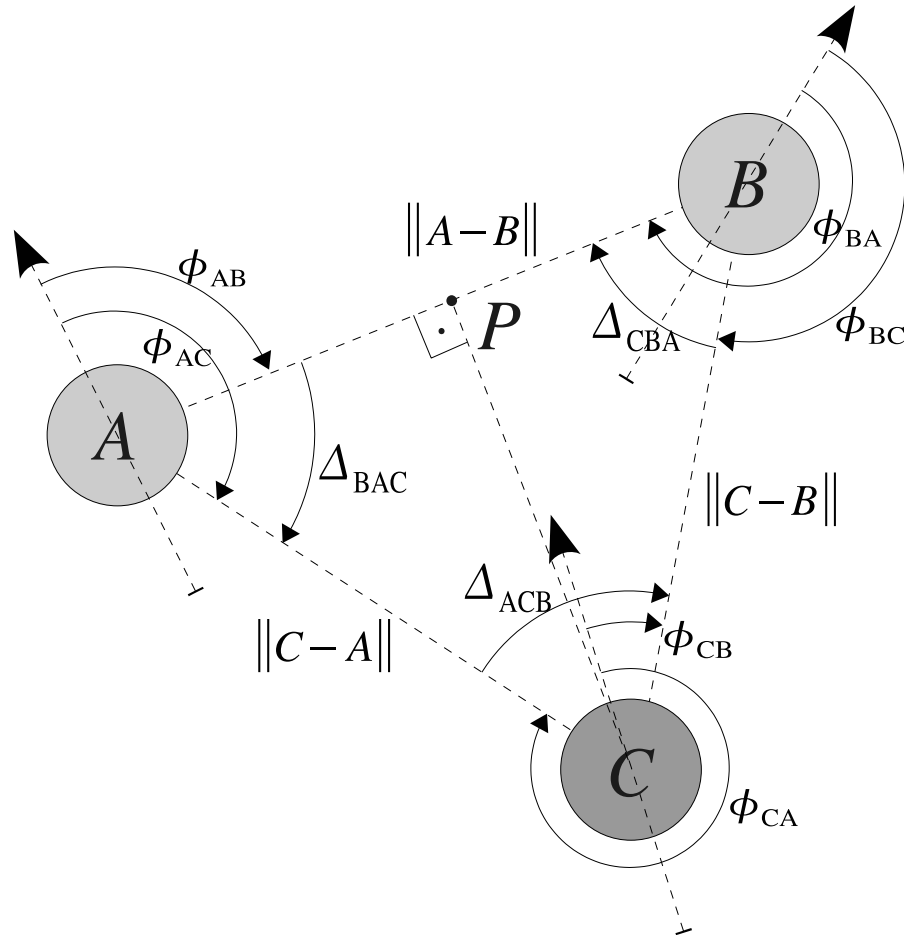
Figure 3.10: The angles and a neighbourhood triangle used for localisation.

The algorithm presented in this research does not require nodes within the network to have a consistent orientation, or known bearing relative to their neighbours. Hence, nodes can only measure angles to neighbours relative to an arbitrary, but locally consistent, bearing. These angles are denoted by ϕ_{ij}, which represents the angle which node i sees node j, relative to node i's local $0°$ bearing. The discrimination angle between nodes can be found by calculating the difference between two ϕ angles. For example, the discrimination angles in Figure 3.10

$(\Delta_{BAC}, \Delta_{CBA}$ and Δ_{BAC}) can be calculated using the following equations.

$$\Delta_{ACB} = (\phi_{CB} - \phi_{CA} + 360)(\mathrm{mod}\,360) \qquad (3.6.1)$$

$$\Delta_{CBA} = (\phi_{BA} - \phi_{BC} + 360)(\mathrm{mod}\,360) \qquad (3.6.2)$$

$$\Delta_{BAC} = (\phi_{AC} - \phi_{AB} + 360)(\mathrm{mod}\,360) \qquad (3.6.3)$$

The distance between the reference nodes ($\|A - B\|$) is calculated from the position estimates obtained from each of the reference nodes (x_A, y_A) and (x_B, y_B) respectively. Using this information, along with the discrimination angles, node C can calculate the distance to each of the reference nodes using the Sine Rule:

$$\|C - A\| = \frac{\|A - B\| \sin(\Delta_{CBA})}{\sin(\Delta_{ACB})}, \qquad (3.6.4)$$

$$\|C - B\| = \frac{\|A - B\| \sin(\Delta_{BAC})}{\sin(\Delta_{ACB})}. \qquad (3.6.5)$$
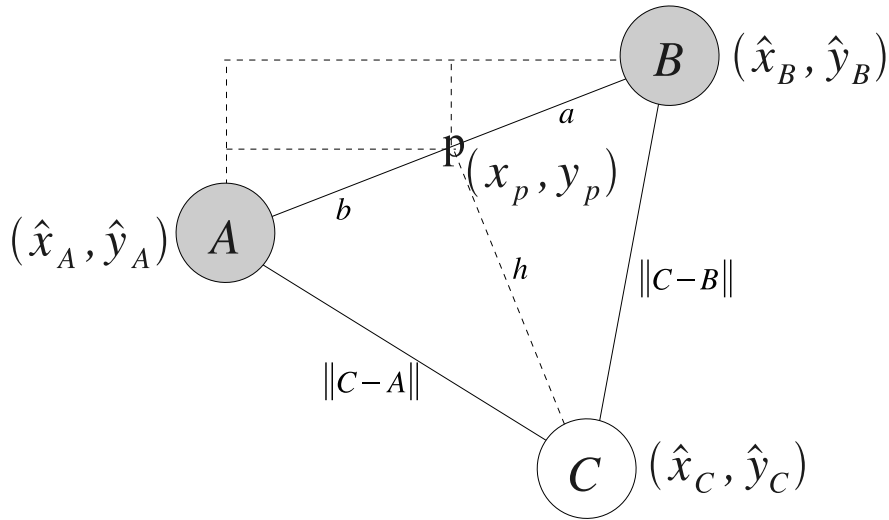
Figure 3.11: The coordinates of Node C can be calculated if the position and distance to each of the reference nodes is known.

From this stage on, the position estimation task has been reduced to a trilateration, or intersection of circles problem. If we consider the example in Figure 3.11 which is the same situation as Figure 3.10 the position of Node C (x_C, y_C) can be

calculated with the introduction of a fictitious point p, using the following steps.

Firstly, consider the two triangles, APC and BPC which give,

$$\|C - A\|^2 = b^2 + h^2, \tag{3.6.6}$$

$$\|C - B\|^2 = a^2 + h^2. \tag{3.6.7}$$

Then, using the fact that $b = \|A - B\| - a$, a can be calculated as,

$$a = \frac{\|C - B\|^2 - \|A - C\|^2 + \|A - B\|^2}{2\,\|A - B\|}. \tag{3.6.8}$$

Then, using the BPC triangle, h can be calculated using,

$$\|C - B\|^2 = h^2 + \|C - B\|^2, \tag{3.6.9}$$

$$h = \sqrt{\|C - B\|^2 - a}. \tag{3.6.10}$$

As points A,B and p lie on the same line the coordinates of point p can be calculated using,

$$y_p = y_B - \frac{a(y_B - y_A)}{\|A - B\|} \tag{3.6.11}$$

$$x_p = x_B - \frac{a(x_B - x_A)}{\|A - B\|} \tag{3.6.12}$$

Which then allows the coordinates for node C to be calculated. However, as it is an underdetermined system there are two symmetric solutions for the position of

(a) $|y_A - y_B| > |x_A - x_B|$ (b) $|y_A - y_B| \leq |x_A - x_B|$
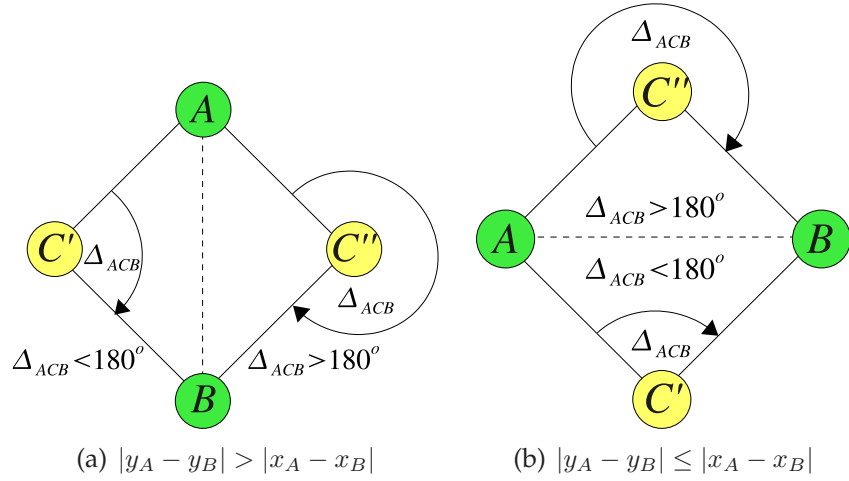
Figure 3.12: Illustration of Algorithm 1 for determining the real location of node C.

node C, C' and C''':

$$x_{C'} = x_p + \frac{h(y_A - y_B)}{\|A - B\|} \tag{3.6.13}$$

$$y_{C'} = y_p - \frac{h(x_A - x_B)}{\|A - B\|} \tag{3.6.14}$$

$$x_{C''} = x_p - \frac{h(y_A - y_B)}{\|A - B\|} \tag{3.6.15}$$

$$y_{C''} = y_p + \frac{h(x_A - x_B)}{\|A - B\|} \tag{3.6.16}$$

Figure 3.12 illustrates the problem of phantom position estimations caused by non unique geometry, which is caused by a limited number of reference points resulting in an under-determined system. In both cases, node A and B know their own positions, as well as the angle between its two neighbours, and node C knows the angle between the two reference nodes A and B (Δ_{ACB}). From this information, node C can determine which position estimate solution is most likely to be correct based on which solution makes the most geometric sense based on all available information.

The procedure for selecting the correct position estimate from the two symmetric

solutions is based on the size of the angle between the two reference nodes. This disambiguation algorithm is run in the vertical or horizontal direction, depending on which direction offers the largest distance between nodes. This helps to increase reliability, especially when there are measurement errors, which could result in the wrong solution being selected, and hence an incorrect position estimate being selected. If node A is located at (x_A, y_A), and B is located at (x_B, y_B), the difference in each direction can be calculated as $|x_A - x_B|$ and $|y_A - y_B|$.

The disambiguation method to be used is chosen based on which direction has the largest difference between reference nodes. If $|y_A - y_B|$ is larger than $|x_A - x_B|$ then the case shown in Figure 3.12 a is used, otherwise Figure 3.12 b is used. For the purposes of this algorithm, reference node A is chosen to be the reference node with the largest y position, or the smallest x position, depending on which case is being used, and the angle between the reference nodes is the clockwise angle from node A to node B (i.e., Δ_{ACB}). The solution selection algorithm is presented in Algorithm 1.

Algorithm 1 Procedure for selecting correct position estimate solution.

> **if** $|y_A - y_B| > |x_A - x_B|$ **then**
>> Set A and B such that $y_A > y_B$
>
> **else**
>> Set A and B such that $x_A < x_B$
>
> **end if**
> **if** $\Delta_{ACB} < 180°$ **then**
>> Use solution C'
>> $x_C \leftarrow$ Equation 3.6.13
>> $y_C \leftarrow$ Equation 3.6.14
>
> **else**
>> Use solution C'''
>> $x_C \leftarrow$ Equation 3.6.15
>> $y_C \leftarrow$ Equation 3.6.16
>
> **end if**

When using the Sine Rule to calculate the distances between nodes based on the

measured angles between nodes, it is important to understand how errors in angle measurements affect the distance estimate. The work presented in [Cha05] describes the procedure for identifying 'well conditioned' triangles; these triangles are less sensitive to errors in angle measurements. The sensitivity to errors in angle measurements of the triangles can be found by taking the partial derivative of Equation (3.6.4) and (3.6.5) with respect to the measured angle, as shown in Equation 3.6.17 and 3.6.18. The larger the derivative the more sensitive the distance estimate is to angle measurement errors.

$$\frac{\partial \, \|A - C\|}{\partial \Delta_{CBA}} = \frac{\|A - B\| \cos(\Delta_{CBA})}{\sin(\Delta_{ACB})} \tag{3.6.17}$$

$$\frac{\partial \, \|C - B\|}{\partial \Delta_{ACB}} = \frac{- \, \|A - B\| \sin(\Delta_{CBA}) \cos(\Delta_{ACB})}{\sin^2(\Delta_{ACB})} \tag{3.6.18}$$

A graphical representation of these equations is shown in Figure 3.13. It can be seen that it is critically important to avoid using triangles with $0°$ and $180°$ angles, which correspond to near colinear configurations. These situations result in increased sensitivity to angle measurement error. Ideally, all three angles would fall into a low noise sensitive region of the graphs. However, this is not always possible if the nodes are randomly positioned.

As the accuracy of the distance estimate is based on the geometry of the triangle, it could be beneficial to include measurement error sensitivity into the weighting coefficients when deciding which position estimate is of higher quality. Obviously, if an estimate was based on a configuration where one (or more) angles were close to $0°$ or $180°$ there is a high probability that errors in angle estimation has greatly affected the quality of the estimate, and therefore the estimate should be weighted down and not heavily relied on for position estimation

(a) Equation (3.6.17) (b) Equation (3.6.18)
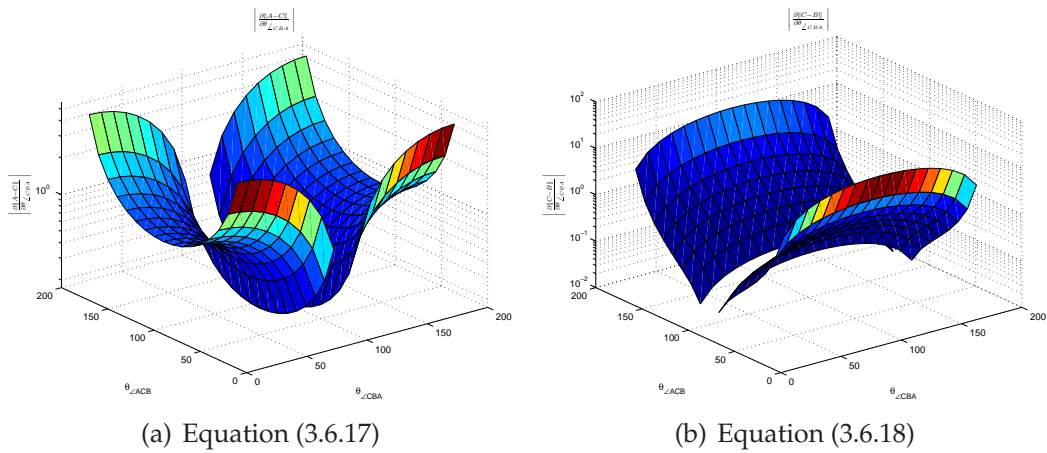
Figure 3.13: Angle measurement sensitivity in triangles.

3.7 Iterative EWMA Algorithm for Localisation in Ad Hoc Networks

In relatively dense ad hoc networks, such as wireless sensor networks, nodes will typically have multiple pairs of neighbours from which position estimations can be formed. Each of these estimations must be combined into a single estimate, such that only one position estimation is kept by each of the nodes. If an iterative approach is taken, as time goes on more nodes in the network will be able to estimate their position, as more nodes learn their position and are able to act as reference nodes for their neighbours. A small number of nodes have a priori position information, these nodes are referred to as anchor nodes which provide fixed points within the network, allowing the remaining nodes to localise themselves.

Using an iterative localisation scheme the accuracy of the position estimates across the network should improve over time as there are more reference nodes being utilised. The ability to average position estimates using filtering techniques allow high frequency fluctuations in the position estimates to be minimised, thus improving the accuracy of the position estimations.

An exponentially weighted moving average (EWMA) algorithm [NIS] is well

suited for situations where older information is to be weighted lower than newer information. This is useful in iterative localisation, where the newest position estimate are likely to be more accurate than the previous estimate. Therefore, EWMA type algorithms provide a good starting point for iterative localisation systems for ad hoc networks. The general EWMA algorithm is usually in the form.

$$S_t = \alpha S_{t-1} + \beta Y_{t-1} \tag{3.7.1}$$

$$\alpha + \beta = 1.0 \tag{3.7.2}$$

Where S_t is the current EWMA value, S_{t-1} is the previous S value and Y_{t-1} is the observation at time $t-1$. The α and β terms are weighting coefficients that must sum to 1.0. The larger β is, the faster the systems with respond to change, at the cost of higher sensitivity to errors in the instantaneous observations.

For the purposes of localisation, the following equation can be used to average observations into a unified continually updating estimate of a nodes current position.

$$\begin{bmatrix} \hat{x} \\ \hat{y} \end{bmatrix}_t = \alpha \begin{bmatrix} \hat{x} \\ \hat{y} \end{bmatrix}_{t-1} + \beta \begin{bmatrix} X \\ Y \end{bmatrix}_{t-1} \tag{3.7.3}$$

Where $\begin{bmatrix} \hat{x} \\ \hat{y} \end{bmatrix}$ is the average position estimate held by the node, and $\begin{bmatrix} X \\ Y \end{bmatrix}$ is the current instantaneous position estimate.

Iterative localisation schemes suffer from a potential accumulation of position estimation errors, as they rely only on immediate neighbours for position information. Any position estimation errors will be passed onto neighbours and, due to

the iterative nature of the algorithm, will begin to propagate across the network.

3.8 Discussion

Based on experimental data collected from five sets of infrared components, it was found that relatively low cost infrared components without explicit RSSI output could be used for inter-node angle estimation by inferring channel quality from packet loss. Angle estimation can be implemented using a sequence of Hello messages sent at different power levels on each transmitter. Depending on channel quality, the receiver will start receiving packets at a different power level. The higher the channel quality, the more packets will be received. However, in low quality channels, only the packets sent with the highest transmission powers will be received correctly.

From the experimental testbed it was found that relative bearing angles could be accurately measured using channel connectivity characteristics from 8 receivers and 16 transmitters mounted on an $8\,\mathrm{cm}$ circular PCB. The angle estimations using this method were typically within $10°$ when using receiver based information, and within $5°$ when using transmitter information. The accuracy of the angle estimation can be further improved by using more infrared components. To save cost, it is possible to increase the number of only the transmitters or the receivers. However, as the transmitters have a narrower beam, and are significantly less expensive than the receivers, it would be advisable to use transmitter ID based angle estimation with more transmitters, provided there was sufficient receivers to ensure $360°$ coverage of neighbours.

The centroid method described by Hoyt [HMB05] relies on the receiver to measure the RSS of the incoming signal. The method presented in section 3.5 relies on the transmitter sending multiple messages at various power levels to estimate

the quality of the channel. In low energy applications, Hoyt's method will reduce the overall transmitted energy required, as only one message needs to be sent by each transmitter, but this method requires additional hardware in order to measure the RSS. In a static network, where inter-node angles remain constant, the power savings of Hoyt's method may be negligible. The simplified hardware requirements of the method presented in this research makes it attractive to nodes with limited abilities (i.e., nodes without ADCs).

Chapter 4

Anchor Hop Distance Weighted Localisation (AHDWL) Algorithm for Improving Localisation Accuracy

4.1 Introduction

The accumulation of position estimation errors limits the accuracy of iterative localisation schemes, where position estimates are calculated at each node and then propagated to neighbours. In these schemes, any estimation errors are inevitably passed onto neighbours, eventually effecting the localisation accuracy of all nodes in the network. The localisation scheme described in the previous chapter is no exception.

This chapter presents a novel algorithm called AHDWL to alleviate the problem which reduces the propagation of position estimation errors. This algorithm was tested on the pulsed infrared light testbed but is applicable to other iterative multihop localisation schemes. The AHDWL algorithm selectively weights individual position estimates depending on their anchor-hop-distance (i.e., how many hops the information has travelled from the anchor nodes).

4.2 Anchor Hop Distance Weighted Localisation (AHDWL) Algorithm

The AHDWL algorithm presented in this chapter belongs to the family of iterative localisation algorithms. It has additional weighting coefficients based on the reference node's distance to the anchor nodes. Position estimates which are calculated from information from reference nodes which are closer to the anchor nodes are considered to be of higher quality and thus receive a higher weighting.

In a network of many nodes trying to localise themselves using neighbours who may, or may not be, anchor nodes, it is important to minimise errors at every node, as any position error will propagate and affect the accuracy of all nodes within the network. A possible advantage of using weighted iterative algorithms for localisation is that nodes are able to decide which nodes are reporting more accurate information, and which nodes are providing estimates with potentially large errors.

The algorithm presented attempts to selectively weight position estimates in such a way that the position estimate errors are kept to a minimum. It assumes that errors in position estimates may not necessarily be normally distributed, and may even contain a bias. Also, not unreasonably, it assumes nodes which are more hops away from the anchor nodes are more likely to have larger position estimation errors than nodes which are closer to the anchor nodes, due to the accumulation of errors at each hop.

To mitigate the accumulation of errors, the individual position estimates are weighted based on their hop count distance from the anchor node. The benefits of this approach are illustrated in Figure 4.1. In the network shown in the
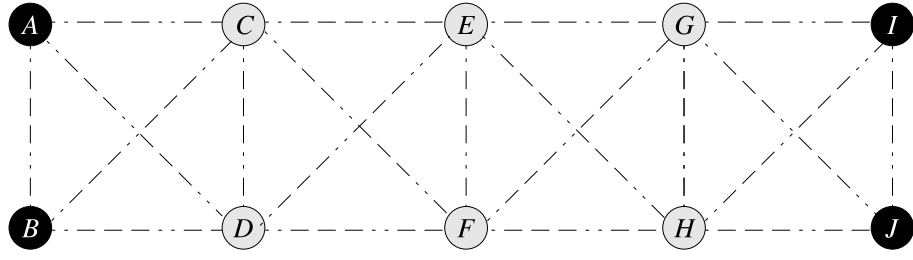
Figure 4.1: Example where anchor hop distance weighting can be used to improve localisation. Nodes A, B, C, I and J know their exact positions (anchors).

figure, it can intuitively be seen that nodes C and D should base their position estimates on the position of A and B (as A and B by definition have perfect position estimates), although it is possible nodes E and F may also be usable to obtain a position estimate, but node E and F's position estimate is considered to be more uncertain than A and B's, due to the fact their estimates are based on position information, which has been passed through multiple hops (n-hop information). Nodes E and F should not favour any nodes, as it is in the middle of the network. Uncertainty in an estimate does not necessarily mean it should be ignored. It is therefore important to try to incorporate all this information together such that a combined estimate is formed based on all available information.

The filtering algorithm for the position estimate is based on,

$$\begin{bmatrix} \hat{x} \\ \hat{y} \end{bmatrix} = \frac{\sum_{i=1}^{i=N} \left(w_i \begin{bmatrix} X \\ Y \end{bmatrix}_i \right)}{\sum_{i=1}^{i=N} w_i}. \tag{4.2.1}$$

Where, $\begin{bmatrix} \hat{x} \\ \hat{y} \end{bmatrix}$ is the averaged position estimate, $\begin{bmatrix} X \\ Y \end{bmatrix}_i$ is the ith instantaneous position estimate, and w_i is the weighting to be applied to the estimate i^{th} position estimate.

The iterative EWMA formula shown in Equation (3.7.3) can be expanded to accept additional weighting coefficients for particular observations, allowing for selective weighting of observations based on estimated certainty of individual observations. Certainty, in this case, is determined by the distance (d) to the anchor nodes (anchor nodes have 100% certainty and a distance of zero). The further from an anchor node the higher the uncertainty.

The weighting factor applied to each position estimate is a function of the anchor hop distance of each neighbour used to calculate the estimate. There are many possible weighting techniques available. For the purposes of this research, the weighting is to be inversely proportional to the anchor hop distance of the two reference nodes being used. One such weighting function could be expressed as

$$w_i(d_a, d_b) = \frac{1}{d_a + d_b + 2.0}, \tag{4.2.2}$$

where w_i is the weighting to be applied, and d_a and d_b is the anchor hop distance of each of the reference nodes being used.

For simplicity the weighting factor (β) of the AHDWL algorithm is based on the average anchor hop distance of the two reference nodes as shown in Equation 4.2.2. β is calculated by multiplying a constant value β_{base} by the weighting coefficient w_i.

$$\beta = w_i \beta_{\text{base}} \tag{4.2.3}$$

An added benefit of using hop-count based algorithms is that each node knows its hop count to the nearest anchor node. If we assume that anchor nodes are also sink nodes, it is possible to efficiently send collected data to the sink nodes, by simply forwarding the message to the neighbour with the lowest anchor hop

distance. This is known as distance vector routing, which is a distributed implementation of the Bellman-Ford algorithm [Sta01]. One main problem associated with Bellman-Ford type algorithms is the formation of routing loops, where nodes or links within the network fail, and incorrect hop count information is propagated throughout the network. Routing failures caused by node mobility or failure are automatically dealt with due to the nodes periodically sending messages to neighbours, including their own current hop-count, to the nearest sink node. There may be short term routing loops while the new anchor hop distance propagates throughout the network, but the network routing should stabilise and allow delivery of messages.

Instead of relying solely on the anchor hop distance to determine the quality of the estimation, an alternative method could be to use the angle measurement sensitivity of the result (as described in the previous chapter) to calculate weighting coefficients. The more sensitive the estimate is to angle measurement errors, the higher the uncertainty of the position estimate and, hence, such estimates should receive a lower weighting. The weighting could be based on anything which may effect the certainty of the position estimate. The only limitation to the weighting function is that the estimated certainty of an estimate value must be cumulative. The parents certainty must be taken into account when calculating weightings, as an estimate is only as good as the data on which it is based. If the estimate is formed from nodes with an uncertain position estimates, any sequential estimate can not be any more certain.

4.3 Implementation of the AHDWL Algorithm

For the implementation of the AHDWL algorithm two different types of messages are defined. The Hello messages allow nodes to broadcast their presence to
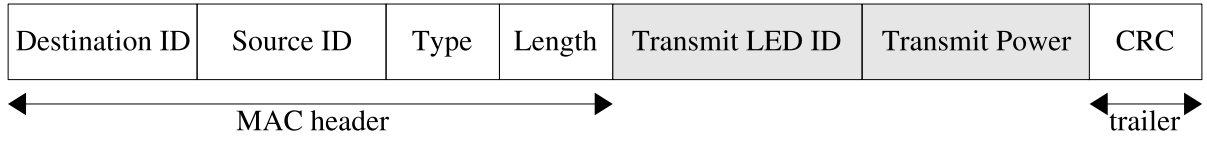
Destination ID	Source ID	Type	Length	Transmit LED ID	Transmit Power	CRC

← MAC header → ← trailer →

Figure 4.2: Hello packet structure. Node periodically broadcasts a sequence of Hello packets with increasing power level from 0.75mW to 3.25mW.

Current Position Est.	Anchor Hop Distance	n_1 ID	Bearing to n_1	...	n_N ID	Bearing to n_N

Figure 4.3: Neighbour table update packet structure. Here, only the payload is shown, the MAC header and trailer are same as the Hello packet shown in Figure 4.2.

neighbours at different power levels. Nodes receiving the Hello packets use the power level sequence, along with local infrared receiver ID, to estimate the angle of the broadcasting neighbour relative to the local $0°$ bearing (using methods discussed in Section 3.5). The node may choose to respond to the Hello message with the transmitter LED ID and minimum power level required for successful communications. This allows the transmitting node to use the minimum power level required for future unicast messages.

The Neighbour Table Update packet contains the position information of the transmitting, node as well as a list of each of its 1-hop neighbours, along with their angles relative to the transmitting nodes local $0°$ bearing. On reception of a Neighbour Table Update message the node updates its local information regarding the remote node and attempts to find triangles (Figure 3.10) (consisting of itself and two mutual neighbours) from which a position estimate can be calculated using equations in section 3.6. Each triangle will produce its own position estimate which is then processed by the AHDWL algorithm such that a single continually updating position estimate is kept by each node.

Nodes store current angle, position and anchor hop distance in their local neighbour table (Figure 4.4). This includes the nodes current position estimate $(\hat{x}_i, \hat{y}_i)$,

ID	Current Pos. Est.	Anchor Hop Dist.	i	n_1	n_2	...	n_N
i (self)	$(\hat{x}_i, \hat{y}_i)$	d_i	-	ϕ_{in_1}	ϕ_{in_2}	...	ϕ_{in_N}
n_1	$(\hat{x}_1, \hat{y}_1)$	d_1	$\phi_{n_1 i}$	-	$\phi_{n_1 n_2}$	...	$\phi_{n_1 n_N}$
$\vdots$	$\vdots$	$\vdots$	$\vdots$	$\vdots$	$\vdots$	$\ddots$	$\vdots$
n_N	$(\hat{x_N}, \hat{y_N})$	d_N	$\phi_{n_N i}$	$\phi_{n_N n_1}$	$\phi_{n_N n_2}$	...	-

Figure 4.4: Neighbour table of node i. The table contents are progressively filled whenever a neighbour table update packet arrives, and a node estimates its own position using this information. It also calculates relative bearings to its neighbours by processing the received Hello packets.

anchor hop distance (d_i) and relative bearing angles to 1-hop neighbours (ϕ_{in_x}). On reception of neighbour table update messages from neighbours, each node updates their local neighbour table with their neighbours latest position estimate, anchor hop distance and bearing angles relative to the neighbouring node. Nodes then attempt to identify triangles of mutual neighbours (Figure 4.6) in order to calculate a new position estimate.

The general outline of the AHDWL algorithm is presented in Figure 4.5. The node will spend most it's time in the idle state (where it can focus on other tasks), and is event driven by timers and incoming message events. Each circle represents a distinct task, which is described in more detail in Algorithms 2 through 6.

Algorithm 2 Initialise

NeighbourTable[] ← NULL
if Anchor Node **then**
    $(\hat{x}, \hat{y})$ ← (X,Y)
    Status ← Anchor
else
    $(\hat{x}, \hat{y})$ ← (null, null)
    Status ← Unknown
end if

Nodes initially have no known neighbours, and the initial position of each node is not known, unless the node is an anchor node, in which case the position is
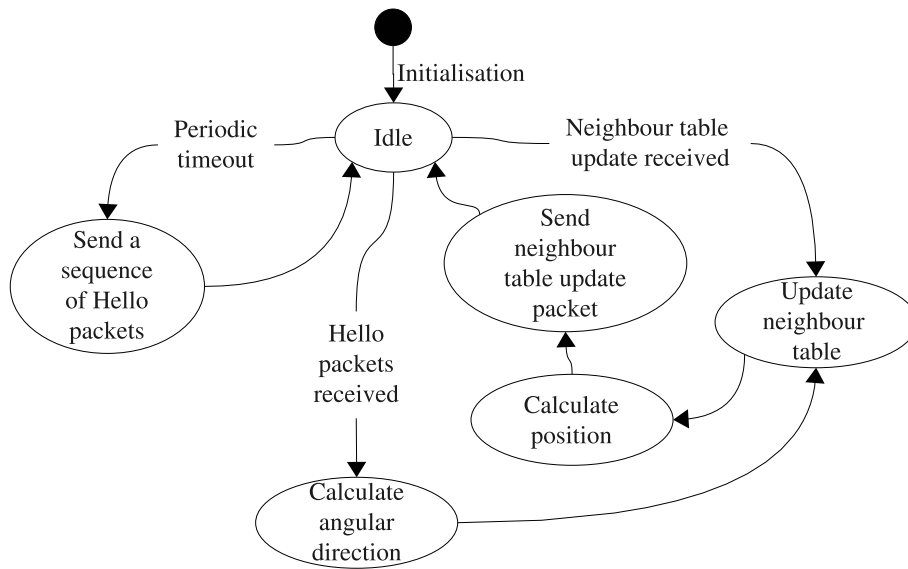
Figure 4.5: Overview of the AHDWL localisation algorithm.

predetermined from an outside source (either preprogrammed, or via another lo-
calisation system such as GPS). Nodes periodically broadcast a sequence of Hello

---

Algorithm 3 Send Hello packet sequence

for each transmitter TX_0 to TX_{15} **do**
    $Power \leftarrow Power_{min}$
    while $Power \leq Power_{max}$ **do**
        SetTXPower(Power)
        SendMsg(DST:ALL, SRC:self.id, TYPE:Hello, TXID:transmitter, TX-
        POWER:Power)
        $Power \leftarrow Power + Power_{step}$
    end while
end for

---

messages at different power levels on each transmitter. The Hello messages act in
two ways: Nodes use the Hello messages to broadcast their presence to their im-
mediate neighbours, also the multiple transmission power allow for the receiving
nodes to estimate the relative bearing angle to their neighbours. This gives nodes
the information required to allow them to calculate a position estimate.

In this implementation, relative bearing angles are calculated based on the re-
ceiver ID of the receivers which correctly decoded the Hello packets. Therefore,

Algorithm 4 Receive message on receiver k- At node C from node A.

$\varphi \leftarrow$ ReceiverAngle[k]
if (Message.type = "Hello") **then**
  $\phi_{CA} \leftarrow$ EstimateAngle(j, φ, message.TXPOWER)
else if (Message.Type = "Neighbour Table Update") **then**
  $d_C \leftarrow \min(d_C, d_A + 1.0)$
  UpdateNeighbourTable(A, $(\hat{x_A}, \hat{y_A})$, d_A)
  for all ($\phi_{Ak} \leftarrow Message.AngleToNeighbour[k]$) **do**
    UpdateNeighbourBearingTable(j, k, ϕ_{Ak})
  end for
  if (Status != Anchor) **then**
    for all nodes C which are mutual neighbours of A and B **do**
      if $(\hat{x_B}, \hat{y_B})$ AND $(\hat{x_C}, \hat{y_C})$ are known **then**
        PositionEstimate(A,B,C)
      end if
    end for
  end if
else
  Non localisation message
end if

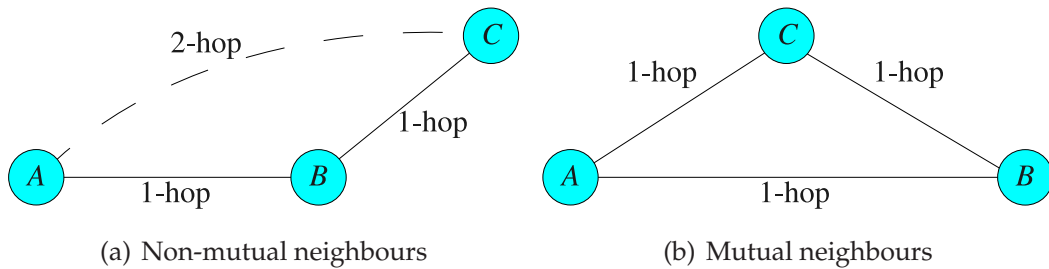(a) Non-mutual neighbours   (b) Mutual neighbours

Figure 4.6: Mutual neighbour triangles.

every time a Hello packet is received, the transmitting node's angle entry in the local neighbour table is updated. Nodes could choose to reply back to the transmitter so that the transmitting node learns which power level, and the transmitter ID of which each of its neighbours can be reached on in order to minimise the transmission energy required for future unicast messages.

When new information becomes available through the reception of Neighbour Table Update messages, the node can attempt to recalculate a new position estimate. Position estimates can be calculated when a triangle can be formed with

Algorithm 5 Position Estimate Update at Node C

$\Delta_{BA} \leftarrow$ DeltaAngle(ϕ_{CB}, ϕ_{CA})
$\Delta_{CA} \leftarrow$ DeltaAngle(ϕ_{BC}, ϕ_{BA})
$\Delta_{BC} \leftarrow$ DeltaAngle(ϕ_{AC}, ϕ_{AB})
if $(|\Delta_{BA}| > \Delta_{min})$ and $(|\Delta_{CA}| > \Delta_{min})$ and $(|\Delta_{BC}| > \Delta_{min})$ **then**
  $(X, Y) \leftarrow$ EstimatePosition($(\hat{x_A}, \hat{y_A}), (\hat{x_B}, \hat{y_B}), \Delta_{BA}, \Delta_{CA}, \Delta_{BC}$)
  $\beta \leftarrow$ CalculateWeighting(d_A, d_B)
  $\alpha \leftarrow 1.0 - \beta$
  $(\hat{x_C}, \hat{y_C}) \leftarrow \alpha(\hat{x_C}, \hat{y_C}) + \beta(X, Y)$
  Status $\leftarrow$ Known
  Send Neighbour Update Table
else
  Co-planar - Can not calculate position estimate
end if

two mutual neighbours (Figure 4.6), where each neighbour has a valid position estimate, and where the three nodes are not colinear (i.e., the angle between any two nodes is greater than $0°$). Once a new position estimate is formed, it is weighted depending on the anchor hop count of the two neighbours and then averaged using the AHDWL algorithm. When a node updates its local neighbour

Algorithm 6 Send Neighbour Table Update at node C

Msg $\leftarrow$ CreateMessage(ID, $(\hat{x}_C, \hat{y}_C)$, d_C)
for all j in Neighbour[] **do**
  Msg $\leftarrow$: AppendMessage(j, ϕ_{Aj})
end for
for all Transmitters TX_i with neighbour(s) associated with them **do**
  Power=max power to reach all neighbours associated with TX_i
  SendMsg(DST:ALL, SRC:self.id, TYPE:update, TXID:TX_i, POWER:Power$_{max}$, Msg)
end for

table it sends a Neighbour Table Update packet to its 1-hop neighbours. In Algorithm 6, the Neighbour Table Updates packets are sent at the minimum power required to reach all known 1-hop neighbours.
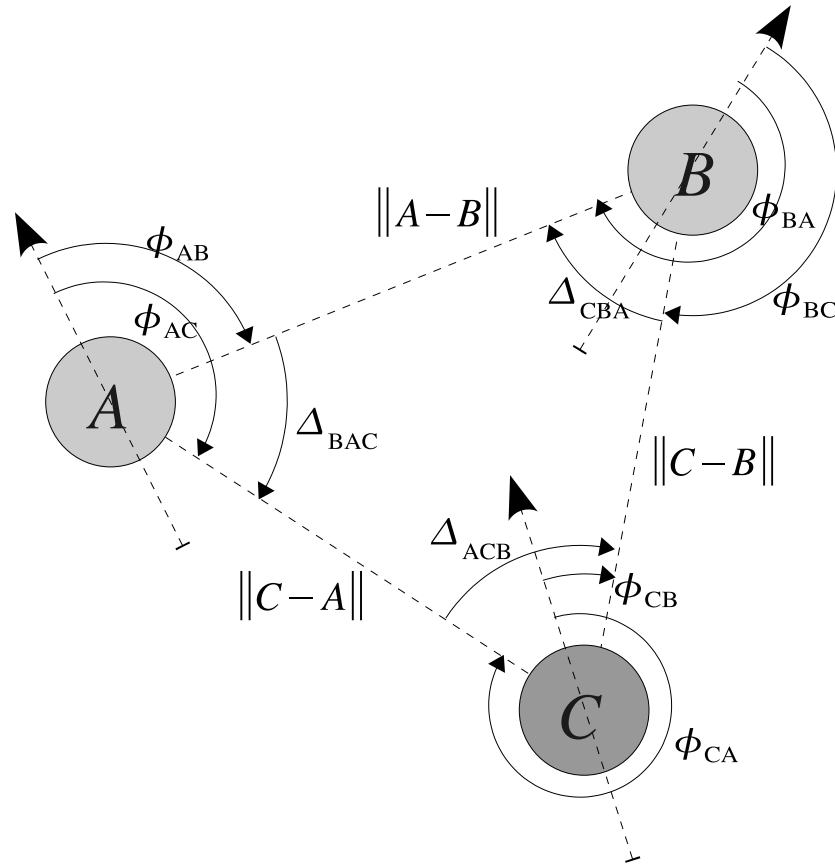
Figure 4.7: A small network of three nodes.

4.3.1 Algorithm Walkthrough

To better understand the localisation algorithm a walk through is presented. In this example, which is based on the small three node network shown in Figure 4.7, nodes A and B each have a valid position estimate, while initially, node C has no known neighbours or position estimate.

Initially, all three nodes have empty neighbour tables and are unaware of their neighbours. Each node broadcasts a sequence of Hello packets at varying power levels in all directions to announce its presence to neighbours. This allows the neighbouring nodes to estimate the relative bearing angle to the node which transmitted the Hello packets, and hence the angle to each of its 1-hop neighbours.

Nodes receive Hello packets from their neighbours, and then use the power level sequence to estimate the relative bearing angles to their immediate neighbours. On completion of the Hello packet sequence the neighbour tables at each node have been populated as follows:

$\mathbf{ID}_A$	$(\hat{x_A}, \hat{y_A})$	d_A
$\mathbf{ID}_B$	ϕ_{AB}	
$\mathbf{ID}_C$	ϕ_{AC}	

Node A

$\mathbf{ID}_B$	$(\hat{x_B}, \hat{y_B})$	d_B
$\mathbf{ID}_A$	ϕ_{BA}	
$\mathbf{ID}_C$	ϕ_{BC}	

Node B

$\mathbf{ID}_C$	invalid	∞
$\mathbf{ID}_A$	ϕ_{CA}	
$\mathbf{ID}_B$	ϕ_{CB}	

Node C

Each node now knows the ID and angle to each of its 1-hop neighbours. Next, all nodes broadcast their neighbour tables to their immediate neighbours. Every node now knows all bearing angles of their neighbours 1-hop neighbours. On completion of the Neighbour Table Update packet exchange node C's local neighbour table will contain the following information about itself, and its 1-hop neighbours:

ID	Current Pos. Est.	Anchor Hop Dist.	C	A	B
C (self)	-	d_C	-	ϕ_{AC}	ϕ_{BC}
A	$(\hat{x_A}, \hat{y_A})$	d_A	ϕ_{CA}	-	ϕ_{BA}
B	$(\hat{x_B}, \hat{y_B})$	d_B	ϕ_{CB}	ϕ_{AB}	-

Node C now uses the bearing angles, from its local neighbour table, to determine which 1-hop neighbours share mutual 1-hop neighbours with itself. If a 1-hop neighbour has a mutual neighbour a triangle can be formed between them. In this example all three nodes are mutual neighbours.

Once node C identifies pairs of mutual neighbours it can calculate all the discrimination angles Δ_{BAC}, Δ_{CBA} and Δ_{ACB}. The distance between nodes A and B

$(\|A - B\|)$ can be calculated as both $(\hat{x}_A, \hat{y}_A)$ and $(\hat{x}_B, \hat{y}_B)$ are known:

$$\|A - B\| = \sqrt{(\hat{x}_A - \hat{x}_B)^2 + (\hat{y}_A - \hat{y}_B)^2}. \qquad (4.3.1)$$

Using the method described in Section 3.6, a position estimate for node C can be calculated. This process is done iteratively to allow nodes to share new information. The AHDWL algorithm governs the way each node updates its local position estimate, with anchor hop count based weighting, to minimise the propagation of errors.

4.4 Evaluation of the AHDWL Algorithm

4.4.1 Evaluation Methodology

The performance of the AHDWL algorithm was conducted using a simulator created for this purpose as described in Appendix C. The simulator is based on the experimental infrared channel characteristics obtained from the infrared ad hoc network testbed, as described in Chapter 3.

The effectiveness of the AHDWL algorithm was evaluated by comparing its absolute position estimation errors of the nodes against the position estimates obtained using the iterative EWMA algorithm. Each algorithm was tested using two different network configurations: 100-node random topology (Figure 4.8) and a 100-node grid (Figure 4.9 . the random network is typical of a network which may be found in real life, where nodes are placed randomly without regard of resulting topology (however the nodes were arranged with minimum connectivity requirements to ensure all nodes in the network were able to calculate their position). The random network results in many poorly conditioned triangles, which provide a poor basis for position estimation using the method described

in Section 3.5. Whereas the grid network was chosen as the nodes are evenly distributed in a grid layout. This provides an excellent geometry for using the position estimation algorithms presented in section 3.5, as all triangles of in-range nodes produce reasonably well conditioned triangles, with a low sensitivity to measurement errors.

Each network topology evaluated contained 12 anchor nodes, with 3 nodes positioned at each corner of the simulation area. The anchor nodes must be placed in clusters of at least two, as the angle-based position estimation algorithm described in Section 3.5 requires at least two reference nodes to calculate a position estimate. The clusters of three anchor nodes at each corner were positioned in an L shape to provide a good geometric basis for localisation. If only two anchor nodes were placed at each corner, it would be possible that the anchor nodes would be colinear with the node attempting to calculate its position, in which case the node would fail to localise itself correctly. Positioning the three anchor nodes in a $90°$ arrangement allows the nodes to localise themselves with low risk of falling into colinear geometry.

Each scenario was simulated 20 times using different random number seeds. This ensured that the results obtained were a good indication of what would be expected to occur in a physical, real life, network. Each algorithm (EWMA and AHDWL) was simulated using the same set of 20 seeds, this ensured that node orientation, IR component placement and message ordering was kept constant for each algorithm. This meant that the only variable changed between experiments was the algorithm used to filter the instantaneous position estimates.

For each experiment the EWMA smoothing factor, β_{base}, was empirically set to 0.7. The larger β_{base}, the faster the algorithm will respond to change. However,
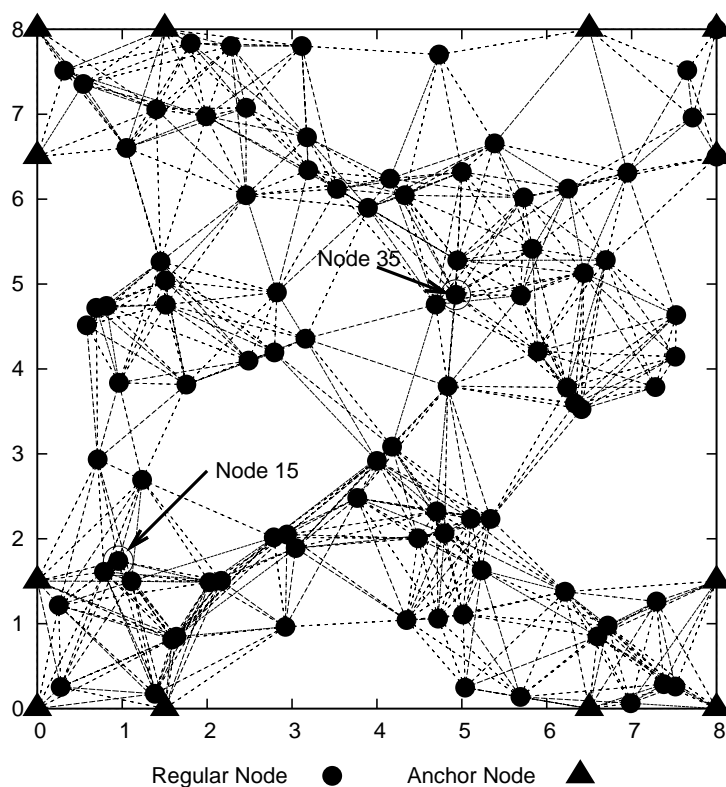
Figure 4.8: 100-node random network.

increasing β_{base} also increases the sensitivity of the algorithm to transient fluctuations. A β_{base} of 0.7 was found to provide quick convergence of position estimates with reasonable noise immunity.

4.4.2 Simulation Results

100-Node Random Topology

The first network presented is a randomly placed 100-node topology (Figure 4.8). Two nodes (nodes 15 and 35) were selected for special attention, to illustrate the expected behaviour at different locations within the network.

The position estimation error distribution is shown in Figure 4.10. The red surface represents the position errors when using the iterative EWMA algorithm. The
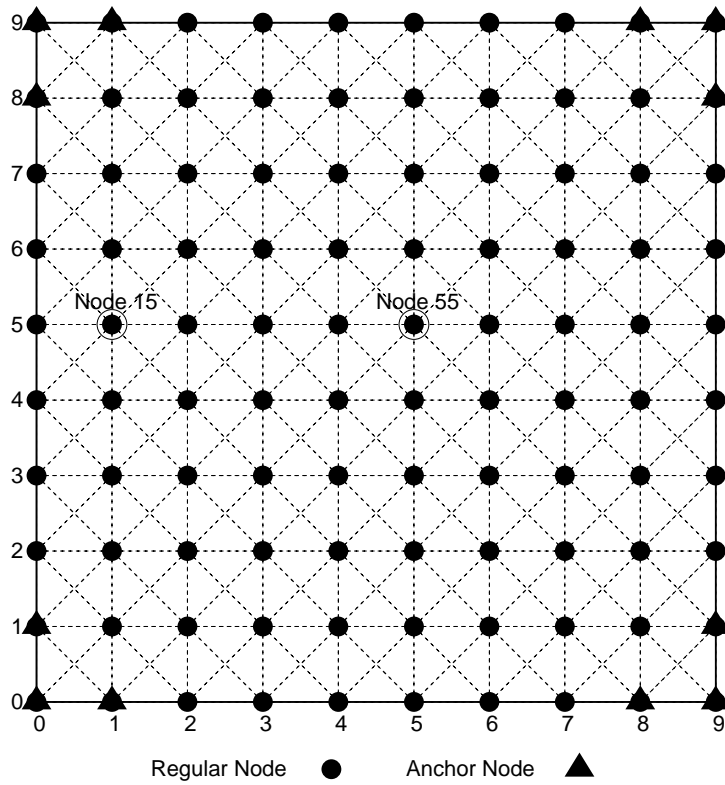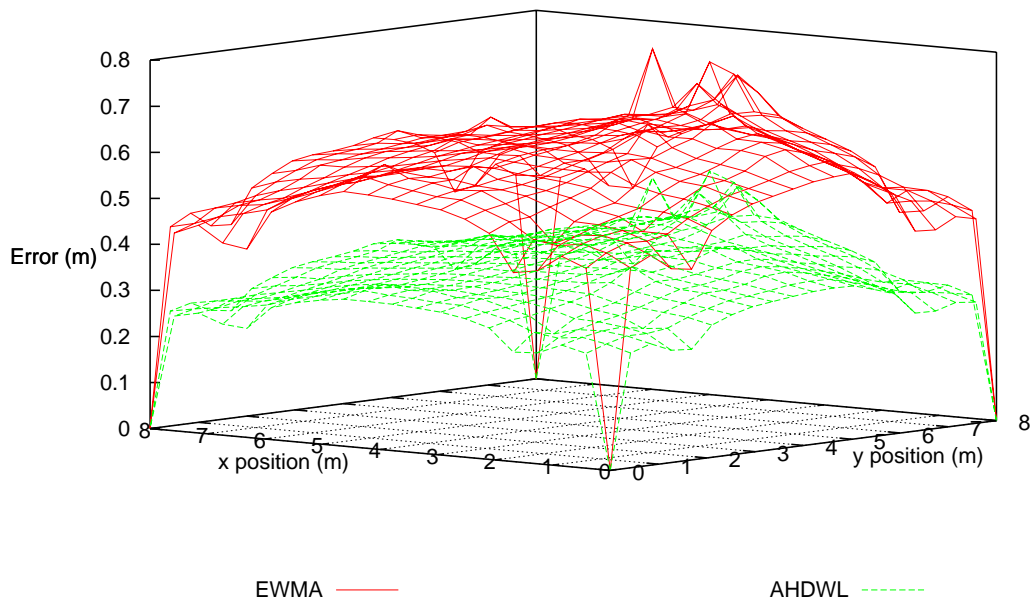
Figure 4.9: 100-node grid topology.

Figure 4.10: Position estimation error for the 100-node random topology.

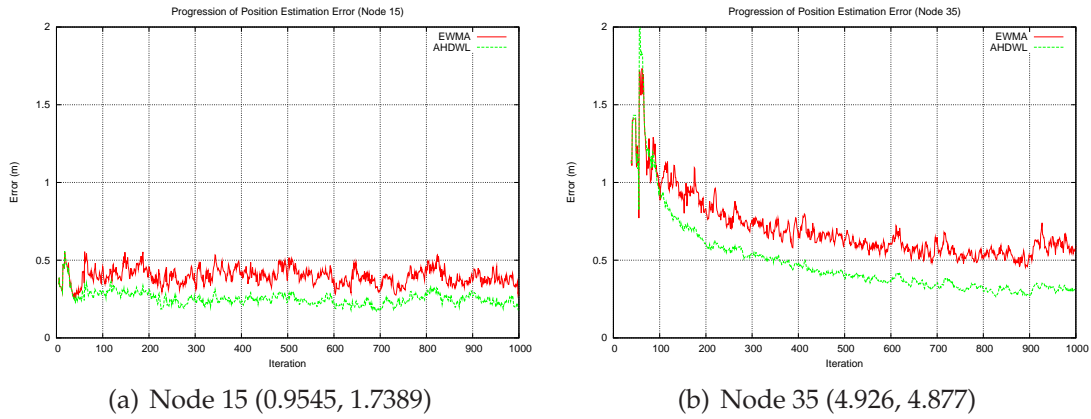(a) Node 15 (0.9545, 1.7389)   (b) Node 35 (4.926, 4.877)

Figure 4.11: Convergence of position estimation errors for the 100-node grid topology.

green surface represents the position estimation errors across the network with the AHDWL algorithm. It can be easily seen that the introduction of weighting factors based on the anchor hop distance greatly improves the position estimates for all nodes within the network.

Figure 4.11 shows the two nodes chosen for special attention in the 100-node random topology. Node 15 was chosen to represent nodes which are close to the anchor nodes, and Node 35 was chosen to represent nodes near the middle of the network. Figure 4.11 show that the AHDWL algorithm converges to a more accurate position estimate than the fixed-weight iterative EWMA algorithm. Node 15 is able to localise itself more accurately than node 35, as it is closer to anchor nodes and thus the position estimates have encountered less hops, and therefore have had less chances to become corrupted by measurement errors.

A histogram of position estimate errors for all nodes in the 100-node random topology network is shown in Figure 4.12. The red bars represent the fixed-weighted iterative EWMA algorithm, and the green bars represent the AHDWL algorithm with anchor hop distance based weighting. It can be seen that the AHDWL algorithm resulted in significantly more nodes being able to estimate their position more accurately, while also significantly reducing the number of
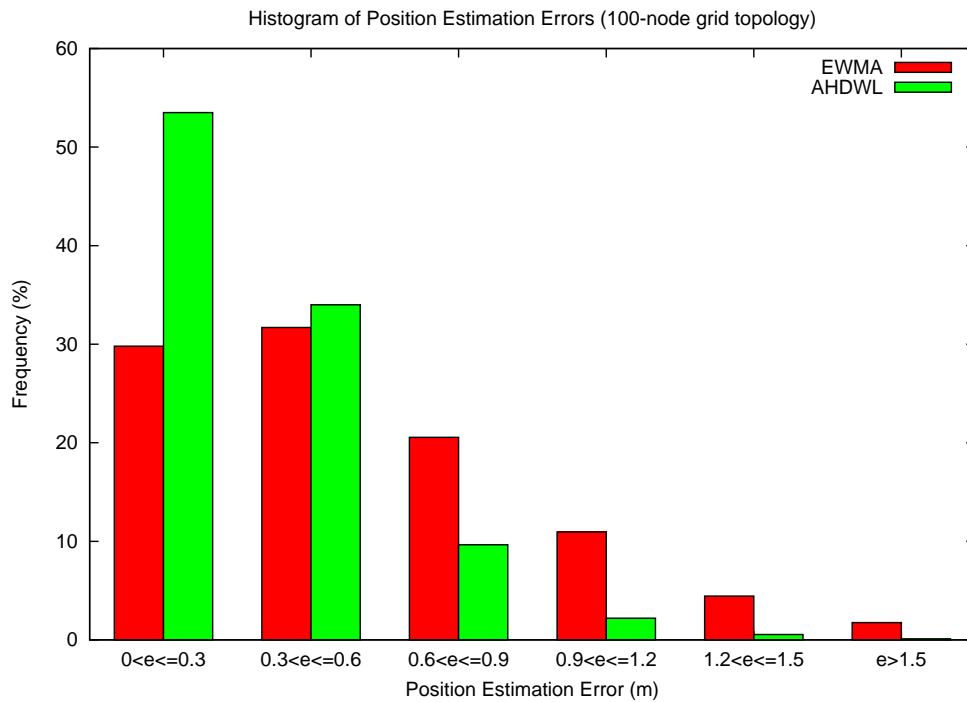
77

Figure 4.12: Position estimation error histogram for the 100-node random topology.

large position estimate errors within the network.

100-Node Grid Topology

A grid topology is presented to demonstrate the effectiveness of the algorithms when nodes are placed in a regular pattern with good geometry for angle-based localisation techniques. The topology consisted of nodes uniformly spaced on a 1 metre grid. Again, 12 anchor nodes in total were placed in L shaped clusters of 3 at each corner of the network.

Figure 4.13 shows the position estimate errors for the 100 node grid topology. The green surface represents the errors when using the AHDWL algorithm, and the red surface represents the fixed-weighted iterative EWMA algorithm. The AHDWL algorithm results in improved localisation accuracy.
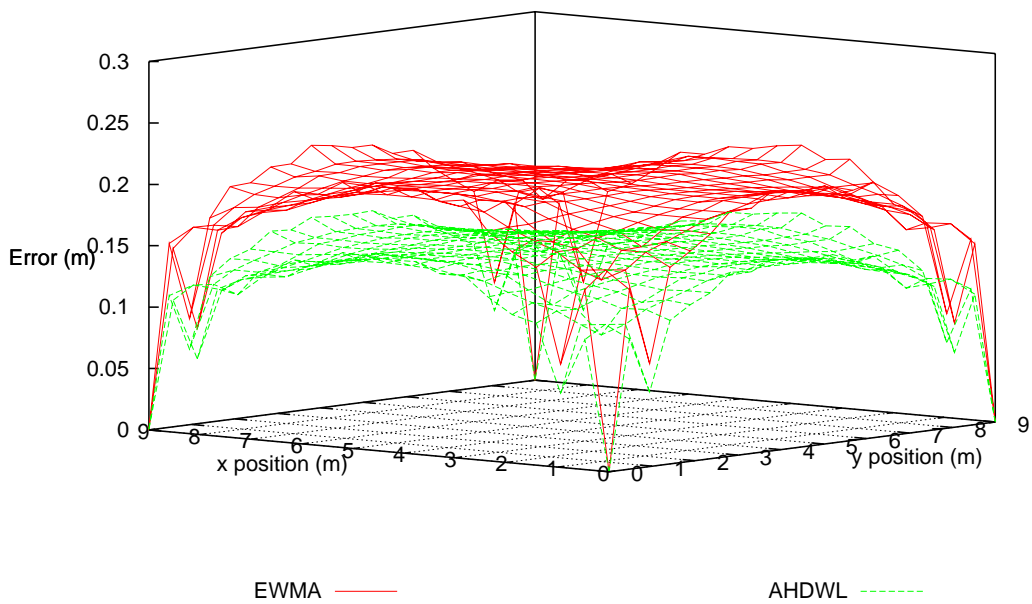
Figure 4.13: Position estimation errors for the 100-node grid topology.

Two nodes were chosen to evaluate the performance of the algorithms at different locations in the network. Figure 4.4.2 shows the position estimate accuracy at two locations: Node 15 represents nodes which are relatively close to the anchor nodes, and Node 55 represents nodes close to the middle of the network.

In this case, both nodes appear to have approximately the same average position error. This is most likely due to the topology being a relatively small, grid based topology, which consists of well conditioned triangles, therefore the sensitivity of the position estimates to angle measurement errors is low.

Furthermore, the node nearer to the centre of the network appears to have a slightly better position estimate, this may be due to the fact that it is receiving information from all anchor nodes with equal weighting (as it in in the centre). For both nodes, the AHDWL algorithm results in more accurate position estimates.

The error histogram for the 100 node grid network is shown in Figure 4.15, the red bars represent the fixed-weight EWMA algorithm, and the green bars represent the AHDWL algorithm. The histogram, again, shows that the use of the AHDWL
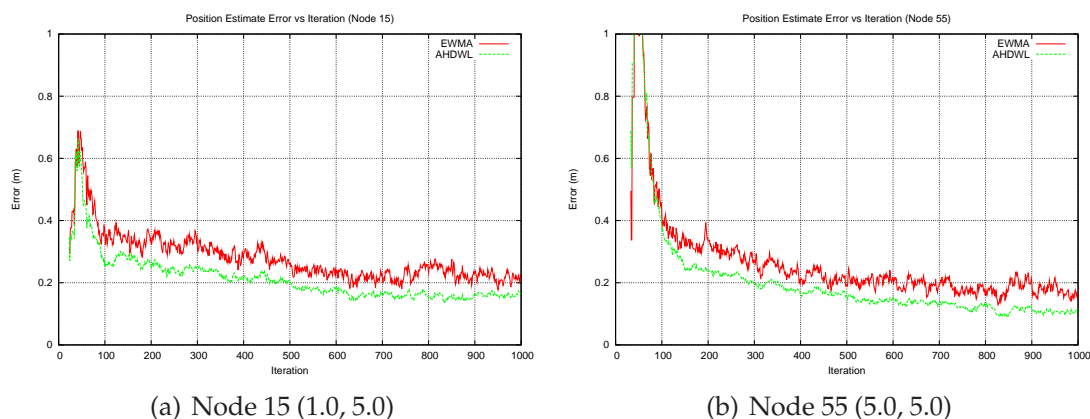
(a) Node 15 (1.0, 5.0)　　　　　　　(b) Node 55 (5.0, 5.0)

Figure 4.14: Convergence of position estimation errors for the 100-node grid topology.

algorithm results in more accurate position estimates.

4.5 Discussion

The results obtained from this experiment using multiple topologies show that it is beneficial to use anchor hop distance as a metric for quality of position estimates in iterative based localisation for ad hoc networks, where nodes rely on neighbouring nodes in order to localise themselves. By selectively weighting estimates based on their anchor hop distance, it is possible to reduce the position estimate errors of each node in the network. This also effectively reduces position estimation error accumulating in multi-hop localisation systems, where nodes rely solely on their neighbours, which may not be anchor nodes, to calculate their own position estimates.

From the results of the experiments, when doing localisation within a multi-hop network where there are a limited number of anchor nodes, it is beneficial to include weighting based on the anchor hop distance of the information.
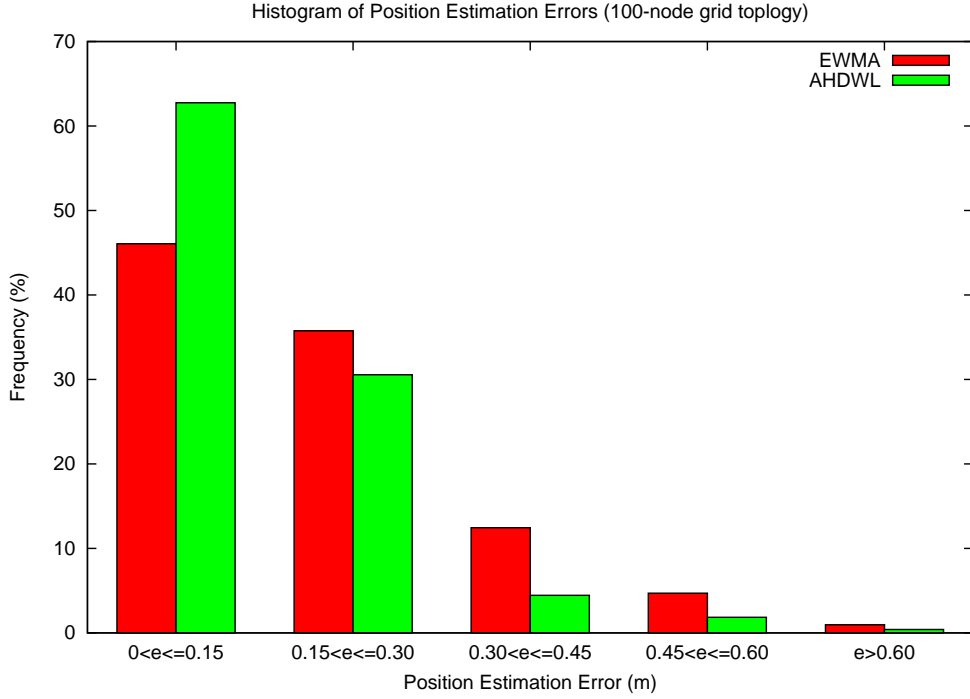
Figure 4.15: Position estimation error histogram for the 100-node grid topology.

It is believed that anchor hop distance could be incorporated into existing lo-
calisation algorithms such as iterative multilateration [SHS01]. Multilateration
attempts to minimise the square of the position estimation errors using a MMSE
type algorithm such as,

$$F\left(x_0, y_0, s\right) = \sum_{i=1}^{N} \alpha^2 f_i \left(x_0, y_0, s\right)^2.\qquad(4.5.1)$$

Where the difference between the measured distance to node 0 (st_{i0}), and the
calculated position based on the current position estimate is,

$$f_i\left(x_0, y_0, s\right) = \text{st}_{i0} - \sqrt{\left(x_i - x_0\right)^2 + \left(y_i - y_0\right)^2}.\qquad(4.5.2)$$

By modifying the weighting factor, α, in Equation (4.5.1) it is possible to weight
each piece of information differently. One such weighting technique may be to
calculate α based on the anchor hop distance of the reference nodes being used.

In this case the MMSE algorithm will attempt to minimise the squared error of the high quality position information (i.e., smaller anchor-hop distance) in favour of minimising the squared error of the lower quality (i.e., larger anchor-hop distance) information.

4.6 Summary

By introducing weighting coefficients based on the hop distances between the anchor nodes and the node running the algorithm, the AHDWL scheme is able to reduce the accumulation of position errors. This results in significantly increased position estimation accuracy of each nodes in the network.

Many existing algorithms, such as multilateration, have the ability to accept unique weighting of individual position estimates. From the results of the AHDWL algorithm, it is clear that using the anchor-hop distance is an effective method of estimating the quality of a particular position estimate. Therefore, introducing weighting based on anchor-hop distance should help to reduce the accumulation of position estimates in existing multihop localisation schemes.

Chapter 5

Conclusions and Recommendations for Future Work

5.1 Conclusion

Localisation in wireless ad hoc networks allows nodes in the network to learn their physical position within the network. In large ad hoc networks, nodes may not be within range of an anchor node, and will rely on position information that has been passed through multiple hops. Traditionally, iterative range-based localisation schemes suffer from an accumulation of errors due to range or angle measurement errors at each node, which effects the accuracy of the position estimates of each node. The anchor hop distance algorithm proposed in this research improves the position estimates of all nodes in the network by selectively weighting individual position estimates based on the number of hops the information has travelled from the anchor nodes. Position estimates formed from information that has travelled through many nodes will receive a lower weighting, whereas, those formed from information which has passed through fewer hops will receive a higher weighting. By giving older information lower weighting, error propagation is reduced as newer information is favoured over older information. This

effectively reduces the distance errors can travel in the network.

A physical testbed was developed to evaluate the anchor hop distance localisation algorithm as well as the ability to estimate angles to neighbours using directional IR channels without explicit RSSI being available. The testbed utilised directional infrared communication channels based on low-cost, readily available components. A method for estimating angles to neighbours based on the inferred quality of the infrared channel between the nodes was developed. The angle estimation algorithm was found to provide accurate inter-node angle estimates without explicit RSSI being available.

Using the infrared channel characteristics from the physical testbed it was shown that weighing individual position estimates based on anchor hop distance in iterative multihop localisation systems greatly improves the position estimate accuracy for all nodes in the network. Many existing distributed localisation algorithms can be modified to apply weightings to individual pieces of information based on anchor hop distance. This should improve the accuracy of these algorithms, while retaining their individual strengths.

5.2 Recommendations for Future Work

The main goal of localisation in ad hoc networks is to provide accurate position estimation while minimising the energy consumption and communication overhead. The AHDWL algorithm presented in this thesis does not attempt to minimise energy consumption, however many existing localisation algorithms have been developed for ad hoc networks which aim to minimise the required energy. It would be possible to adapt these algorithms to incorporate the AHDWL scheme while retaining their original low energy and communication overhead properties.

In chapter 3 it was shown that transmission based angle estimation yielded more accurate angle estimates. However, transmission based angle estimation requires MAC to ensure effective communication between nodes. The presented AHDWL algorithm should be implemented on a network which provides MAC. The efficiency of the MAC algorithm should be considered and modifications may be required, particularly in the angle estimation phase where effective collision free communication is required, in order to accurately calculate angle estimates.

In multihop localisation systems, anchor nodes are relatively expensive, either in terms of required hardware (eg, GPS) or initial configuration (eg, manually configuring each node's position). It is therefore important that the network does not contain unnecessary anchor nodes. The number of anchor nodes should be minimised by carefully positioning the nodes in optimal locations, while ensuring that they provide a good basis for regular nodes to estimate their positions.

Mobile ad hoc networks are being deployed where nodes are able to move. Obviously localising mobile nodes accurately is important in order to establish the location of each node within the network. Mobility presents challenges to networks as they have dynamic topologies, and links between nodes will be broken and formed as nodes begin to move relative to one another. The anchor hop count algorithm presented should gracefully deal with mobility. However, due to the EWMA filtering the algorithm may respond slowly to change. While EWMA weighting can be modified to respond faster to change, this will result in higher sensitivity to erroneous position estimates and measurement errors. Some existing algorithms have been presented which attempt to overcome the problem of mobility in ad hoc networks, and anchor hop distance could also be incorporated into these algorithms to improve localisation accuracy in these networks.

Ad hoc networks are being deployed in many different environments. One exciting area of research is the deployment of wireless nodes in aquatic environments to measure environmental parameters, which then can be used to create models of bodies of water in order to develop ways of improving the quality of such systems. Infrared has been shown to work in underwater environments. The infrared angle estimation presented in this work should be tested underwater to understand limitations of the system in water, and to develop methods to improve the accuracy and range of the infrared system presented.

Furthermore, underwater networks will typically require 3D localisation. It is believed that by creating a sphere shaped node with infrared components located evenly around the surface, that the algorithm presented can be extended to allow 3D localisation with the addition of another angle measurement. The direction of neighbours will then be represented by an azimuth and zenith angle. Position estimation in 3D will require at least one more reference node than the 2D case in order to unambiguously localise itself. The presented angle estimation algorithm estimates angles in a 2D plane. The algorithm could be extended to estimate angles in 3D space, this would require infrared channel characteristics in both the azimuth and zenith angles.

Appendix A

Sens-R: Pulsed Infrared Light Network Node

A.1 Overview of the Sens-R Testbed

The Sens-R testbed was developed to evaluate the angle based localisation algorithm presented in this thesis. Each node consists of two circuit boards: The main processing board which is responsible for high level algorithms, and the communication board which contains the IR transmitters and receivers. The Sens-R nodes are based on Atmel 8-bit AVR microcontrollers as there is a portable, well maintained and open source tool chain based on the GNU C Compiler (GCC) [Fou]. Atmel AVRs also offer a rich set of on-chip peripherals, such as analog to digital converters (ADCs), timers and pulse width modulator (PWM) outputs. The number of devices in the AVR family also provides an easy upgrade path to more capable AVRs in the future, without significantly changing the underlying code base. In some cases, such as the ATmega2561, the upgrade does not require any circuit modifications either, as it is pin compatible with the ATmega128 device used.
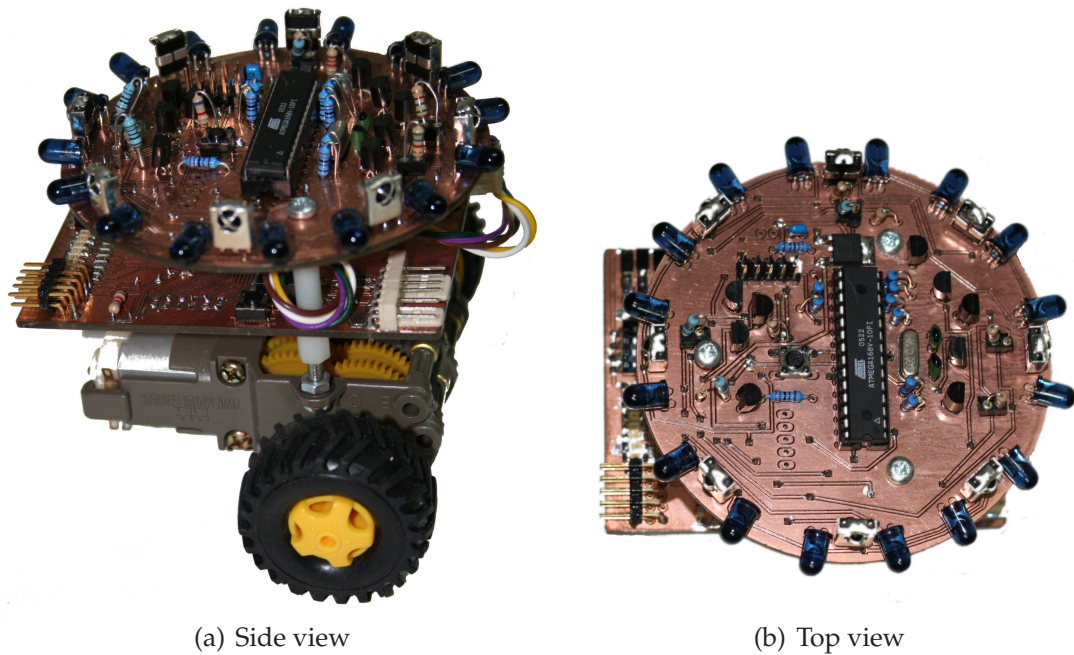
(a) Side view   (b) Top view

Figure A.1: Sens-R node with directional infrared channels.

MAIN PROCESSING SUBSYSTEM
• Atmel ATmega128 microcontroller [Atma]
• Micro-C/OSII real time operating system (RTOS) [Lab02]
• 8 10-bit analog to digital (ADC) channels
• 8 LED status indicators
• 4 mode selection switches
• Serial and JTAG debug port
COMMUNICATIONS SUBSYSTEM
• Atmel ATmega168 microcontroller [Atmb]
• 16 30° half-power cone with variable intensity infrared transmitter modules
• 8 90° half-power cone infrared receiver modules (BRM-1030 [Bri])
MOBILITY SUBSYSTEM
• Tamiya 70097 twin-motor gearbox
• Dual pulse width modulated controlled motors
• Dual optical rotary encoders for measuring wheel rotation

Table A.1: Subsystems and major components of the Sens-R nodes.
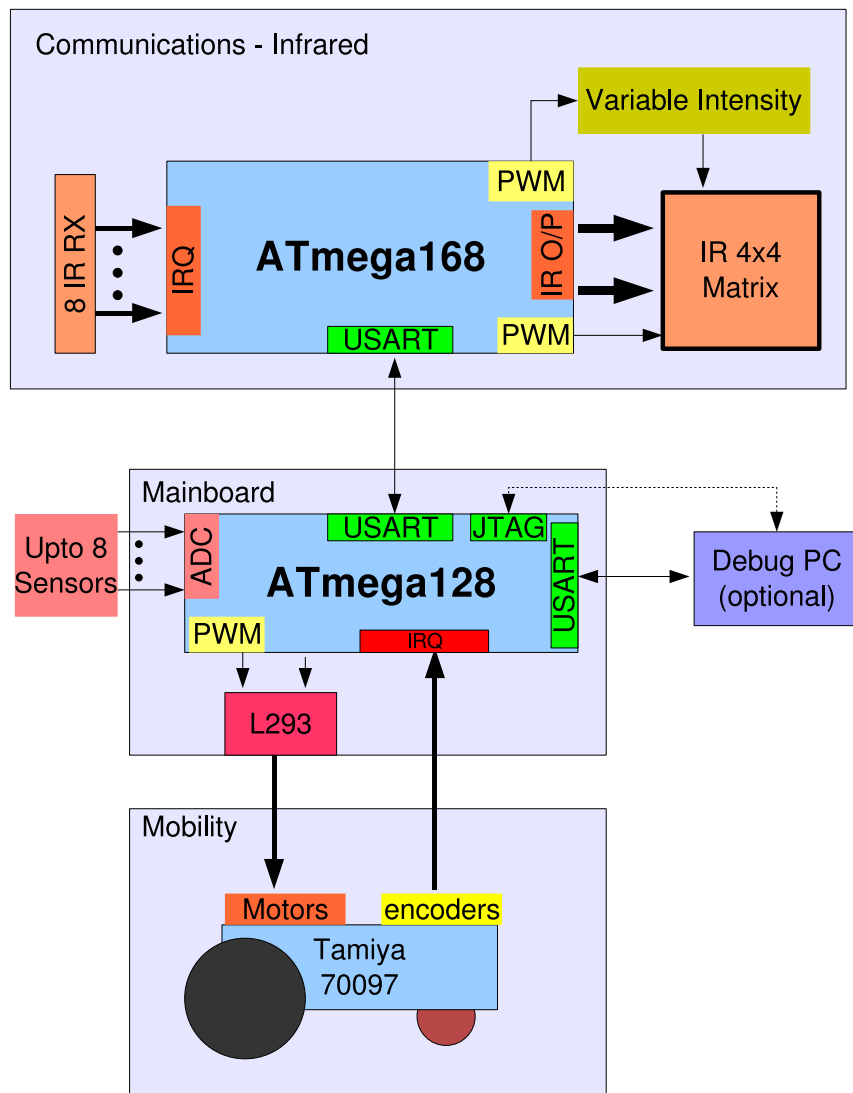
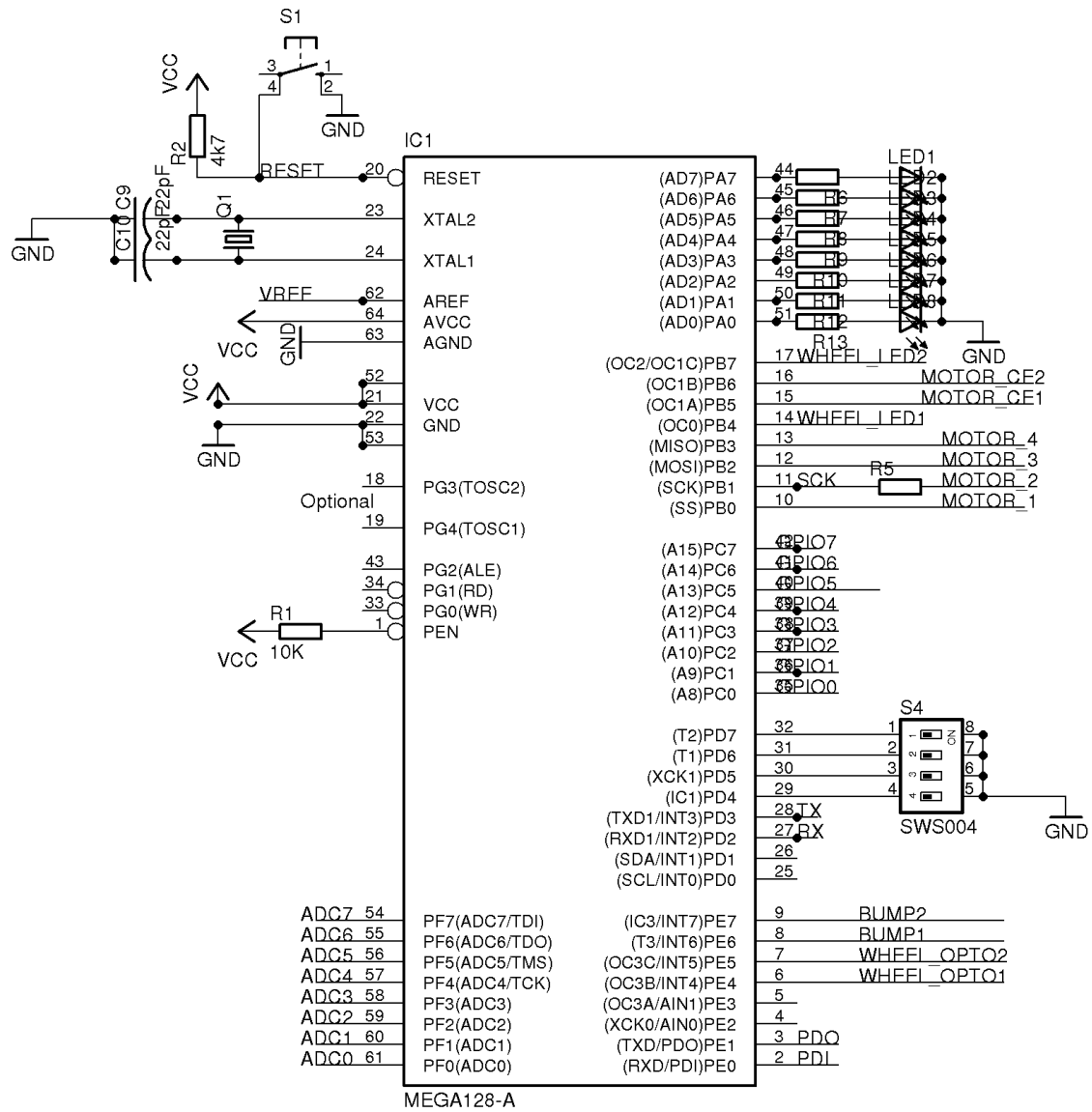Figure A.2: Interconnection of the subsystems of a Sens-R node.

Figure A.3: Main processing board circuit diagram: Microcontroller.
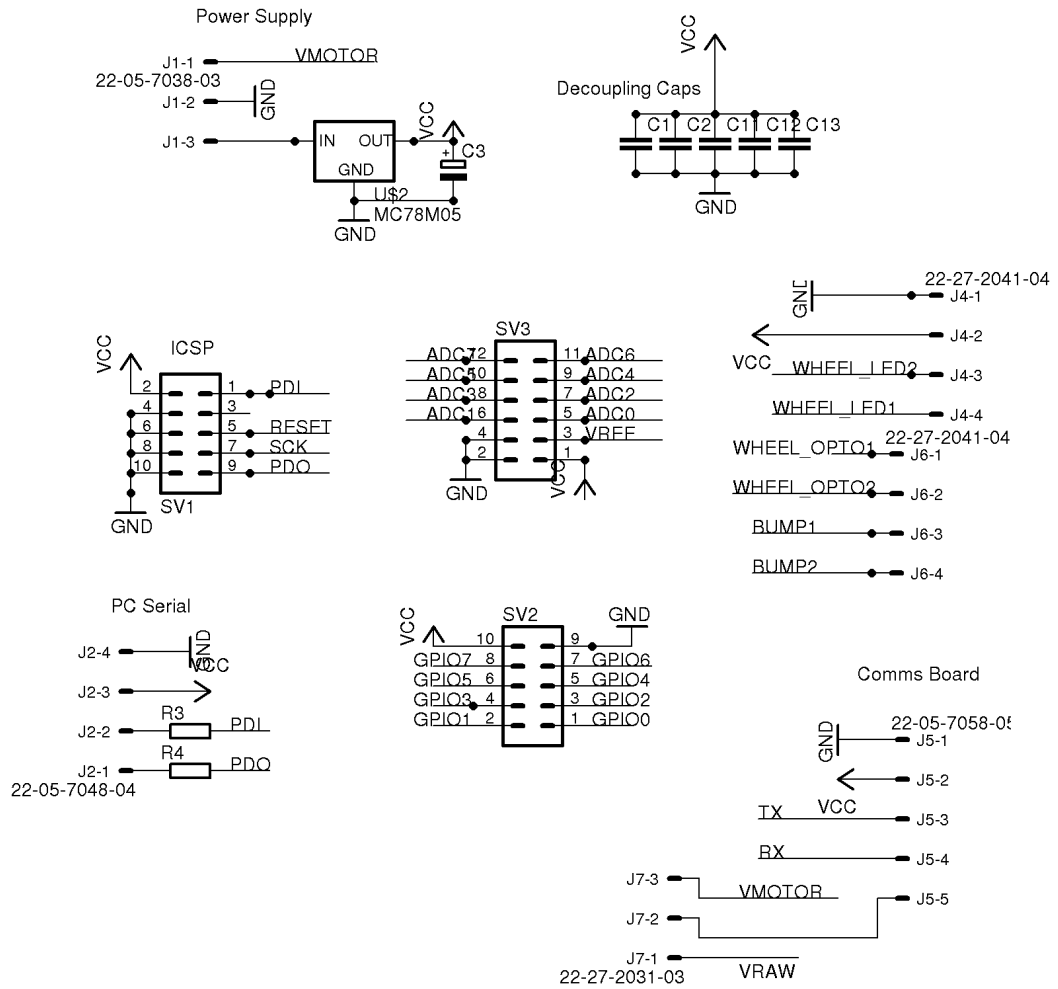
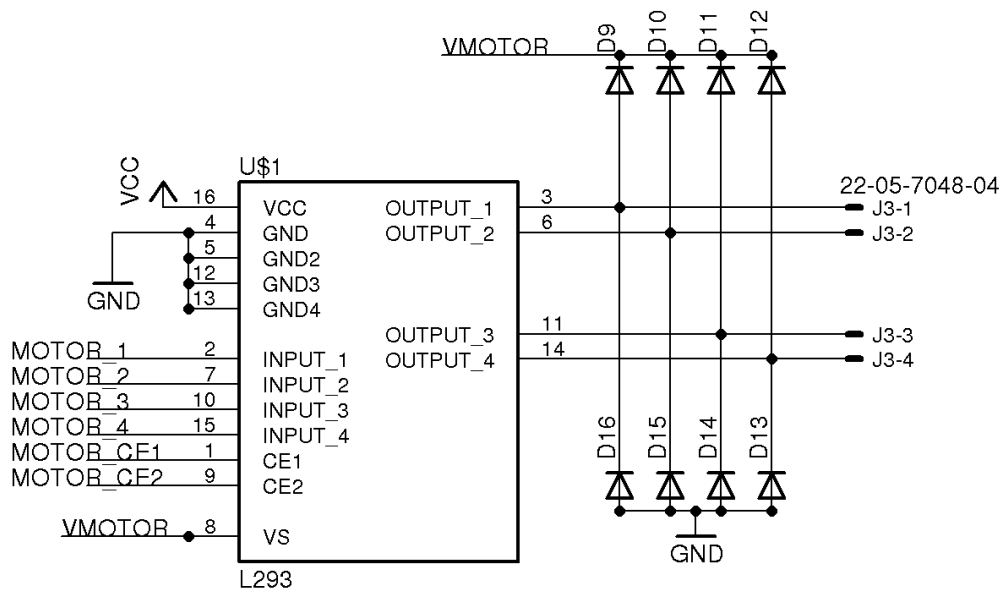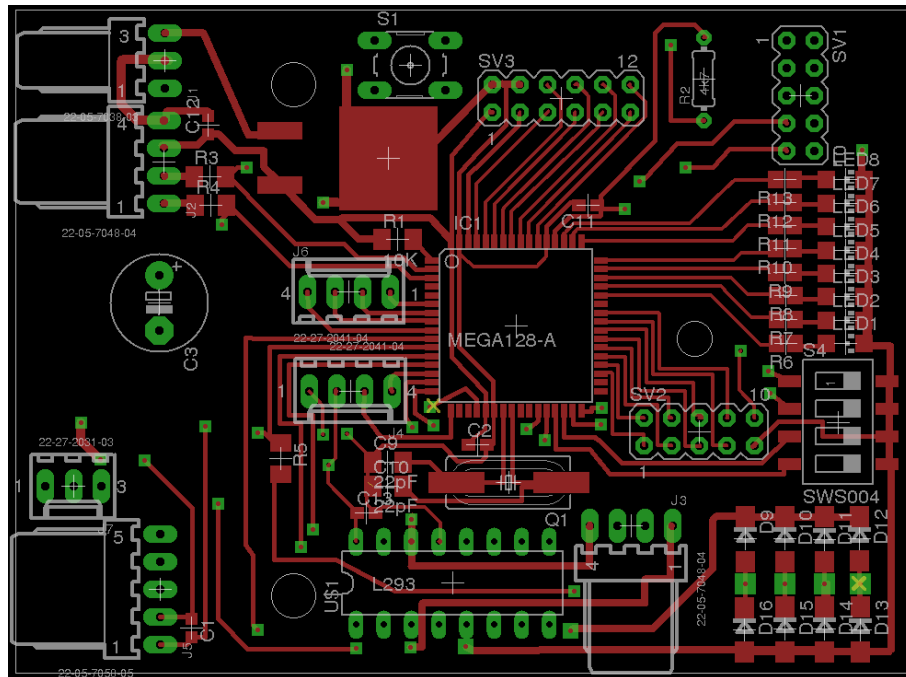Figure A.4: Main processing board circuit diagram: Power and connectors.
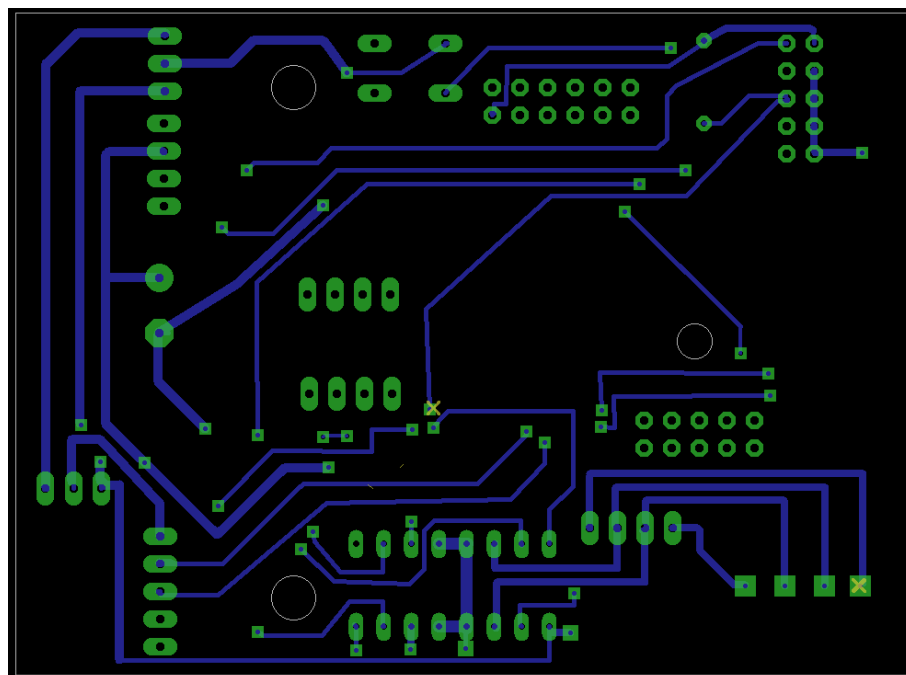
Figure A.5: Main processing board circuit diagram: Motor control.

(a) Top layer

(b) Bottom layer

Figure A.6: Processing board layout (Dimensions: 8cm x 6cm).

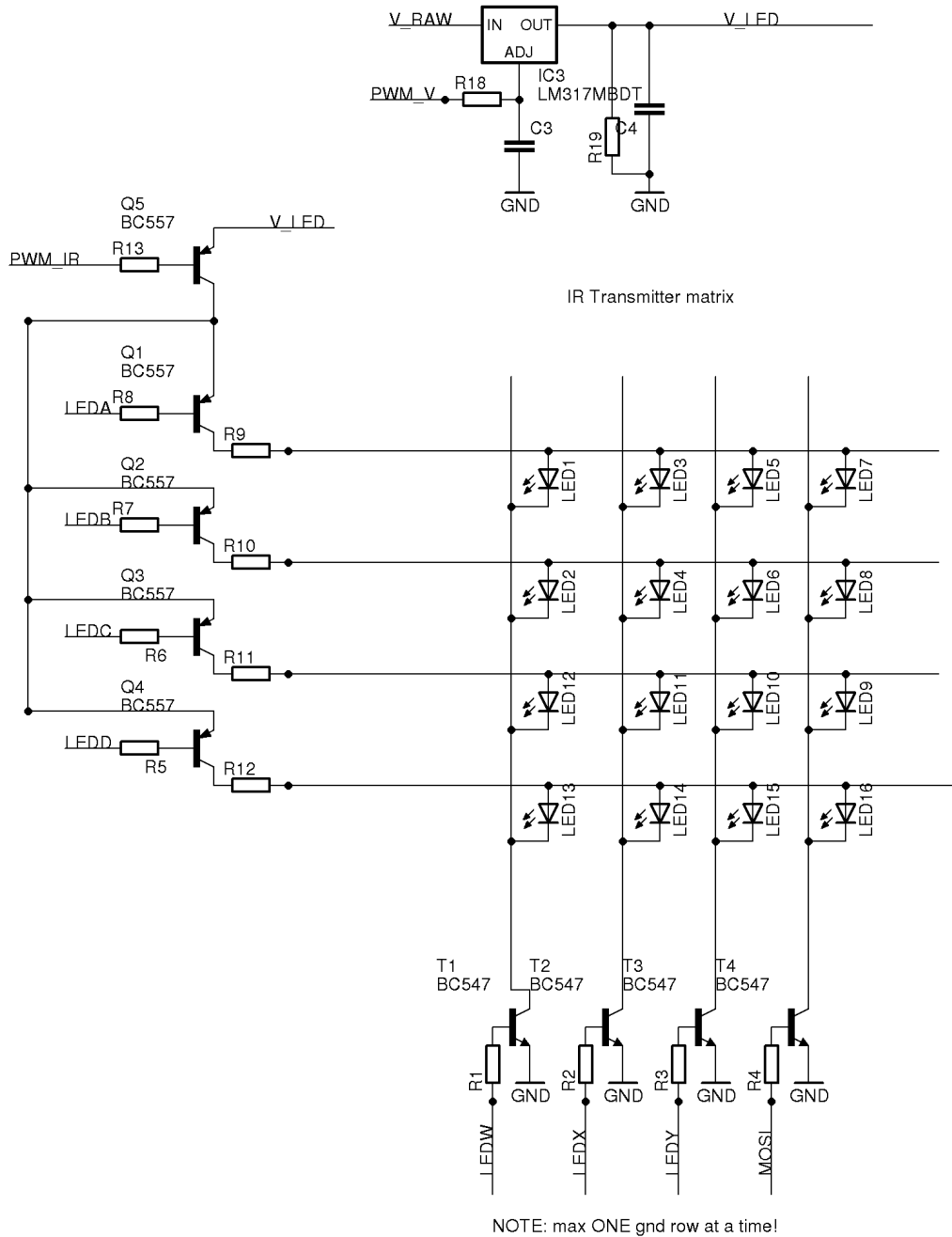Figure A.7: Communication board circuit diagram: Microcontroller.

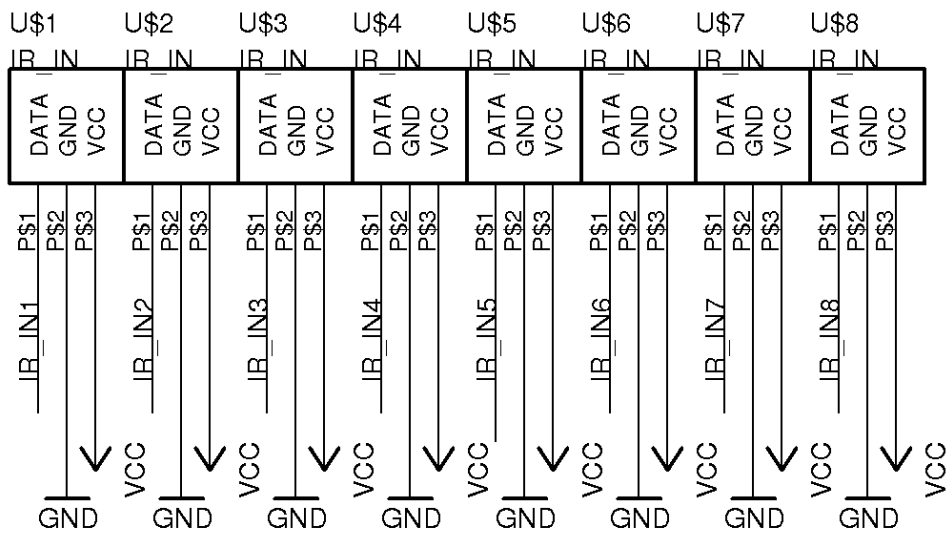Figure A.8: Communication board circuit diagram: Infrared transmitters.
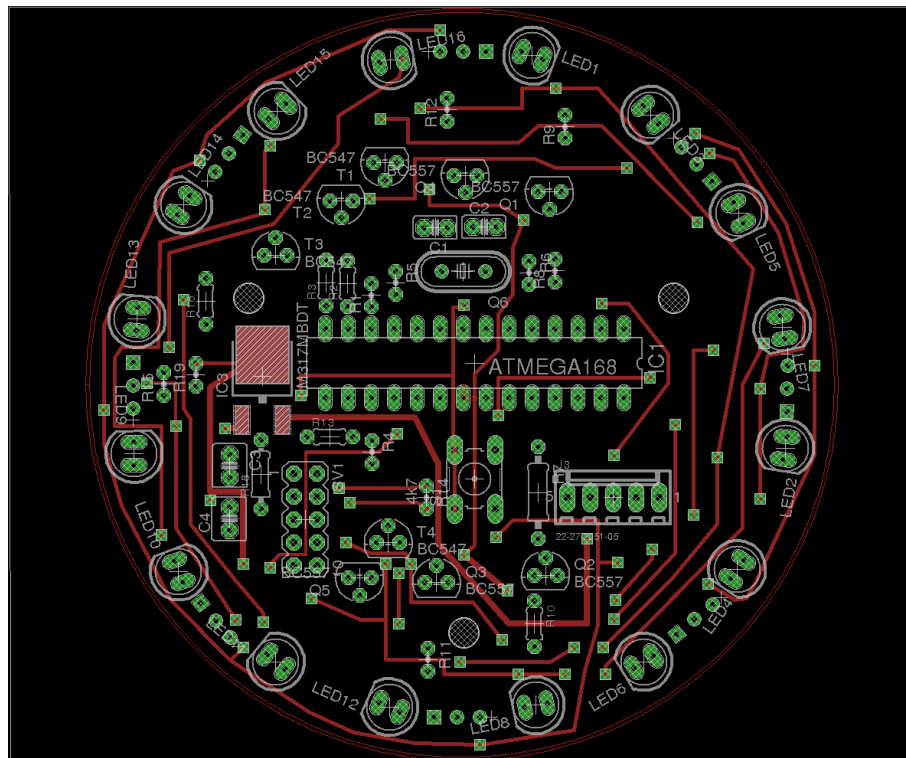
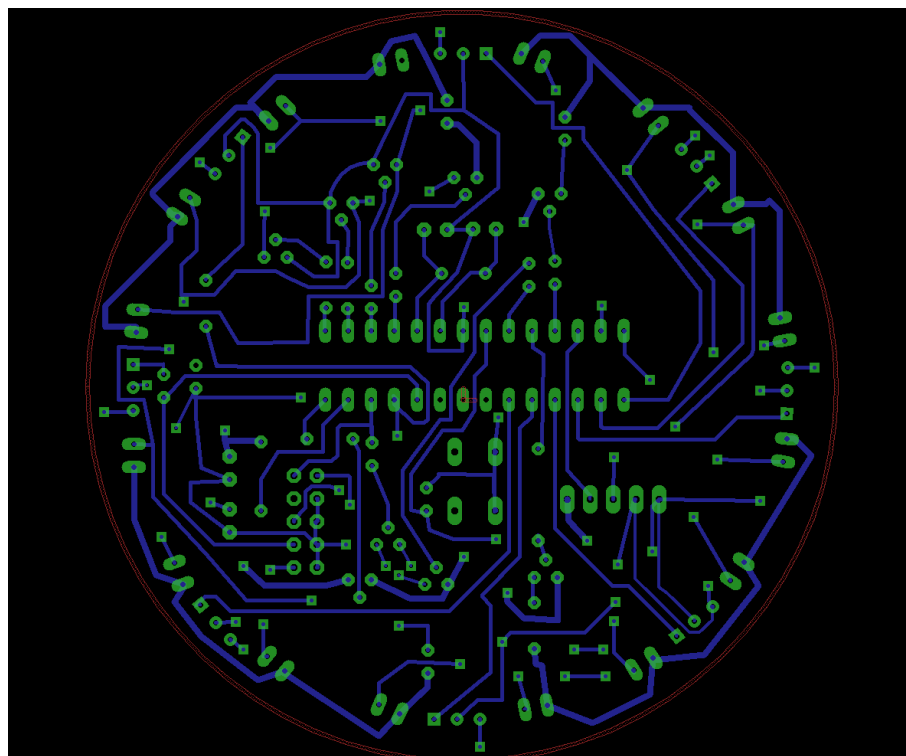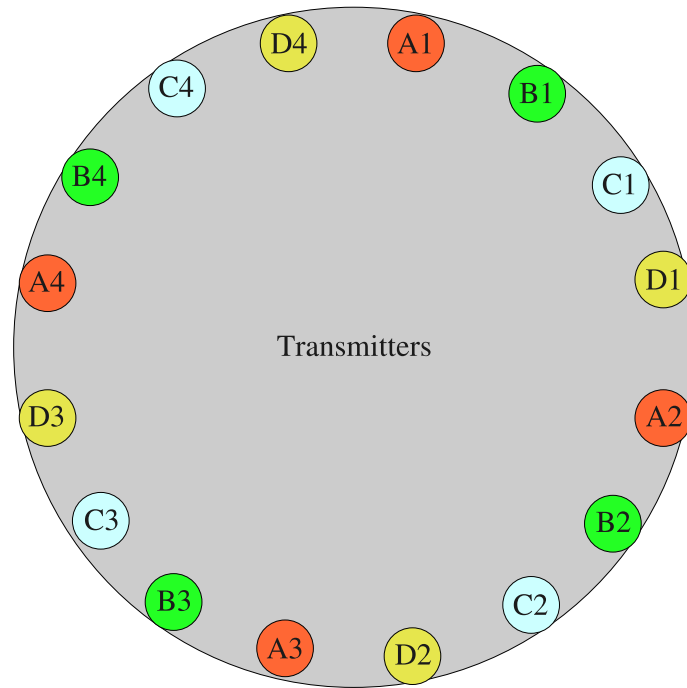Figure A.9: Communication board circuit diagram: Infrared receivers.
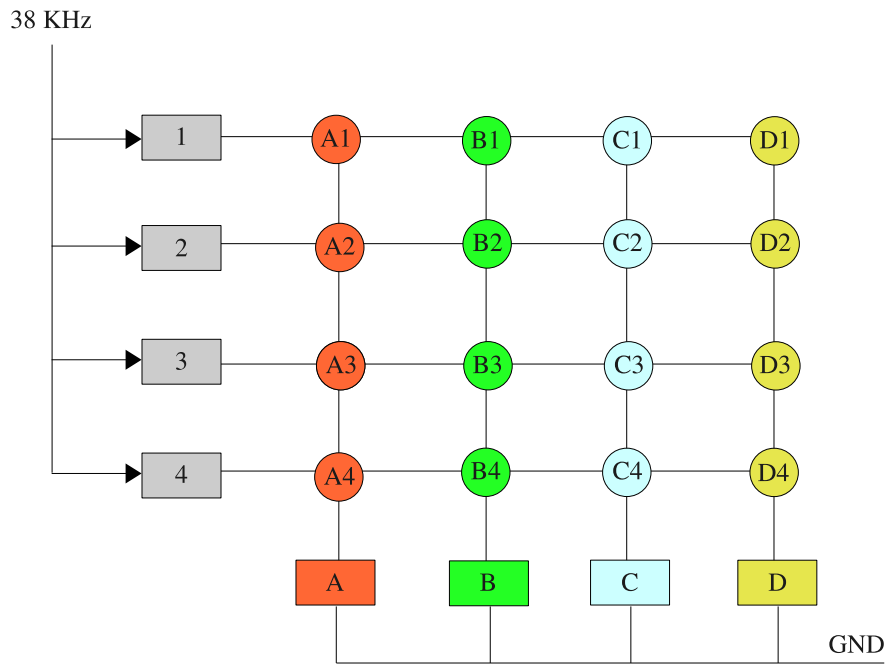
(a) Top layer

(b) Bottom layer

Figure A.10: Communication board layout (Diameter: 8cm)

(a) Component layout

(b) Infrared switching logic

Figure A.11: Sens-R infrared transmitter configuration - 16 IR LEDs in 4×4 matrix. To ensure consistent transmission power, only one ground switch can be activated at a time.

A.2 Details of the Infrared Communication System

The communication system allows decoding of messages on all eight receiver modules simultaneously. The transmitters, however, were arranged in a 4x4 matrix, partially due to the limited availability of I/O pins on the ATmega168 microcontroller. The transmitting matrix was designed to allow up to four independent transmissions using four of the IR LEDs spaced $90°$ apart. This limitation also ensures neighbouring transmitter LEDs transmissions do not overlap and interfere with each other, and additionally reduces the instantaneous current required to power the array of the infrared LEDs .

The infrared transmission power is controlled using a variable voltage source with a software controlled pulse width modulated (PWM) output from the ATmega168 to set the output voltage. The larger the PWM duty cycle, the higher the supply voltage to the infrared LED and series resistor combination, and hence higher the transmission power. As the IR LEDs theoretically have a constant forward voltage of approximately 1.4 V, the current though the resistor-LED circuit should ideally be linearly dependant on the supply voltage. The power ($\mathrm{P_{LED}}$) dissipation in the LED element can be calculated as,

$$\mathrm{P_{LED} = V_D \left(\frac{V_R}{R} \right)} \tag{A.2.1}$$

where $\mathrm{V_D}$ is the voltage drop across the LED and $\mathrm{V_R}$ is the voltage drop across the series $R\,\Omega$ resistor. This was taken to be a reasonable approximation of actual transmitted power. However, it did neglect non-infrared power being dissipated by the device and any non-linearities of the components.

Figure A.12 shows the relationship between the duty cycle of the variable voltage supply control signal and the power dissipation of the LED based on an experiment of five separate LEDs. The larger uncertainly of the higher supply voltages
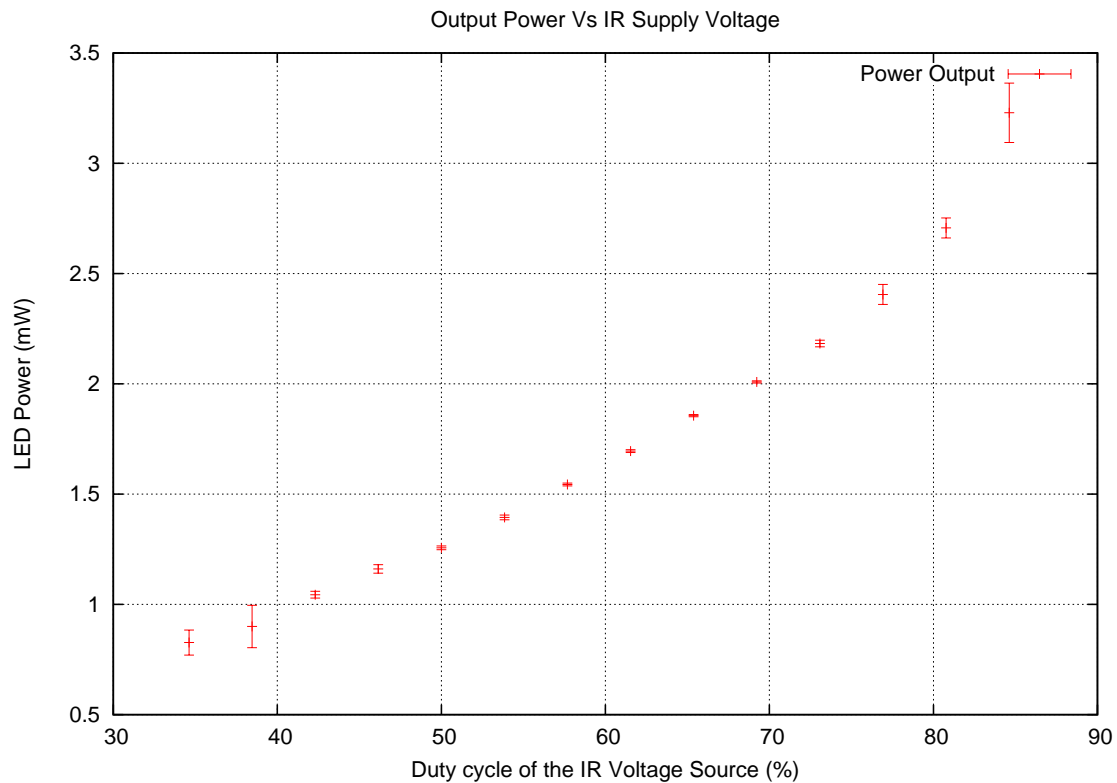
Figure A.12: LED power dissipation vs PWM duty cycle.

is likely caused by differences in the voltage regulator, switching logic and LED components.

Each of the receiver modules were connected to a dedicated input pin of the ATmega168 with edge triggered interrupts. This provided fully interrupt driven reception and decoding of eight separate data streams simultaneously, without significant processing overhead.

The variable intensity LED supply was implemented using a variable linear voltage regulator (LM317 [Sem]) (Figure A.13). The LM317 is a variable linear positive voltage regulator which essentially maintains an output voltage of 1.2 V above the (high impedance) adjustment voltage pin. The microcontroller used PWM, with a low pass R-C filter, to create an adjustable analog voltage. This was used as the adjustment voltage reference for the LM317. As the logic supply of
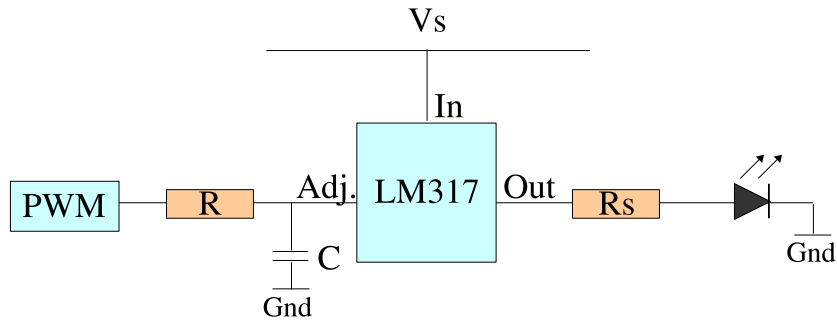
Figure A.13: Variable transmission intensity control.

the microcontrollers was set at 5V, the output range of the LM317 was between 1.2 V (duty cycle = 0%) and 6.2 V (duty cycle = 100%), provided that the input voltage (V_s) is sufficiently large enough to provide a 6.2 V output from the LM317 regulator.

The voltage output of the LM317 is given by,

$$V_{\text{out}} = V_{\text{cc}} \left(\frac{\text{Duty Cycle}}{100} \right) + 1.2. \tag{A.2.2}$$

Therefore, the current (I) through the LED and series resistor R_S where the forward voltage drop across the LED is V_{LED} is given by,

$$I = \frac{(V_{\text{out}} - V_{\text{LED}})}{R_S}. \tag{A.2.3}$$

Then the power dissipated by the infrared LED (P_{LED}) is,

$$P_{\text{LED}} = V_{\text{LED}} \times I. \tag{A.2.4}$$

The infrared transmitters were arranged in a 4x4 matrix which allowed a maximum of four simultaneous unique transmissions on LEDs spaced 90° apart. The number of data streams being transmitted did not significantly effect the transmission power of the LEDs, as each set of LEDs had a separate series resistor and

the current drain of the LEDs had minimal effect on the variable voltage output.

Linear regulators are not ideal for low energy applications as they dissipate excess energy as heat. However, linear regulators are simple to implement and control, and do offer energy reduction due to the fact that the lower voltage output causes less current to be drawn by the LED-resistor combination. The power dissipation of a linear regulator can be described as:

$$\text{Power} = (V_{in} - V_{out}) \times I \tag{A.2.5}$$

Where V_{in} is the input voltage to the regulator, V_{out} is the output voltage, and I is the current being drawn by the circuit.

Ideally, for low energy applications, the variable intensity supply should be implemented in the form of a switching variable current regulator, as LEDs have a sharp current-voltage relationship, making it difficult to accurately control the intensity of a LED using voltage alone. The use of linear regulators, resistors and other devices which dissipate energy unnecessarily, when other less wasteful options are available, is not energy efficient.

Appendix B

Pulsed Infrared Light Channel Characteristics

B.1 Experimental Setup for Obtaining Channel Characteristics

The infrared channel experiments consisted of two servo motor platforms acting as goniometers (Figure B.1) which allowed accurate rotation of the infrared components(IR LED and IR receiver module) independently. This allowed recording of pulse width and pulse loss at different transmission and reception angles, as well as multiple distances and transmission powers. The lighting was kept constant throughout the experiments to eliminate the effect of ambient lighting, which may have affected the readings.

The experiments were repeated using five different transmitter/receiver pairs of components in order to identify the likely variation between different physical components. If the channel characteristics varied greatly between components it may indicate that the method would be unreliable for localisation purposes, unless each node or component was individually calibrated.
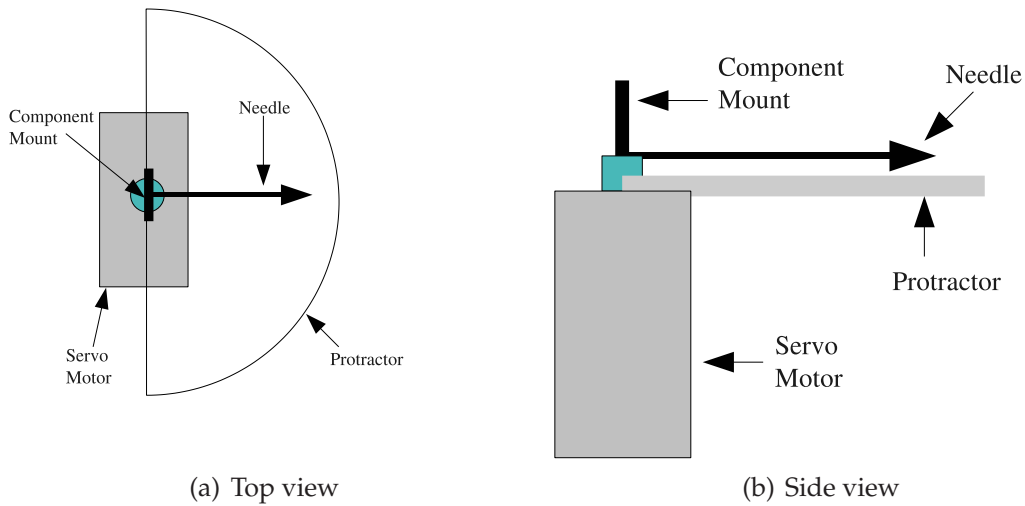
(a) Top view

(b) Side view

Figure B.1: Experimental platform for measuring IR channel characteristics.

Parameter	Start	End	Increment
Distance	0.2m	2.0m	0.2m
TX Angle	0°	20°	5°
RX Angle	0°	50°	10°
TX Power	10%	100%	10%

Table B.1: Experimental infrared test parameters.

For the experiments, the transmitter and receiver devices each had a dedicated ATmega168 [Atmb] microcontroller which formed a skeletal representation of the communication systems found on the nodes. A computer was used to simultaneously control the sending of pulses, logging of received pulses and movement of the two servo motor platforms (Figure B.2). Once the servo motor platforms were calibrated, all measurements were conducted using batch scripts, to ensure consistency in experimental procedure.

Five pairs of components were tested to determine expected variation in infrared characteristics across the physical network. Each pair was subjected to identical tests, which involved a total of 300 individual data collection points for each component pair, as shown in Table B.1.

At each test position a total of 600 received pulses were transmitted in 20 blocks
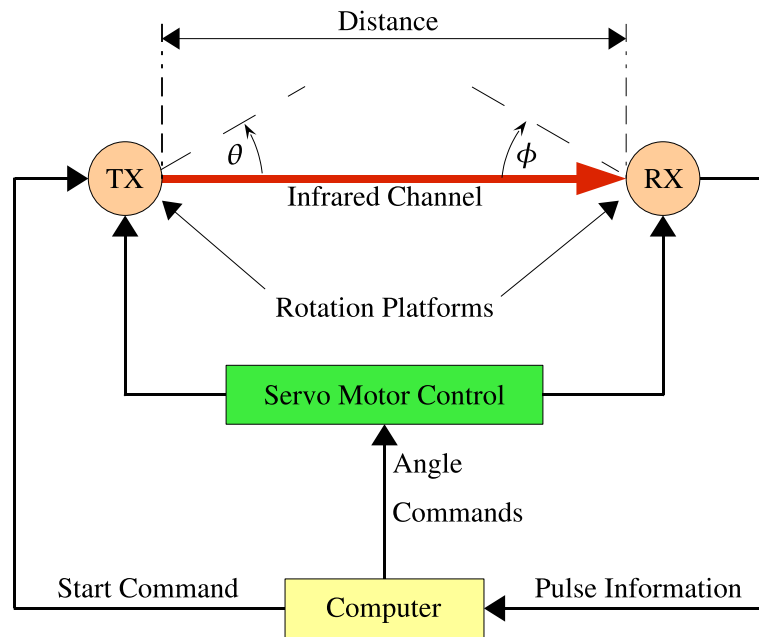
Figure B.2: Experimental system overview.

of 30 pulses, as shown in Figure B.3. The receiver logged the received pulses and recorded the pulse width, with a resolution of $6.4\,\mu s$. These measurements allowed the number of pulses correctly received at each position to be determined.

The output from the experimental receiver microcontroller was a continuous byte stream, consisting of pairs of numbers representing logic level, and the time spent at that logic level. The logic level byte was included for stream synchronisation and to allow accurate measurement of arbitrarily long pulse periods. The resolution of the period timer was $6.4\,\mu s$, and measurements were rounded down to the nearest timing increment. Therefore, the maximum timing error of the pulse width was $6.4\,\mu s$. With respect to the $38\,kHz$ IR carrier frequency used for the IR communications, the timing resolution provides four counts per cycle of the carrier frequency, and the test pulses of $500\,\mu s$ resulted in a count of $78 \times 6.4\,\mu s$. Therefore, the maximum timing error due to rounding for a $500\,\mu s$ pulse is approximately 1.3%.
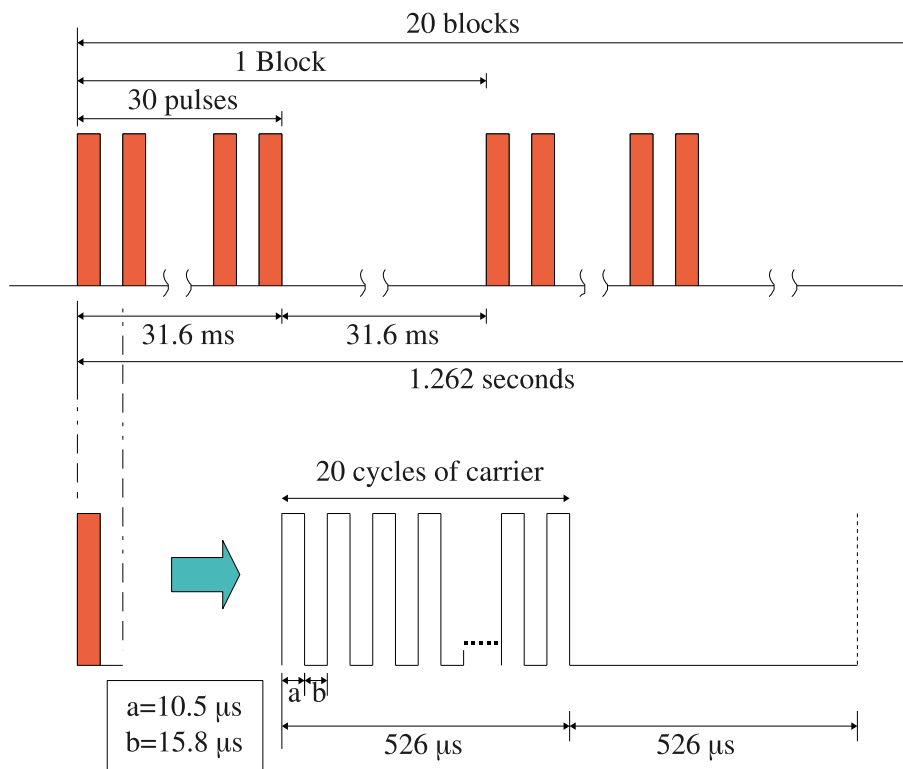
Figure B.3: Transmitted pulse structure: 20 blocks of 30 pulses.

The experimental data captured by the receiver, shown in Figure B.4, closely matches the transmitted waveform pattern as shown in Figure B.3. This captured dataset represents a high quality, low loss, communication channel. If the received waveform had missing pulses and/or blocks, it would indicate pulse losses, resulting in transmission errors, and hence an unreliable communication channel
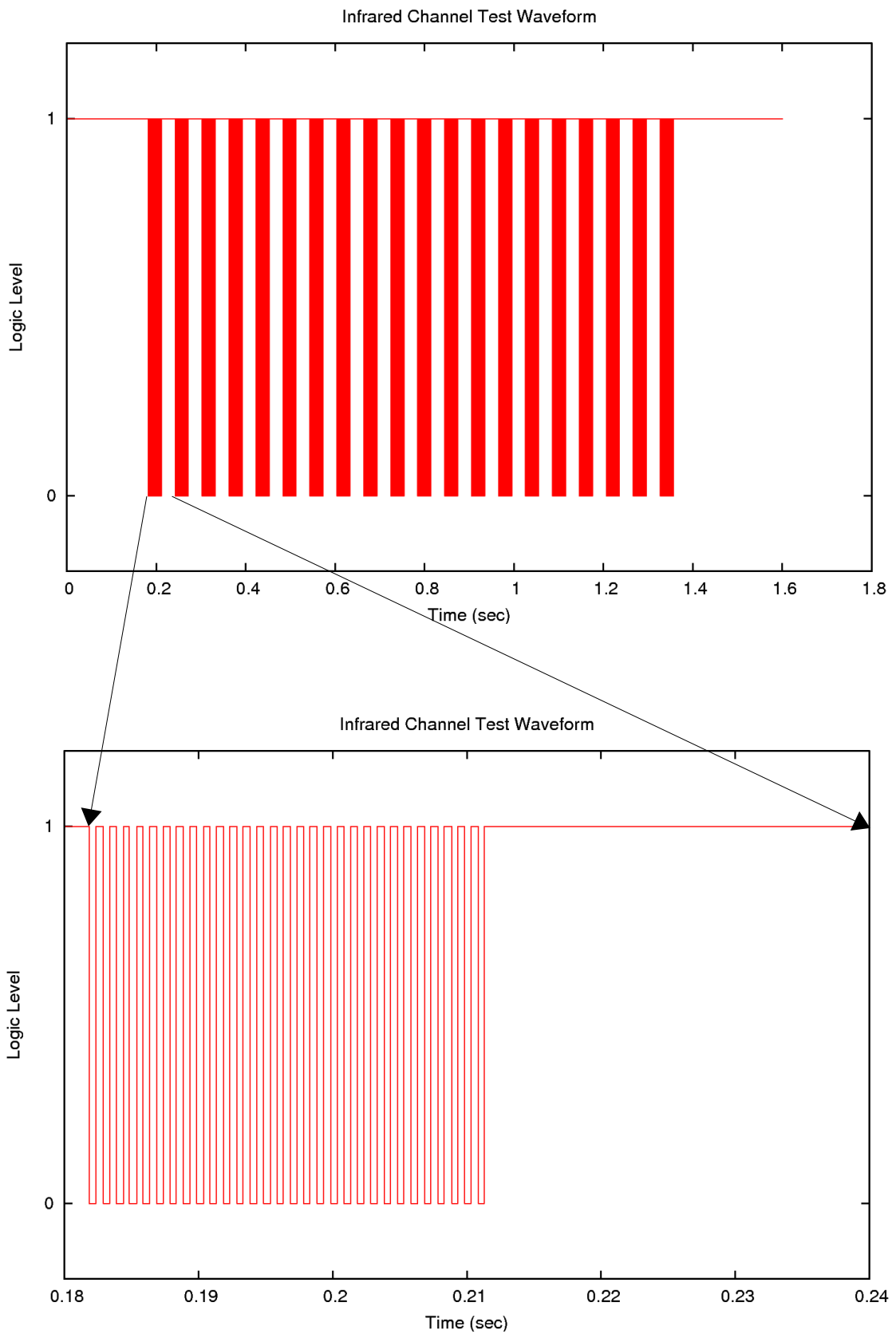
Figure B.4: Captured waveform, each of the 20 blocks contains 30 pulses.

B.2 Channel Characteristics

Figures B.5 through B.9 represent the channel characteristics of each of the five transmitter-receiver pairs tested. The shaded areas represent a usable channel (i.e., lower than 10% pulse loss), outside this area the IR channel displays high pulse loss and does not provide an effective communication medium. See Section 3.2.2 for further details on interpreting these graphs.

Figure B.5: Pair 1: Communication channel characteristics

Figure B.6: Pair 2: Communication channel characteristics

Figure B.7: Pair 3: Communication channel characteristics
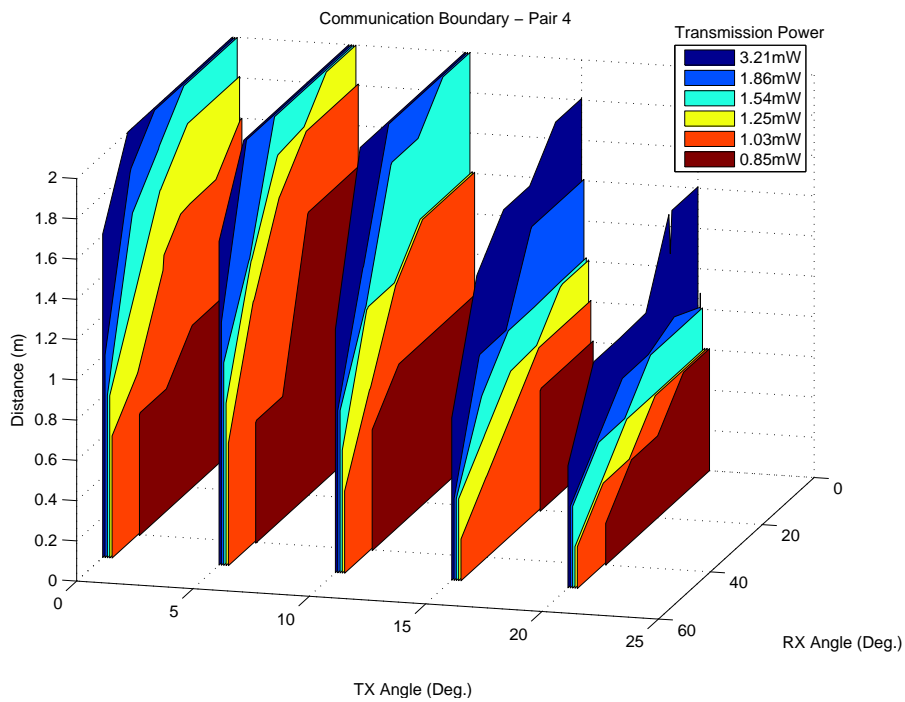
Figure B.8: Pair 4: Communication channel characteristics
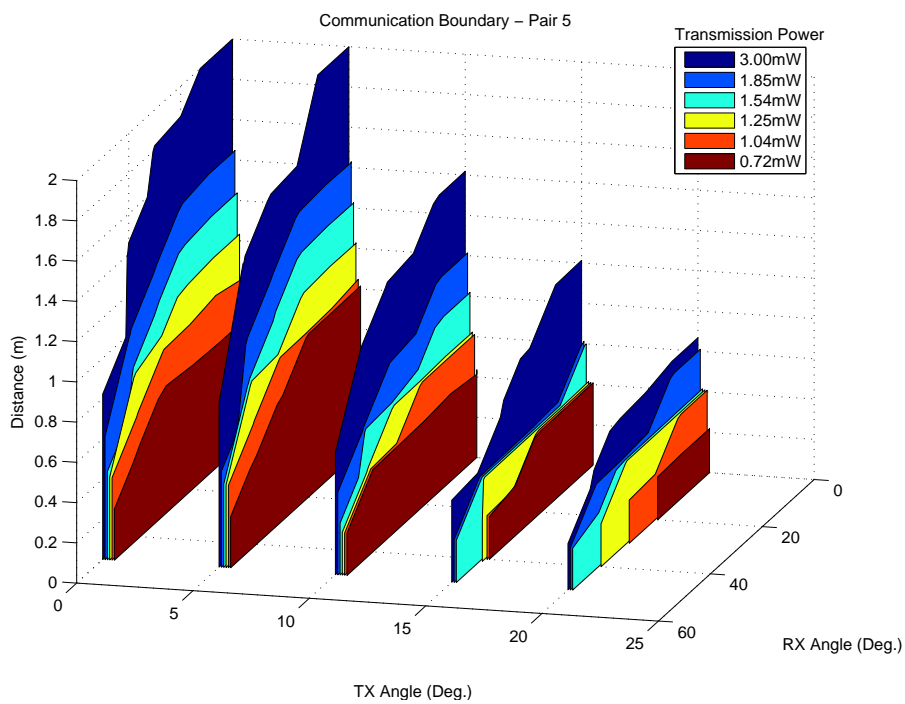
Figure B.9: Pair 5: Communication channel characteristics

Appendix C

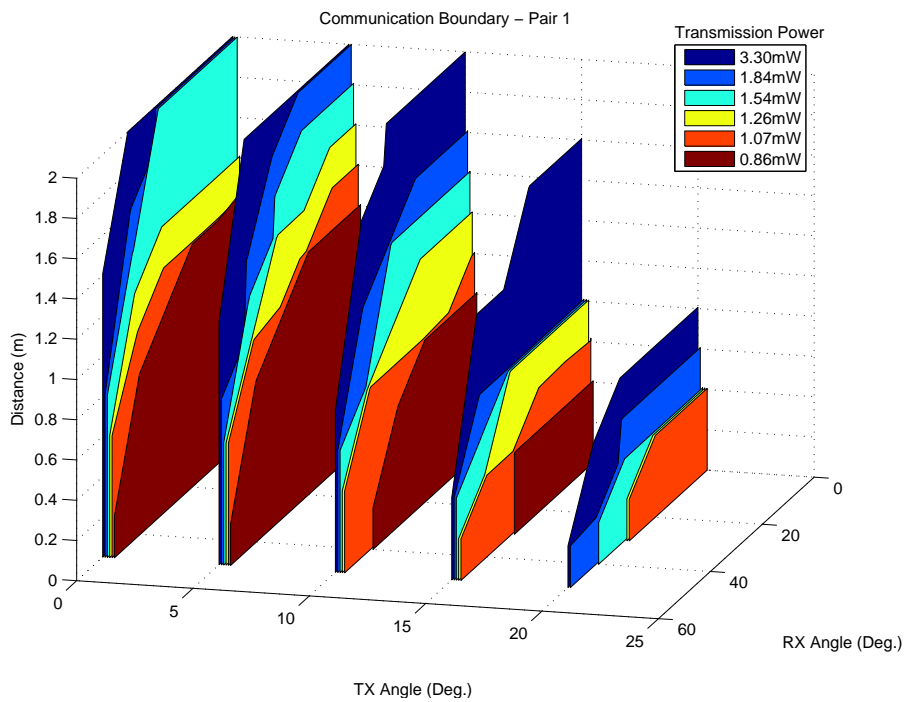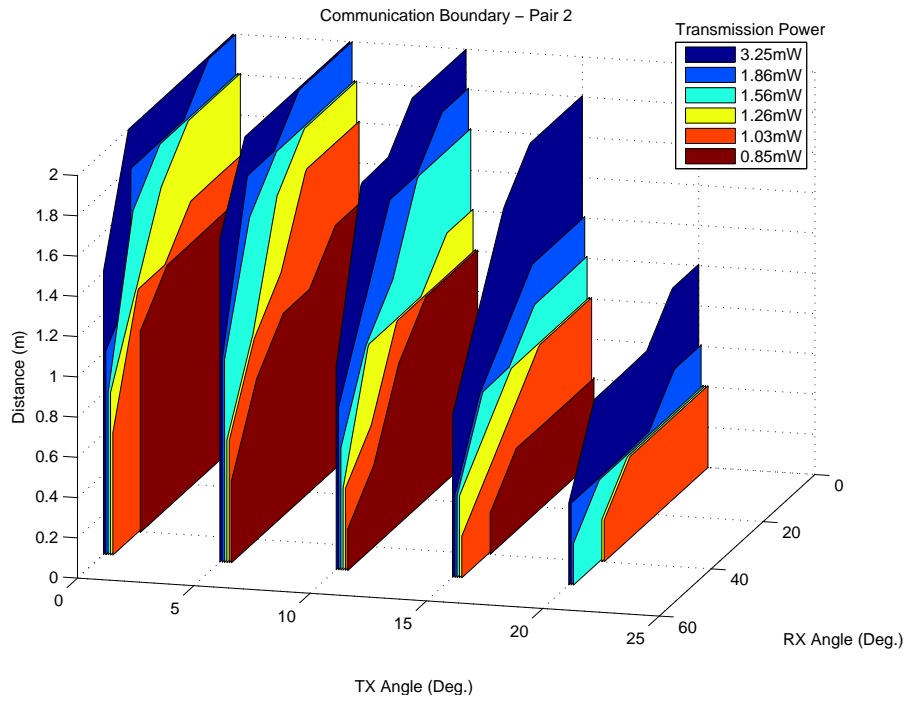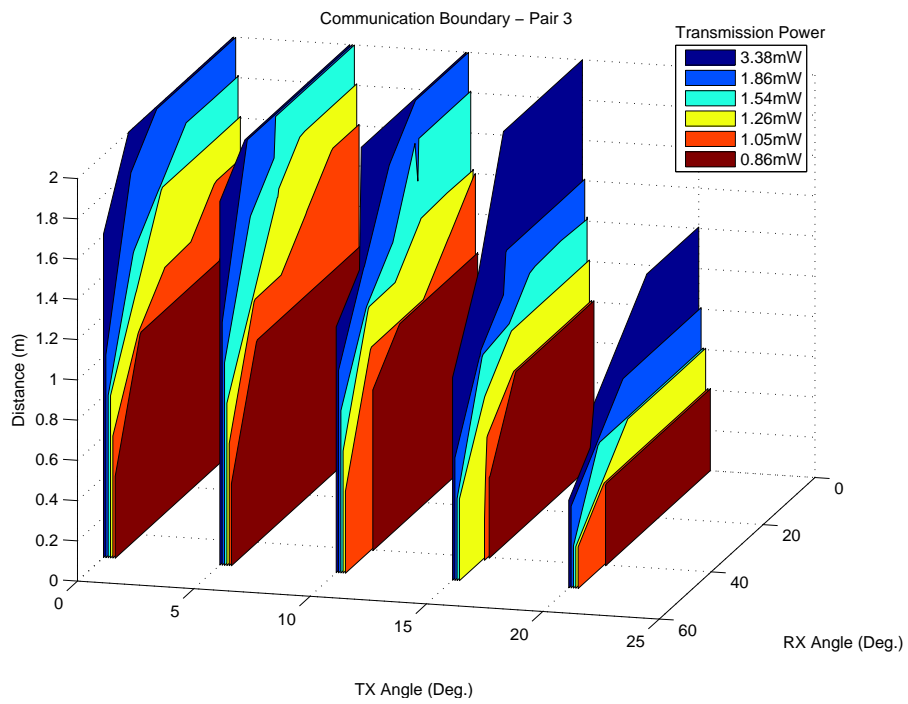# Simulator for Ad Hoc Networks with Pulsed Infrared Light Links

C.1 Simulator Details

As part of this research, a simulator was developed to evaluate the use of directional infrared channels for localisation in wireless ad hoc networks. The simulator incorporated experimental channel characteristics, obtained from the physical infrared testbed, in order to accurately model the infrared channels between nodes. A discretised channel model was developed based on the experimental results obtained in Chapter 3. This allowed nodes to use one of the five experimental data sets to accurately simulate the infrared channels between nodes, along with the expected variation in infrared components for each transmitter-receiver pair.

The simulator was implemented in C, with an optional OpenGL [Ope] front-end to provide an interactive environment with visual indication of the position of each node in the network, along with the estimated channel quality between each connected IR pair. The OpenGL front-end allowed users to relocate and rotate nodes with instant feedback of the channel characteristics between each

transmitter-receiver pair in the network. However, for most simulations, the OpenGL front-end was disabled to reduce the runtime of non-interactive batch simulations.

The simulation environment consisted of a two dimensional field which contains all nodes. The dimensions of the simulated environment were not specifically set, and change dynamically depending on the position of nodes within the network. All distances within the simulator were represented in metres, while angles were measured in degrees, clockwise, from a due north bearing. The global coordinate system for all simulated entities were in the form (x,y), relative to the lower left hand corner of the field.

Nodes within the simulation environment had independent orientations, which affected the placement of transmitter and receiver components around the edge of the node. The position of the IR components on each node is dependant on the node's orientation ($\theta°$), and the number of transmitters and receivers (N_{TX} and N_{RX} respectively). Receivers were placed every Δ°_{RX} around the edge of the nodes, and transmitters were placed at every Δ°_{TX}, as shown in Equations (C.1.2) and (C.1.1).

The angular separation of the transmitters (Δ_{TX}) and receivers (Δ_{RX}) is given by,

$$\Delta_{\mathrm{TX}} = \frac{360°}{N_{\mathrm{TX}}}, \tag{C.1.1}$$

$$\Delta_{\mathrm{RX}} = \frac{360°}{N_{\mathrm{RX}}}. \tag{C.1.2}$$

Therefore, the angular position of each component can be calculated as,

$$\varphi_{\mathrm{TX_n}} = \theta + n\Delta_{\mathrm{TX}} + \frac{\Delta_{\mathrm{TX}}}{2} \qquad \text{for } n = 0, 1, \ldots, N_{\mathrm{TX}} - 1, \tag{C.1.3}$$

$$\varphi_{\mathrm{RX_n}} = \theta + n\Delta_{\mathrm{RX}} \qquad \text{for } n = 0, 1, \ldots, N_{\mathrm{RX}} - 1. \tag{C.1.4}$$

Finally the (x,y) coordinates of each infrared component is given by,

$$(X_{\mathrm{TX_n}}, Y_{\mathrm{TX_n}}) \;=\; (X + r\cos(\varphi_{\mathrm{TX_n}}), Y + r\sin(\varphi_{\mathrm{TX_n}})), \qquad\text{(C.1.5)}$$

$$(X_{\mathrm{RX_n}}, Y_{\mathrm{RX_n}}) \;=\; (X + r\cos(\varphi_{\mathrm{RX_n}}), Y + r\sin(\varphi_{\mathrm{RX_n}})). \qquad\text{(C.1.6)}$$

Where (X,Y) is the midpoint, and r is the radius, of the node.

To ensure accurate simulation of the infrared channel characteristics, all angles and distances were calculated taking into account the radius (r) of the physical nodes (4cm in this case). Figure C.1 shows the 4 angles which must be considered when simulating the infrared channel characteristics between nodes. The angles $\varphi_{\mathrm{TX_n}}$ and $\varphi_{\mathrm{RX_n}}$ represent the angle of the transmitter LED and IR receiver modules respectively, relative the line joining the centre of both nodes. The angles ϕ_{TX} and ϕ_{RX} represent the transmitter and receiver angle relative to the optical axis (zero angle) of the device (ie, normal to the circumference of the circular node).
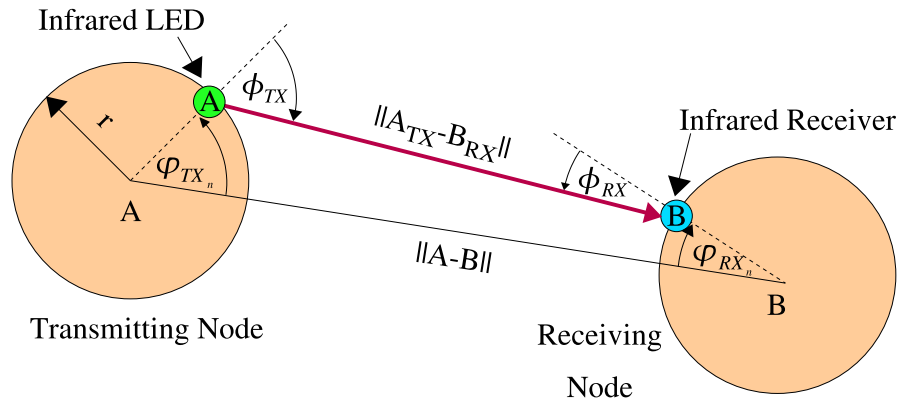
Figure C.1: Simulation of transmission and reception angles.

The transmission and reception angles (ϕ_{TX} and ϕ_{RX}) can be calculated using the Sine Rule. By forming two triangles as shown in Figure C.2, Equation (C.1.7) can be used to calculate $\mathrm{D_{TX}}$ and $\mathrm{D_{RX}}$, which can then be substituted into Equation (C.1.8) to find ϕ_{TX} and ϕ_{RX}.
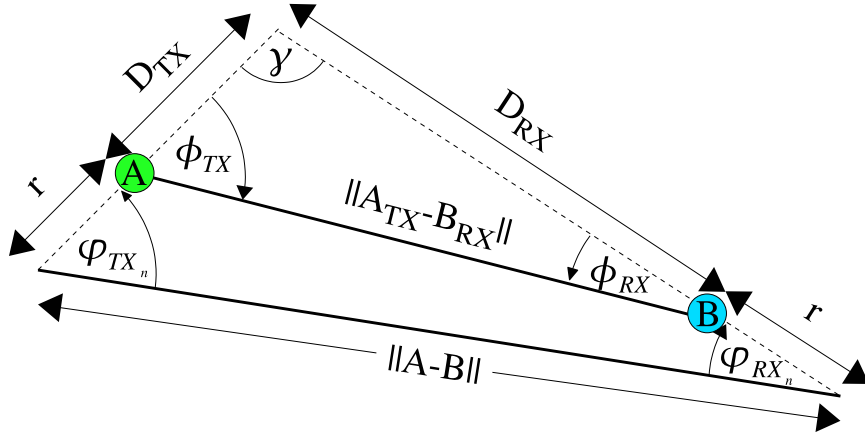
Figure C.2: Calculating the transmission and reception angles.

$$\frac{D_{\mathrm{TX}} + r}{\sin(\varphi_{\mathrm{RX_n}})} = \frac{D_{\mathrm{RX}} + r}{\sin(\varphi_{\mathrm{TX_n}})} = \frac{\|A - B\|}{\sin(\gamma)} \tag{C.1.7}$$

$$\frac{D_{\mathrm{TX}}}{\sin(\phi_{\mathrm{RX}})} = \frac{D_{\mathrm{RX}}}{\sin(\phi_{\mathrm{TX}})} = \frac{\|A_{\mathrm{TX}} - B_{\mathrm{RX}}\|}{\sin(\gamma)} \tag{C.1.8}$$

C.1.1 Simulation Environment

The simulator allowed simulation of arbitrarily large networks, while allowing observation of all active IR pairs and connected neighbours. Figure C.3 shows an example of a simulated two node network. The channel quality for each transmitter-receiver pair is represented with different coloured lines: blue indicates a low power (high quality) link, green indicated medium power and red indicates a high power (low quality) link.

In interactive graphics mode, the simulator allowed users to adjust parameters of the network, including node position and node orientation, to visualise the connectivity of the infrared nodes for different topologies. The simulator outputted debug information including a list of in-range infrared transmitter-receiver pairs, as shown in Table C.3, along with the transmission and reception angles, and the
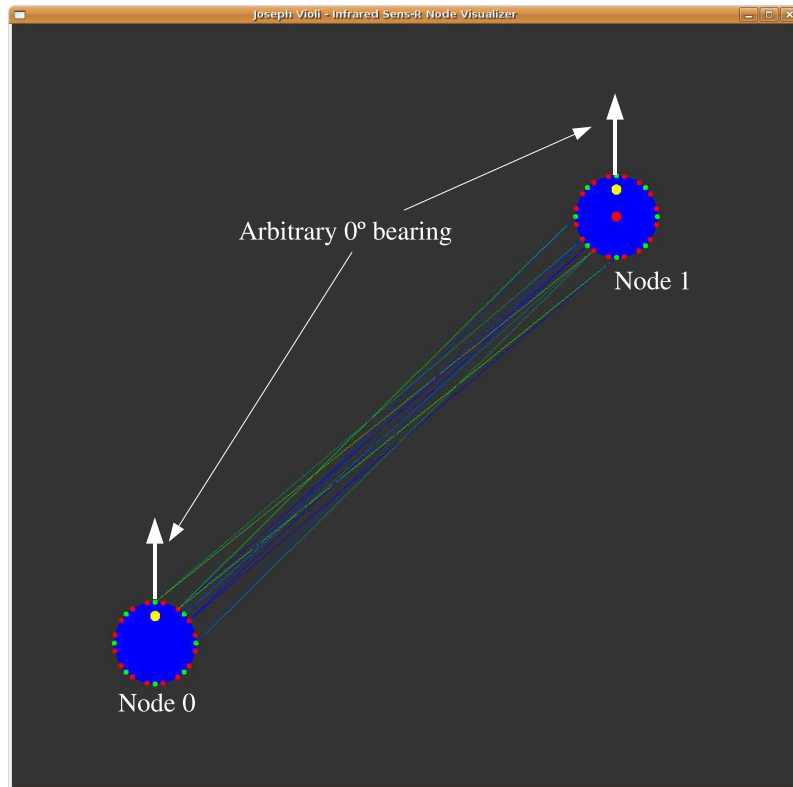
Figure C.3: Simulated two node network.

Node 0 to Node 1					
TXID	**RXID**	ϕ_{TX}	ϕ_{RX}	**Distance**	**Power**
1	4	17.523	51.273	0.549	9
2	4	6 .600	49.650	0.548	1
1	5	14.649	3.399	0.535	1
2	5	9 .521	1.729	0.535	1
1	6	11.612	44.638	0.546	7
2	6	12.525	46.275	0.546	2
Real Angle = 47.233809; Est. Angle = 48.730000					
Node 1 to Node 2					
TXID	**RXID**	ϕ_{TX}	ϕ_{RX}	**Distance**	**Power**
9	0	17.523	51.273	0.549	10
10	0	6 .600	49.650	0.548	5
9	1	14.649	3.399	0.535	4
10	1	9 .521	1.729	0.535	2
9	2	11.612	44.638	0.546	5
10	2	12.525	46.275	0.546	2
Real Angle = 227.233809; Est. Angle = 229.180000					

Table C.1: Simulator output for Figure C.3.

Figure C.4: Simulated 100 node grid network.

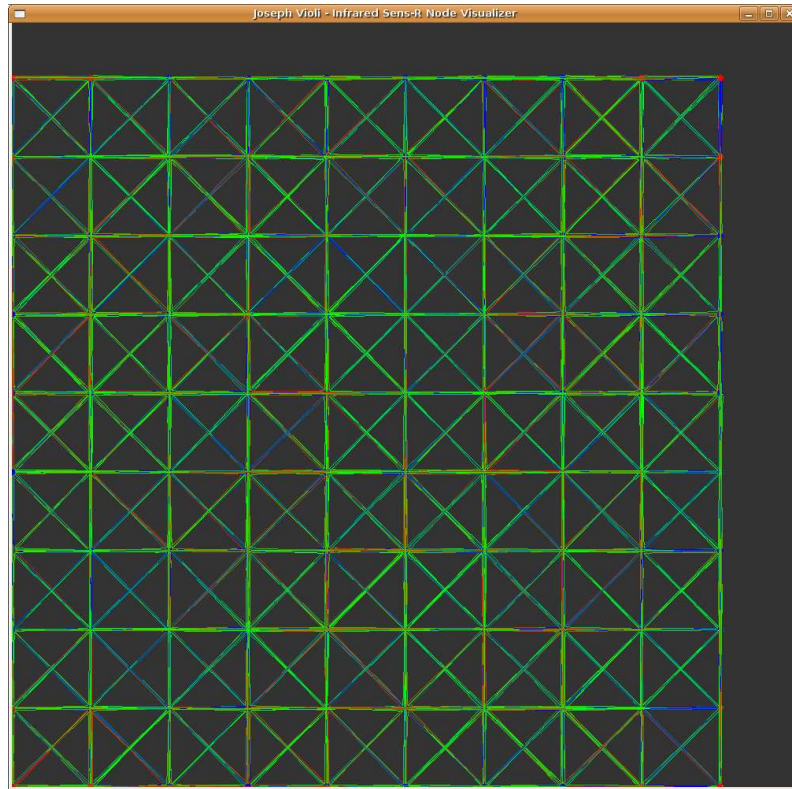minimum power required to achieve successful communications based on a randomly selected experimental data set. The simulator also outputted the actual and estimated angle of nodes based on Equation (3.5.2), from this the accuracy of the angle estimation algorithm could be established.

Large networks could also be simulated interactively. Figure C.4 shows the simulation window of a 100 node network with a grid topology. However, due to the number of interconnections and angle calculations required for large networks, it was not practical to allow real-time interactivity for large networks, as the time required to calculate connectivity between nodes made the simulation unresponsive. Therefore, large networks were typically run in a non-interactive batch mode with static networks, such that connectivity between nodes remains constant and all angles and distances could be precomputed, thus dramatically reducing the runtime of simulations of large scale networks.

116

Bibliography

[ABKR07] J. Arnold, N. Bean, M. Kraetzl, and M. Roughan. Node localisation in wireless ad hoc networks. *Proceedings of the 15th IEEE International Conference on Networks (ICON 2007)*, Nov. 2007.

[ASSC02] I. F. Akyildiz, Weilian S., Y. Sankarasubramaniam, and E. Cayirci. A survey on sensor networks. *IEEE Communications Magazine*, 40(8):102–114, Aug. 2002.

[Atma] Atmel. 8-bit AVR Microcontroller with 128 KByte In-System Programmable Flash. URL reference http://www.atmel.com/dyn/resources/prod_documents/doc2467.pdf.

[Atmb] Atmel. 8-bit AVR Microcontroller with 8 KByte In-system Programmable Flash. URL reference http://www.atmel.com/dyn/resources/prod_documents/doc2545.pdf.

[BHE00] N. Bulusu, J. Heidemann, and D. Estrin. GPS-less low-cost outdoor localization for very small devices. *IEEE Personal Communications Magazine*, 7(5):28–34, Oct. 2000.

[BLP06] M. Broxton, J. Lifton, and J. A. Paradiso. Localization on the push-pin computing sensor network using spectral graph drawing and mesh relaxation. *ACM SIGMOBILE Mobile Computing and Communications Review*, 10(1):1–12, 2006.

[Bri] Bright LED Electronics Corp. BRM-1030. URL reference http://www.brightled.com.tw/Downloads/Products/Receiver_Module/BRM-1030.pdf.

[CCL03] I. Chlamtac, M. Conti, and J. J. Liu. Mobile ad hoc networking: imperatives and challenges. *Ad Hoc Networks*, 1(1):13–64, Jul. 2003.

[Cha05] A. M. Chandra. *Higher Surveying*. New Age International Ltd., 2005.

[CHH01] S. Capkun, M. Hamdi, and J.-P. Hubaux. GPS-free positioning in mobile ad hoc networks. *Proceedings of the 34th Annual Hawaii International Conference on System Sciences.*, pages 1–10, Jan. 2001.

[Cro] Crossbow. Crossbow Technology Inc. URL reference http://xbow.com.

[CV04] R. R. Choudhury and N. H. Vaidya. Deafness: a mac problem in ad hoc networks when using directional antennas. *Proceedings of the 12th IEEE International Conference on Network Protocols (ICNP 2004)*, pages 283–292, Oct. 2004.

[Dal93] P. Daly. Navstar GPS and GLONASS: global satellite navigation systems. *Electronics & Communication Engineering Journal*, pages 349–357, December 1993.

[ECC03] J. S. Esteves, A. Carvalho, and C. Couto. Generalized geometric triangulation algorithm for mobile robot absolute self-localization. *2003 IEEE International Symposium on Industrial Electronics (ISIE '03)*, 1:346–351, Jun. 2003.

[EH07] F. Engel and M. Hedley. A comparison of cooperative localisation techniques for wireless mobile sensor networks. *International Symposium on Communications and Information Technologies (ISCIT '07)*, pages 887–892, Oct. 2007.

[Feh95] K. Feher. *Wireless Digital Communications: Modulation and Spread Spectrum*. Prentice-Hall, 1995.

[Fes] Festo. URL reference http://www.festo.com.

[FKZL03] S. Feldmann, K. Kyamakya, A. Zapater, and Z. Lue. An indoor Bluetooth-based positioning system: Concept, Implementation and Experimental Evaluation. In *International Conference on Wireless Networks*, pages 109–113, 2003.

[Fou] Free Software Foundation. AVR C Runtime Library. URL reference http://www.nongnu.org/projects/avr-libc.

[Gas02] M. S. Gast. *802.11 Wireless Networks: The Definitive Guide*. O'Reilly & Associates, Inc., Sebastopol, CA, USA, 2002.

[GBBE06] Y. Gu, D. Bozdağ, R. W. Brewer, and E. Ekici. Data harvesting with mobile elements in wireless sensor networks. *Computer Networks*, 50(17):3449–3465, 2006.

[GZT+05] P. Gober, A. Ziviani, P. Todorova, M.D. Amorim, P. Hunerberg, and S. Fdida. Topology control and localization in wireless ad hoc and sensor networks. *Ad Hoc & Sensor Networks*, 1:301–322, 2005.

[HHB+03] T. He, C. Huang, B. M. Blum, J. A. Stankovic, and T. Abdelzaher. Range-free localization schemes for large scale sensor networks. In

Proceedings of the 9th annual international conference on Mobile computing and networking (MobiCom'03), pages 81–95, New York, NY, USA, 2003. ACM.

[HHB+05] T. He, C. Huang, B. M. Blum, J. A. Stankovic, and T. F. Abdelzaher. Range-free localization and its impact on large scale sensor networks. *Transactions on Embedded Computing Systems*, 4(4):877–906, 2005.

[HLM01] R. M. Harlan, D. B. Levine, and S. McClarigan. The Khepera robot and the kRobot class: a platform for introducing robotics in the undergraduate curriculum. *ACM SIGCSE Bulletin*, 33(1):105–109, 2001.

[HMB05] S. Hoyt, S. McKennoch, and L. G. Bushnell. An autonomous multi-agent testbed using infrared wireless communication and localisation. Technical report, Department of Electrical Engineering, University of Washington, March 2005.

[JCLR99] Jr J. C. Liberti and T. S. Rappaport. *Smart Antennas for Wireless Communications: IS-95 and Third Generation CDMA Applications*. Prentice Hall PRT, 1999.

[Kav07] M. Kavehrad. Broadband room service by light. *Scientific American*, pages 82–87, July 2007.

[KH06a] K. W. Kolodziej and J. Hjelm. *Local Positioning Systems: LBS Applications and Services*. CRC, May 2006.

[KH06b] Krzysztof W. Kolodziej and Johan Hjelm. *Local Positioning systems: LBS Applications and Services*. CRC Press, 2006.

[KKK07] J. Kang, D. Kim, and Y. Kim. RSS self-calibration protocol for WSN localization. *Second International Symposium on Wireless Pervasive Computing (ISWPC '07)*, pages –, 5-7 Feb. 2007.

[Lab02] J. Labrosse. *MicroC/OS-II: The Real-Time Kernel*. CMP Books, 2002.

[LBP05] J. Lifton, M. Broxton, and J.A. Paradiso. Experiences and directions in pushpin computing. *Fourth International Symposium on Information Processing in Sensor Networks (IPSN 2005)*, pages 416–421, Apr. 2005.

[LR03] K. Langendoen and N. Reijers. Distributed localization in wireless sensor networks: a quantitative comparison. *Computer Networks*, 43(4):499–518, 2003.

[LWH04] C. Liu, K. Wu, and T. He. Sensor localization with ring overlapping based on comparison of received signal strength indicator. *Proceedings of the IEEE International Conference on Mobile Ad-hoc and Sensor Systems*, pages 516–518, 25-27 Oct. 2004.

[Mar04] A. Martinoli. A Scalable, On-Board Localisation and Communication System for Indoor Multi-Robot Experiments. *Sensor Review*, 24:167–180(14), 1 February 2004.

[Nic04] D. Niculescu. Positioning in ad hoc sensor networks. *IEEE Network*, 18(4):24–29, Jul.-Aug. 2004.

[NIS] e-Handbook of Statistical Methods: Single Exponential Smoothing. URL reference http://www.itl.nist.gov/div898/handbook/pmc/section4/pmc431.htm.

[NN03] D. Niculescu and B. Nath. DV based positioning in ad hoc networks. *Telecommunication Systems*, 22:267–280, 2003.

[NSGPK02] L. E. Navarro-Serment, R. Grabowski, C. J. J. Paredis, and P. K. Khosla. Millibots: The Development of a Framework and Algorithms for a Distributed Heterogeneous Robot Team. In *IEEE Robotics and Automation Magazine*, volume 9, Dec. 2002.

[Ope] OpenGL. URL reference http://www.opengl.org.

[OWB04] K. J. O'Hara, D. B. Walker, and T. R. Balch. The GNATS low-cost embedded networks for supporting mobile robots. In *Third International Multi-Robot Systems Workshop*, June 2004.

[Pat00] B. Pattan. *Robust Modulation Methods & Smart Antennas in Wireless Communications*. Prentice Hall PTR, 2000.

[PLY+00] K. Pahlavan, X. Li, M. Ylianttila, R. Chana, and M. Latva-aho. An overview of wireless indoor geolocation techniques and systems. In *Proceedings of the IFIP-TC6/European Commission International Workshop on Mobile and Wireless Communication Networks (NETWORKING '00)*, pages 1–13, London, UK, 2000. Springer-Verlag.

[RRS+05] R. Ramanathan, J. Redi, C. Santivanez, D. Wiggins, and S. Polit. Ad hoc networking with directional antennas: A complete system solution. *IEEE Journal on Selected Areas in Communications*, 23(3):496–506, Mar. 2005.

[RS03] V. Ramadurai and M. Sichitiu. Localization in wireless sensor networks: A probabilistic approach. In *Proceedings of the 2003 International Conference on Wireless Networks (ICWN 2003)*, pages 275–281, Las Vegas, NV, 2003.

[RS06] P. Rong and M. L. Sichitiu. Angle of arrival localization for wireless sensor networks. 3rd *Annual IEEE Communications Society on Sensor and Ad Hoc Communications and Networks (SECON '06)*, 1:374–382, Sept. 2006.

[San05] P. Santi. Topology control in wireless ad hoc and sensor networks. *ACM Computing Surveys (CSUR)*, 37(2):164–194, 2005.

[Sem] National Semiconductor. LM317 - 3-Terminal Adjustable Regulator. URL reference http://www.national.com/mpf/LM/LM317.html.

[SF04] M. Smith and B. Freisleben. Self-Healing Wireless Ad Hoc Networks Based On Adaptive Node Mobility. In *Proceedings of the First IFIP International Conference on Wireless and Optical Communications Networks, Muscat, Oman*, pages 121–124. IFIP, 2004.

[SHS01] A. Savvides, C-C. Han, and M. B. Strivastava. Dynamic Fine-Grained Localization in Ad-Hoc Networks of Sensors. In *Mobile Computing and Networking*, pages 166–179, 2001.

[SKOM06] M. Sugano, T. Kawazoe, Y. Ohta, and M. Murata. Indoor localization system using RSSI measurement of wireless sensor network based on ZigBee standard. In *Wireless and Optical Communications*, 2006.

[SPS03] A. Savvides, H. Park, and M. B. Srivastava. The n-hop multilateration primitive for node localization problems. *Mobile Networks and Applications*, 8(4):443–451, 2003.

[Sta01] W. Stallings. *High Speed Networks and Internets: Performance and Quality of Service*. Prentice Hall PTR, Upper Saddle River, NJ, USA, 2001.

[Sto02] I. Stojmenovic. Position-based routing in ad hoc networks. *IEEE Communications Magazine*, pages 128–134, July 2002.

[SWH06] T. Scott, K. Wu, and D. Hoffman. Radio propagation patterns in wireless sensor networks: new experimental results. In *Proceedings of the 2006 international conference on Wireless Communications and Mobile Computing (IWCM '06)*, pages 857–862, New York, NY, USA, 2006. ACM.

[TR05] F. Thomas and L. Ros. Revisiting trilateration for robot localization. *IEEE Transactions on Robotics*, 21(1):93–101, Feb 2005.

[VCdSdM03] M.A.M. Vieira, Jr. Coelho, C.N., Jr. da Silva, D.C., and J.M. da Mata. Survey on wireless sensor network devices. *Proceedings of IEEE Conference on Emerging Technologies and Factory Automation (ETFE '03)*, 1:537–544 vol.1, Sep. 2003.

[VWG+03] M. Vossiek, L. Wiebkin, P. Gulden, J. Wieghardt, C. Hoffmann, and P. Heide. Wireless Local Positioning. *IEEE Microwave Magazine*, 4:77–86, Dec. 2003.

[WB] G. Welch and G. Bishop. An introduction to the kalman filter. URL reference http://www.cs.unc.edu/~welch/kalman/kalmanIntro.html.

[WX07] C. Wang and L. Xiao. Sensor Localization under Limited Measurement Capabilities. *IEEE Network*, pages 16–23, May/June 2007.

[XGB02] K. Xu, M. Gerla, and S. Bae. How effective is the IEEE 802.11 RTS/CTS handshake in ad hoc networks. *IEEE Global Telecommunications Conference (GLOBECOM '02)*, 1:72–76 vol.1, Nov. 2002.

[ZG04] F. Zhao and L. J. Guibas. *Wireless Sensor Networks: An Information Processing Approach*. Morgan Kaufmann, 2004.

[ZHKS04] G. Zhou, T. He, S. Krishnamurthy, and J. A. Stankovic. Impact of radio irregularity on wireless sensor networks. In *Proceedings of the 2nd international conference on Mobile systems, applications, and services (MOBISYS '04)*, pages 125–138, New York, NY, USA, 2004. ACM.

[ZWCF06] H. Zhai, J. Wang, X. Chen, and Y. Fang. Medium access control in mobile ad hoc networks: challenges and solutions: Research articles. *Wireless Communication and Mobile Computing*, 6(2):151–170, Mar. 2006.